Applications of The Coupled-Cluster Theory On the Novel H, Si, C, and Ge Containing Small Molecules; Effects of Scalar Relativity

by

Levent Sari

(Under the direction of H. F. Schaefer)

Abstract

The highly correlated ab initio coupled-cluster theories have been employed on the ground and first excited electronic states of the HCSi and HCGe tri-atomic molecules, and on the ground electronic states of the GeC_2, Si_2H_3, and Si_2H_4. The main reason for the choice of these molecules is that very little or even nothing is known about the structure, energetic, and other first and second order molecular properties. Also, these molecules are of interest because of their potential applications in semiconductors and optoelectronics, in surface growth processes, and their possible existence in the circumstellar atmospheres of evolved carbon stars. Large basis sets (e.g. TZ3P(2f,2d)+2$diff$ and cc-pVQZ) have been employed in conjunction with the very sophisticated quantum mechanical methods such as CCSD(T), CCSD(2), and CCSDT. Equation of motion coupled cluster theories were employed in order to determine some excited state properties, which cannot be determined using standard quantum mechanical methods due to possible variational collapses. Challenging problems such as characterization of the Renner-Teller splitting in the ground $\tilde{X}\ ^2\Pi$ states of HCSi and HCGe, determination of the true ground state equilibrium geometry for the elusive GeC_2, and searching the unanticipated mono- and di-bridged isomers of the Si_2H_3 and Si_2H_4 molecules have been focused. Investigation of the effects of the scalar relativistic corrections on some molecular properties as well as on the Renner-Teller splitting has been another focus of interest throughout the study. In some cases, corrections due to zero-point vibrational energies (ZPVE) and core-valence interactions have been determined in order to predict reliable spectroscopic constants. The theoretical predictions for the HCSi and HCGe tri-atomic molecules were compared with the few existent experimental and theoretical works in literature. It has been observed that coupled cluster theory in conjunction with large basis sets is able to predict bond distances within ± 0.1 Å and energetic properties within ± 1 kcal/mol accuracy. Inclusion of the scalar relativistic corrections

even produced better estimates. The equilibrium geometry for the GeC_2 molecule in its ground state is predicted to be L-Shaped rather than T-shaped as in the case of SiC_2. For the structural predictions on the Si_2H_3 and Si_2H_4 molecules, collaboration with the Harvard experimentalists showed excellent agreements.

INDEX WORDS: Ab initio methods, Coupled Cluster Theory, Dirac Equation, Breit-Pauli Hamiltonian, Scalar Relativistic Corrections, Renner Teller Effects, Variational Collapse, Spinor, Excited States, Correlation Consistent Basis Set, Core Valence Corrections, Zero Point Vibrational Energy, Circumstellar Atmosphere, Chemical Vapor Deposition

Applications of The Coupled-Cluster Theory On the Novel H, Si, C, and Ge Containing Small Molecules; Effects of Scalar Relativity

by

Levent Sari

B.S., Bogazici University, Istanbul, Turkey, 1999

A Dissertation Submitted to the Graduate Faculty
of The University of Georgia in Partial Fulfillment
of the
Requirements for the Degree

Doctor of Philosophy

Athens, Georgia

2003

Applications of The Coupled-Cluster Theory On the Novel H, Si, C, and Ge Containing Small Molecules; Effects of Scalar Relativity

by

Levent Sari

Approved:

Major Professor: H. F. Schaefer

Committee: Lucia Babcock
Henning Meyer
Lionel Carreira

Electronic Version Approved:

Maureen Grasso
Dean of the Graduate School
The University of Georgia
May 2003

To my parents and lovely wife...

Acknowledgments

First of all, I am very grateful to my parents, Ali and Kafiye, who spent all their efforts for my education beginning from the primary school. Although both of them could not find chances to complete a higher education, they always did everything that they can in order to provide me with the best possible education. Therefore, their contribution is the fundamental part in my success. Also, I want to thank my sister Sema and brothers Mufrettin and Furkan. Especially, my elder brother Mufrettin has an important part in my success because he helped me very much throughout my education.

I am also very grateful to the support of my wife, Nuray. She always tried to provide me with the best atmosphere in which I can study and work efficiently. Although She entered into my life just about a year ago, her presence accelerated my productivity and success.

I thank my undergraduate professors, Victoria Aviyente and Yuksel Inel, whose quantum and physical chemistry courses made quantum mechanics attractive for me. Especially, Dr. Aviyente encouraged me a lot for a graduate study in the U.S.

I am very thankful to Dr. Yukio Yamaguchi for his unending help in my research. He taught me not only the fundamentals of almost all ab initio methods but also detail usages of our program package Psi. I also found a very good chance to increase my programming skills through his class.

I thank Jason M. Gonzales very much for being my mentor during my first year at CCQC and also in the U.S. He helped me a lot in learning Psi2 program package

and Latex. I also appreciated his advices and suggestions pertinent to the American life-style.

I thank Nicholas Petraco, Lubos Horny, and Chae Pak for being my close friends at CCQC. I also want to thank my Turkish friends, Kursat Erbas, Zubeyr Cinkir, Ismail Budak Arpinar, Ozer Cinar, and Bedri Karakas. They always provided me with atmospheres I am familiar with.

I also want to thank all other CCQC members. I thank Linda Rowe, Amy Peterson, and Karen Branch for taking care of so many details. I thank Richard Remington for keeping the computers going and teaching me helpful things about the art of AIX.

I thank Prof. L. Babcock, Prof. H. Meyer, and Prof. L. Carreira as being my committee members. I appreciate their efforts and valuable suggestions.

Lastly, I am deeply grateful and thankful to Professor Henry. F. Schaefer for the opportunities he provided for me to gain best research skills. I appreciate his encouragement, sense of humor, and very nice personality. I believe that I worked for one of the best bosses on the planet.

Table of Contents

List of Figures

List of Tables

Chapter 1

Introduction and Background Material

Once we decide to carry atoms and molecules to the computers, and deal with them without any experimental data, we should have extremely sophisticated quantum mechanical tools. The complexity of the atomic and molecular systems makes the mathematical equations hard to comprehend and cumbersome to implement. I think, the most dangerous quantum mechanical theory is that it relies on the one or two physical concepts of the molecular systems rather than comprising all the physics. For instance, any theory that does not include some kind of relativistic treatments is incomplete, because the special theory of relativity is valid even for a hydrogen atom. Any ab initio theory that does not have a proper treatment of electron correlation is insufficient for describing the molecular structure. Therefore, when we work on a molecular system not only we should employ highly correlated wave-functions but also all possible physical facts such as core-valence interactions and relativity should be taken into account.

Another very important aspect of the ab initio quantum chemical treatments is the choice and/or size of the basis set. A value obtained from calculations which is performed with a specific basis set cannot be a reliable prediction, even if a very sophisticated level of theory is used. Because the basis set used might not describe the system properly or it might not be large enough. For instance, if the basis set does not include diffuse functions for a loosely bound system or for an anion, any treatment with this basis set will not give the correct result even if we do a

complete basis set extrapolation with the cc-pV5Z and cc-pV6Z, or any other kind of extrapolation scheme. The same is true for the core-valence interactions. If the basis set does not have any function, which accounts for the core-core or core-valence interactions, we are not in the true path even if we do the most sophisticated quantum mechanical treatments. Therefore, we should employ multiple basis sets and monitor the changes as we increase the size of the basis set. Also, effects of the adding diffuse functions should be clearly understood. Then, functions which describe the core-valence interactions should be added. After a careful analysis of the effects of basis set expansion, adding diffuse functions, and core-valence functions, we may come to a definitive result.

Therefore, throughout this study, not only I employed highly level quantum mechanical methods which solve the problem of electron correlations but also I tried to incorporate other physics such as relativity and core-valence interactions. I believe that such treatment is necessary for a true description of the molecular systems, and for reliable theoretical predictions. Also, depending on the result of a single basis set has been strictly avoided.

1.1 A Brief History of the Coupled Cluster Theory

Coupled cluster theory was introduced into quantum chemistry in the late 1960s by Čížek and Paldus.[1–3] It has been become the most reliable and computationally affordable method for the approximate solution of the electronic Schrödinger equation. Quantum chemists were slow to accept coupled cluster theory, perhaps because the earliest people in the field used elegant but unfamiliar mathematical tools such as Feynman-like diagrams and second-quantization. Almost ten years after the essential contributions of Paldus and Čížek, Hurley presented a re-derivation of the coupled cluster doubles (CCD) equations[4] which were more familiar to quantum chemists.

In 1977, Monkhorst[5] reported a general coupled cluster response theory for calculating molecular properties. The computer implementations of the theory began to appear by the end of the 1970s. The Pople[6] and Bartlett[7] groups developed and tested spin-orbital CCD programs. In 1982, Purvis and Bartlett derived the coupled cluster singles and doubles (CCSD) equations and implemented them in a practical computer code.[8] Thereafter, the popularity of coupled cluster methods has increased, and tremendous efforts have been made in the production of highly efficient CCSD energy codes.[8–14]

I strongly suggest interested readers to look at a very nice review paper on coupled cluster theory, written by T. D. Crawford and H. F. Schaefer.[15]

1.2 Cluster Expansion of the Wavefunction

The Slater determinant for a system of four electrons moving in an arbitrary electrostatic field can be written as

$$\Phi_0 = \frac{1}{\sqrt{4!}} \begin{vmatrix} \phi_i(\mathbf{x}_1) & \phi_j(\mathbf{x}_1) & \phi_k(\mathbf{x}_1) & \phi_l(\mathbf{x}_1) \\ \phi_i(\mathbf{x}_2) & \phi_j(\mathbf{x}_2) & \phi_k(\mathbf{x}_2) & \phi_l(\mathbf{x}_2) \\ \phi_i(\mathbf{x}_3) & \phi_j(\mathbf{x}_3) & \phi_k(\mathbf{x}_3) & \phi_l(\mathbf{x}_3) \\ \phi_i(\mathbf{x}_4) & \phi_j(\mathbf{x}_4) & \phi_k(\mathbf{x}_4) & \phi_l(\mathbf{x}_4) \end{vmatrix}, \tag{1.1}$$

Expansion of this determinant produces a linear combination of products of the four functions, ϕ_i, ϕ_j, ϕ_k, and ϕ_l, with the electronic coordinates $\mathbf{x}_n$ distributed among them in all possible ways. The component functions ϕ_i can be chosen in a variety of ways. For instance, if the nuclear field were only a single carbon nucleus, the one-electron spatial functions could be constructed to represent the atomic $1s$, $2s$, and $2p$ orbitals. For a molecular system, the functions can be constructed as a linear combination of atomic orbitals (AOs) in which each one-electron function represents

a molecular orbital (MO) whose AO coefficients are determined via the Hartree-Fock self-consistent-field (SCF) procedure. Since permutation of any two rows in the determinant — which is equivalent to interchanging the coordinates of any two electrons — changes the sign of Φ_0, the antisymmetry principle is maintained. A convenient shorthand notation for this wavefunction consists of a Dirac-notation ket containing only the diagonal elements of the above matrix:

$$\Phi_0 = |\phi_i(\mathbf{x}_1)\phi_j(\mathbf{x}_2)\phi_k(\mathbf{x}_3)\phi_l(\mathbf{x}_4)\rangle, \tag{1.2}$$

We can improve this so-called independent-particle approximation such that the motions of the electrons are correlated. To do this, often the set of *occupied* orbitals is chosen from a larger set of one-electron functions. These "extra" functions are frequently referred to as *virtual* orbitals and arise as a byproduct of the SCF procedure. These functions will be donated as

- Orbitals of the **occupied** space have subscripts i, j, k, ...
- Orbitals within the **virtual** space have subscripts a, b, c, ...
- Arbitrary functions which may lie in **eitherspace** have subscripts p, q, r, ...

Within the space described by the full set of orbitals, any function of N variables may be written in terms of N-tuple products of the ϕ_p. For example, a function of two variables may be constructed by using all possible binary products of the set of one-electron functions, e.g.,

$$f(\mathbf{x}_1, \mathbf{x}_2) = \sum_{p>q} c_{pq}\phi_p(\mathbf{x}_1)\phi_q(\mathbf{x}_2), \tag{1.3}$$

Instead of correlating the motions of a specific pair of electrons, however, we may use a modified form of this expansion to correlate the motions of any two electrons within a selected pair of occupied orbitals, say functions i and j, using a two-particle

cluster function:

$$f_{ij}(\mathbf{x}_m, \mathbf{x}_n) = \sum_{a>b} t_{ij}^{ab} \phi_a(\mathbf{x}_m)\phi_b(\mathbf{x}_n), \tag{1.4}$$

The t_{ij}^{ab} are the cluster coefficients determined via the electronic Schrödinger equation. Inserting this into Φ_0 leads to the somewhat-improved electronic wavefunction:

$$\Psi = | \left[\phi_i(\mathbf{x}_1)\phi_j(\mathbf{x}_2) + f_{ij}(\mathbf{x}_1, \mathbf{x}_2)\right] \phi_k(\mathbf{x}_3)\phi_l(\mathbf{x}_4)\rangle, \tag{1.5}$$

Inclusion of the cluster function, f_{ij}, in the wavefunction produces a linear combination of Slater determinants involving replacement of occupied orbitals ϕ_i and ϕ_j by virtual orbitals ϕ_a and ϕ_b, such that:

$$\Psi = \Phi_0 + \sum_{a>b} t_{ij}^{ab} |\phi_a(\mathbf{x}_1)\phi_b(\mathbf{x}_2)\phi_k(\mathbf{x}_3)\phi_l(\mathbf{x}_4)\rangle. \tag{1.6}$$

In addition, the determinantal form of the individual terms in this expansion implies antisymmetrization of the cluster coefficients, such that $t_{ij}^{ab} = -t_{ji}^{ab} = -t_{ij}^{ba} = t_{ji}^{ba}$. Note the cluster function, $f_{ij}(\mathbf{x}_1, \mathbf{x}_2)$, correlates the motions of *any* pair of electrons placed in orbitals i and j. The Slater determinant produces a linear combination of orbital products, including terms such as:

$$\left[\phi_i(\mathbf{x}_1)\phi_j(\mathbf{x}_2) + f_{ij}(\mathbf{x}_1, \mathbf{x}_2)\right] \phi_k(\mathbf{x}_3)\phi_l(\mathbf{x}_4) \tag{1.7}$$

and

$$\left[\phi_i(\mathbf{x}_3)\phi_j(\mathbf{x}_4) + f_{ij}(\mathbf{x}_3, \mathbf{x}_4)\right] \phi_k(\mathbf{x}_1)\phi_l(\mathbf{x}_2), \tag{1.8}$$

which differ only in their distribution of electronic coordinates. Therefore, the cluster function correlates the motion of *every* pair of electrons found in orbitals ϕ_i and ϕ_j.

A more intelligent approach might be to correlate all possible pairwise combinations of orbitals in this four-electron system:

$$\begin{aligned} \Phi \;=\; & |\phi_i\phi_j\phi_k\phi_l\rangle + |f_{ij}\phi_k\phi_l\rangle - |f_{ik}\phi_j\phi_l\rangle + |f_{il}\phi_j\phi_k\rangle + |\phi_i f_{jk}\phi_l\rangle - \\ & |\phi_i f_{jl}\phi_k\rangle + |\phi_i\phi_j f_{kl}\rangle + |f_{ij}f_{kl}\rangle - |f_{ik}f_{jl}\rangle + |f_{il}f_{jk}\rangle, \end{aligned} \tag{1.9}$$

Note that there is no need to limit this approach to only orbital pairs. We could introduce three-orbital cluster functions and include these in our new wavefunction to give:

$$\begin{aligned}\Phi &= |\phi_i\phi_j\phi_k\phi_l\rangle + |f_{ij}\phi_k\phi_l\rangle - |f_{ik}\phi_j\phi_l\rangle + |f_{il}\phi_j\phi_k\rangle + |\phi_i f_{jk}\phi_l\rangle - \\ &\quad |\phi_i f_{jl}\phi_k\rangle + |\phi_i\phi_j f_{kl}\rangle + |f_{ij}f_{kl}\rangle - |f_{ik}f_{jl}\rangle + |f_{il}f_{jk}\rangle + \\ &\quad |f_{ijk}\phi_l\rangle - |f_{ijl}\phi_k\rangle + |f_{ikl}\phi_j\rangle + |\phi_i f_{jkl}\rangle. \end{aligned} \tag{1.10}$$

If one continues this process to include all cluster functions for up to N orbitals, we would obtain the exact wavefunction, Ψ, within the space spanned by the $\{\phi_p\}$. We might assume that clusters larger than pairs are less important to an adequate description of the system. This assumption supported by the fact that the electronic Hamiltonian contains operators describing pairwise electronic interactions at most. We could therefore write a four-electron wavefunction which includes all clusters of only one and two orbitals as:[15]

$$\begin{aligned}\Psi &= |\phi_i\phi_j\phi_k\phi_l\rangle + |f_i\phi_j\phi_k\phi_l\rangle + |\phi_i f_j\phi_k\phi_l\rangle + |\phi_i\phi_j f_k\phi_l\rangle + |\phi_i\phi_j\phi_k f_l\rangle + \\ &\quad |f_i f_j\phi_k\phi_l\rangle + |f_i\phi_j f_k\phi_l\rangle + |f_i\phi_j\phi_k f_l\rangle + |\phi_i f_j f_k\phi_l\rangle + |\phi_i f_j\phi_k f_l\rangle + \\ &\quad |\phi_i\phi_j f_k f_l\rangle + |f_i f_j f_k\phi_l\rangle + |f_i f_j\phi_k f_l\rangle + |f_i\phi_j f_k f_l\rangle + |\phi_i f_j f_k f_l\rangle + \\ &\quad |f_{ij}\phi_k\phi_l\rangle - |f_{ik}\phi_j\phi_l\rangle + |f_{il}\phi_j\phi_k\rangle + |\phi_i f_{jk}\phi_l\rangle - |\phi_i f_{jl}\phi_k\rangle + \\ &\quad |\phi_i\phi_j f_{kl}\rangle + |f_{ij}f_{kl}\rangle - |f_{ik}f_{jl}\rangle + |f_{il}f_{jk}\rangle + |f_i f_j f_k f_l\rangle + \\ &\quad |f_{ij}f_k\phi_l\rangle + |f_{ij}\phi_k f_l\rangle + |f_{ij}f_k f_l\rangle - |f_{ik}f_j\phi_l\rangle - |f_{ik}\phi_j f_l\rangle - |f_{ik}f_j f_l\rangle + \\ &\quad |f_{il}f_j\phi_l\rangle + |f_{il}\phi_j f_l\rangle + |f_{il}f_j f_l\rangle + |f_i f_{jk}\phi_l\rangle + |\phi_i f_{jk}f_l\rangle + |f_i f_{jk}f_l\rangle - \\ &\quad |f_i f_{jl}\phi_k\rangle - |\phi_i f_{jl}f_k\rangle - |f_i f_{jl}f_k\rangle + |f_i\phi_j f_{kl}\rangle + |\phi_i f_j f_{kl}\rangle + |f_i f_j f_{kl}\rangle. \end{aligned} \tag{1.11}$$

1.3 The Exponential Ansatz and Formal Coupled-Cluster Theory

The complicated notation of Eq. [1.11] can be drastically reduced by defining a *creation* and an *annihilation* operator.[15] The *creation* operator accts on a Slater

determinant as;

$$a_p^\dagger|\phi_q \dots \phi_s\rangle = |\phi_p\phi_q \dots \phi_s\rangle, \tag{1.12}$$

And similarly, the *annihilation* operator;

$$a_p|\phi_p\phi_q \dots \phi_s\rangle = |\phi_q \dots \phi_s\rangle, \tag{1.13}$$

A given Slater determinant may be written as a chain of creation operators acting on the true vacuum (a state containing no electrons or orbitals):

$$a_p^\dagger a_q^\dagger \dots a_s^\dagger|\ \rangle = |\phi_p\phi_q \dots \phi_s\rangle. \tag{1.14}$$

Using these second-quantized operators, we may define the single-orbital cluster operator:

$$\hat{t}_i \equiv \sum_a t_i^a a_a^\dagger a_i\,, \tag{1.15}$$

Similarly, a two-orbital cluster operator which substitutes orbital ϕ_a for ϕ_i and ϕ_b for ϕ_j is given as:

$$\hat{t}_{ij} \equiv \sum_{a>b} t_{ij}^{ab} a_a^\dagger a_b^\dagger a_j a_i\,, \tag{1.16}$$

Equations [1.15] and [1.16] may be used to rewrite the long one- and two-orbital cluster wavefunction in Eq. [1.11] above as:

$$\begin{aligned}\Psi \;=\; & \left(1 + \sum_i \hat{t}_i + \frac{1}{2}\sum_{ij}\hat{t}_i\hat{t}_j + \frac{1}{6}\sum_{ijk}\hat{t}_i\hat{t}_j\hat{t}_k + \frac{1}{2}\sum_{ij}\hat{t}_{ij} + \right. \\ & \left. \frac{1}{8}\sum_{ijkl}\hat{t}_{ij}\hat{t}_{kl} + \frac{1}{24}\sum_{ijkl}\hat{t}_i\hat{t}_j\hat{t}_k\hat{t}_l + \frac{1}{2}\sum_{ijk}\hat{t}_{ij}\hat{t}_k + \frac{1}{4}\sum_{ijkl}\hat{t}_{ij}\hat{t}_k\hat{t}_l\right)\Phi_0. \end{aligned} \tag{1.17}$$

We may simplify this expression even further by defining the total one- and two-orbital cluster operators:

$$\hat{T}_1 \equiv \sum_i \hat{t}_i = \sum_{ia} t_i^a a_a^\dagger a_i\,, \tag{1.18}$$

and

$$\hat{T}_2 \equiv \frac{1}{2}\sum_{ij}\hat{t}_{ij} = \frac{1}{4}\sum_{ijab} t_{ij}^{ab} a_a^\dagger a_b^\dagger a_j a_i\,, \tag{1.19}$$

More generally, an n-orbital cluster operator may be defined as:

$$\hat{T}_n = \left(\frac{1}{n!}\right)^2 \sum_{ij\ldots ab\ldots}^{n} t_{ij\ldots}^{ab\ldots} a_a^\dagger a_b^\dagger \ldots a_j a_i \,. \tag{1.20}$$

This reduces the wavefunction expression to:

$$\Psi = \left(1 + \hat{T}_1 + \frac{1}{2!}\hat{T}_1^2 + \frac{1}{3!}\hat{T}_1^3 + \hat{T}_2 + \frac{1}{2!}\hat{T}_2^2 + \frac{1}{4!}\hat{T}_1^4 + \hat{T}_2\hat{T}_1 + \frac{1}{2!}\hat{T}_2\hat{T}_1^2\right)\Phi_0. \tag{1.21}$$

All of the terms from the above equation match those from the power series expansion of an exponential function! Thus, the general expression for Eq. [1.21] is:

$$\Psi = e^{\hat{T}_1 + \hat{T}_2}\Phi_0 \equiv e^{\hat{T}}\Phi_0, \tag{1.22}$$

The exponentiated cluster operator (ansatz), $e^{\hat{T}}$, when applied to the reference determinant, produces a new wavefunction containing cluster functions, each of which correlates the motion of electrons within specific orbitals. If $\hat{T}$ includes contributions from all possible orbital groupings for the N-electron system (that is, $\hat{T}_1, \hat{T}_2, \ldots, \hat{T}_N$), then the exact wavefunction within the given one-electron basis may be obtained from the reference function. Truncation of the cluster operator at specific substitution/excitation levels leads to a hierarchy of coupled cluster techniques (e.g., $\hat{T} \equiv \hat{T}_1 + \hat{T}_2 \rightarrow$ CCSD; $\hat{T} \equiv \hat{T}_1 + \hat{T}_2 + \hat{T}_3 \rightarrow$ CCSDT, etc.

We do not yet have a recipe for determining the so-called "cluster amplitudes" (t_i^a, t_{ij}^{ab}, etc.) which parameterize the power series expansion implicit in Eq. [1.22]. Starting point for this analysis is the electronic Schrödinger equation:

$$\hat{H}|\Psi\rangle = E|\Psi\rangle, \tag{1.23}$$

The coupled cluster wavefunction, $\Psi_{\mathrm{CC}}^{\hat{T}}\Phi_0$, is used to approximate the exact solution, Ψ:

$$\hat{H}e^{\hat{T}}|\Phi_0\rangle = Ee^{\hat{T}}|\Phi_0\rangle. \tag{1.24}$$

Using a "projective" technique, one may left-multiply this equation by the reference, Φ_0, to obtain an expression for the energy:

$$\langle\Phi_0|\hat{H}e^{\hat{T}}|\Phi_0\rangle = E\langle\Phi_0|e^{\hat{T}}|\Phi_0\rangle = E, \tag{1.25}$$

Additionally, one may obtain expressions for the cluster amplitudes by left-projecting the Schrödinger equation by the excited determinants produced by the action of the cluster operator, $\hat{T}$, on the reference:

$$\langle\Phi^{ab\ldots}_{ij\ldots}|\hat{H}e^{\hat{T}}|\Phi_0\rangle = E\langle\Phi^{ab\ldots}_{ij\ldots}|e^{\hat{T}}|\Phi_0\rangle, \tag{1.26}$$

Projection by the determinant $|\Phi^{ab}_{ij}\rangle$, for example, will produce an equation for the specific amplitude t^{ab}_{ij} (coupled to other amplitudes).

Recall that the exponentiated operator may be expanded in a power series as:

$$e^{\hat{T}} = 1 + \hat{T} + \frac{\hat{T}^2}{2!} + \frac{\hat{T}^3}{3!} + \ldots. \tag{1.27}$$

Inserting this into the energy expression Eq. [1.25] we obtain:

$$\langle\Phi_0|\hat{H}(1 + \hat{T} + \frac{\hat{T}^2}{2!} + \frac{\hat{T}^3}{3!} + \ldots)|\Phi_0\rangle = E, \tag{1.28}$$

which becomes, after distributing terms:

$$\langle\Phi_0|\hat{H}|\Phi_0\rangle + \langle\Phi_0|\hat{H}\hat{T}|\Phi_0\rangle + \langle\Phi_0|\hat{H}\frac{\hat{T}^2}{2!}|\Phi_0\rangle + \langle\Phi_0|\hat{H}\frac{\hat{T}^3}{3!}|\Phi_0\rangle + \ldots = E. \tag{1.29}$$

Note that $\hat{H}$ is at most a two-particle operator and that $\hat{T}$ is at least a one-particle excitation operator. Then, assuming that the reference wavefunction is a single determinant constructed from a set of one-electron functions, Slater's rules state that matrix elements of the Hamiltonian between determinants that differ by more than two orbitals are zero. Thus, the fourth term on the left-hand side of Eq (1.29) contains, at the least, threefold excitations, and, as a result, that matrix element (and *all* higher-order elements) necessarily vanish. The energy equation then simplifies to

$$\langle\Phi_0|\hat{H}|\Phi_0\rangle + \langle\Phi_0|\hat{H}\hat{T}|\Phi_0\rangle + \langle\Phi_0|\hat{H}\frac{\hat{T}^2}{2!}|\Phi_0\rangle = E. \tag{1.30}$$

This truncation depends *only* on the form of $\hat{H}$ and not on that of $\hat{T}$ or on the number of electrons.

1.4 Relativity in Chemistry

In the vicinity of nucleus the electrons acquire high velocities, a substantial fraction of speed of light, and the mass increases;

$$M = M_0(\frac{(1-v^2)}{c^2})^{-1/2} \tag{1.31}$$

$$R_{bohr} \ \alpha \ \frac{1}{M} \tag{1.32}$$

The outer s and (to a lesser extent) also the outer p electrons are close to the nucleus for a certain fraction of their "revolution time". In a stationary picture, one would say that their orbitals have "inner tails" or that they are "core-penetrating orbitals". Therefore the outer s and p electrons experience direct relativistic effect as well as indirect effects.[16] The shells with higher angular momentum, d and f, are not core-penetrating due to the their large centrifugal barrier. Therefore, they only experience indirect relativistic effects which is expanding or destabilization of the d and f -like orbitals due to the fact that inner electrons shield the nuclei more by shrinking as a result of the direct relativistic effects.[16,17] Therefore, by affecting the stability and shape of the atomic —and in turn molecular orbitals — special theory of relativity is quite important for any kind of ab initio treatment on the atomic and molecular systems. Especially, the effects are very prominent for those molecular processes which are directly related with the energy and/or shape of the molecular orbitals, such as ionization and excitation energies [see chapter 3 and 4].

One of the first attempts as a relativistic quantum mechanical wave equation was the Klein-Gordon equation. Although it is theoretically sound from the perspective that it is consistent with both classical quantum mechanics and the special theory

of relativity, it has several features which keep it from being a very powerful tool in relativistic quantum mechanics. Dirac later developed his own relativistic wave equation which did not have some of the shortcomings of the Klein-Gordon equation and that some of the supposed "errors" that the KG equation gave rise to were actually illustrating some new physics. The Dirac equation is only rigorous for a one particle system, but has been used as a starting point for a number of approximate many electron methods.

1.4.1 Klein-Gordon Equation

The special-relativistic expression for the kinetic energy may be used to form the classical free particle Hamiltonian

$$\mathrm{E} = \mathrm{c}(\mathrm{m}^2\mathrm{c}^2 + \mathbf{p}^2)^{1/2}. \tag{1.33}$$

The analogous quantum mechanical expression may be constructed by replacing the classical momentum, $\mathbf{p}$, with its quantum mechanical operator, $\hat{\mathbf{p}}$ which yields the free particle wave equation

$$(i\hbar\frac{\partial}{\partial t})\psi = [c((m^2c^2 + \hat{\mathbf{p}}^2)^{1/2}]\psi \tag{1.34}$$

This equation, however, does not satisfy some of the conditions required by special relativity. The wave equation is not invariant to a Lorentz transform, and the square root term introduces ambiguity. The Klein-Gordon equation rectifies both of these problems simply by taking the square of the original energy expression and extending the result to a quantum mechanical wave equation:

$$\mathrm{E}^2\psi = (\mathrm{i}\hbar\frac{\partial}{\partial \mathrm{t}})^2\psi = (\mathrm{m}^2\mathrm{c}^4 + \hat{\mathbf{p}}^2\mathrm{c}^2)\psi \tag{1.35}$$

The resulting wave equation is Lorentz invariant and well defined, but suffers from other problems. Negative energy solutions to this equation are possible, which do

not have a readily obvious explanation, and the probability density, $\psi^*\psi$, fluctuates with time as does its integral over all space. The problems of the Klein-Gordon equation may make it a poor equation for an electron, but those weaknesses helped to point Dirac in the right direction and to develop a single particle equation which successfully surmounted all these problems.

1.4.2 Dirac's Free Particle Equation

In order for a wave equation to satisfy the special relativistic requirement of lorentz invariance, derivatives in space and time must all appear in the same order. The K-G equation illustrates that an expression which satisfies this condition but is non-linear in the space and time derivatives gives rise to anomalous results. Dirac set out to find an equation which was first order in space and time derivatives. The result of his efforts, the Dirac equation, is difficult to motivate, impossible to prove, and far more complicated that the non-relativistic analog. However, Dirac's wave equation for a single particle satisfies all the requirements of special relativity and quantum mechanics, and is able to predict the properties of one particle systems with remarkable accuracy.

Dirac's equation for an electron in field-free space is given by[18–20]

$$(\hat{\mathrm{p}}_0 - \alpha \cdot \hat{\mathbf{p}} - \beta \mathrm{mc})\psi = 0 \tag{1.36}$$

where

$$\hat{\mathrm{p}}_0 = i\frac{\hbar}{c}\frac{\partial}{\partial t} \tag{1.37}$$

and $\hat{\mathrm{p}}$ is simply the three component momentum. In order to determine the nature of the three components of α and β, it is useful to compare the modified equation

$$(\hat{\mathrm{p}}_0 - \alpha \cdot \hat{\mathbf{p}} - \beta \mathrm{mc})^*(\hat{\mathrm{p}}_0 - \alpha \cdot \hat{\mathbf{p}} - \beta \mathrm{mc})\psi = 0 \tag{1.38}$$

to the Klein-Gordon equation. Equations (1.35) and (1.38) are equivalent if we enforce the conditions

$$[\alpha_{\rm i}, \alpha_{\rm j}]_+ = \alpha_{\rm i}\alpha_{\rm j} + \alpha_{\rm j}\alpha_{\rm i} = \partial_{\rm ij} \tag{1.39}$$

where α_i represents β for i=0 and α_x,α_y, and α_z for i= 1-3, respectively. In order for this set of four objects to fulfill these anti-commutation relations, each α must be four-dimensional.

One set of matrices which obey similar anti-commutation relations are the Pauli spin matrices: $\sigma_{x,y,z}$. These are 2×2 matrices, however, and there are only three of them, so they are not useful in their usual form. If the α_i's are defined as[19]

$$\alpha_0 = \begin{pmatrix} I_{2\times 2} & 0 \\ 0 & -I_{2\times 2} \end{pmatrix}, \tag{1.40}$$

$$\alpha_i = \begin{pmatrix} 0 & \sigma_i \\ \sigma_i & 0 \end{pmatrix} \quad (i = 1-3) \tag{1.41}$$

Where $I_{2\times 2}$ is a two by two identity matrix and σ_i are the Pauli spin matrices. Though these four by four matrices do not represent the only set of matrices which satisfy the anti-commutation relations, they may only differ by a similarity transform from this set.

Because the Dirac equation contains operators represented by four dimensional matrices, the solutions { ψ } must be represented by a four component vector

$$\psi = \begin{pmatrix} \psi_1 \\ \psi_2 \\ \psi_3 \\ \psi_4 \end{pmatrix} \tag{1.42}$$

The interpretation of the components of this four-vector is not readily evident. Expressing the Dirac equation in full matrix form provides some elucidation

$$\begin{pmatrix} (\hat{p}_0 - mc) & 0 & -\hat{p}_z & -(\hat{p}_x - i\hat{p}_y) \\ & (\hat{p}_0 - mc) & -(\hat{p}_x + i\hat{p}_y) & \hat{p}_z \\ -\hat{p}_z & -(\hat{p}_x - ip_y) & (\hat{p}_0 + mc) & 0 \\ -(\hat{p}_x + i\hat{p}_y) & \hat{p}_z & 0 & (\hat{p}_0 + mc) \end{pmatrix} \begin{pmatrix} \psi_1 \\ \psi_2 \\ \psi_3 \\ \psi_4 \end{pmatrix} = 0 \quad (1.43)$$

The non-relativistic electronic wave-function has two components corresponding to the α and β components of spin angular momentum. In the non-relativistic limit, p_0 approaches mc, and the terms which couple ψ_1 with ψ_2 drop out. What remains are four eigenvector equations, with approximate eigenvalues of $+m_0c^2$ for ψ_1 and ψ_2, and $-m_0c^2$ for ψ_3 and ψ_4. ψ_1 and ψ_2, then, may be interpreted as the α and β components of positive energy, electron-like solutions, but the solutions which are dominated by ψ_3 and ψ_4 do not possess a readily evident interpretation. Dirac deduced that these solutions correspond to a particle with the same mass as the electron but an opposite charge, and dubbed these particles positrons. Far from being figments of a theorist's imagination, only three years after Dirac First suggested them in 1930, positrons were observed experimentally.

1.5 The Nature of Four-Component Wave-function

The four-component nature of the Dirac eigenfucntions gives rise to many interesting differences when compared to the non relativistic solutions. The contributions from the first two components of the wave-function tend to be much larger than the contributions from the final two components for electron-like solutions. For this reason the upper two-component spinor is known as the large component of the wave-function, while the lower spinor is known as the small component. By orthogonality the opposite is true for the positron-like solutions. Since the angular and spin portions of

the wave-functions are normalized, the magnitude of the large and small contributions is determined entirely by the radial functions, $f(r)$ and $g(r)$. The ratio of their contributions may be expressed as

$$\frac{g(r)}{f(r)} \simeq \frac{Z\alpha}{2n} \tag{1.44}$$

In general, the ratio will probably be larger than this approximate value in regions close to the nucleus, where the contribution of $g(r)$ is the greatest. The contribution of the small component, then, may be significant for sufficiently heavy nuclei. Though hydrogenic ions with very heavy nuclei may not be of great practical interest, this relationship will have implications for heavy many-electron atoms where the innermost electrons experience a large portion of the full nuclear charge and hence are closely related to the analogous hydrogenic systems.

One interesting consequence of the four component wave-function may be observed in the associated probability density. Scalar wave-functions, ψ, which possess radial and angular nodes will have the same radial and angular nodes in their probability density, $\psi^*\psi$ The four-component wave-function, however, gives rise to a probability density which sis the sum of the probability densities associated with the large and small wave-functions, ϕ and χ, respectively. The radial component of ϕ and χ posses different numbers of nodes and, in general, none of these nodes will coincide. Similarly, the angular contributions of ϕ differ from those of χ by a single unit of angular momentum. Therefore, although $\phi^*\phi$ and $\chi^*\chi$ may possess either radial of angular nodes individually, their sum, their sum will be node-less.

The energy eigenvalues of the hydrogenic solutions to the Schrödinger equation are only dependent upon n, the principal quantum number, while the Dirac hydrogenic eigenvalues are dependent on both n and j. The spectral dependence on j is upheld by experimental observation, however the degeneracy of eigenvalues for solutions with the same j values but differing l values is not observed in nature.

The breaking of this degeneracy is known as the Lamb shift and its origin has been attributed to the difference in the interaction of the different j eigenfunctions with the vacuum fluctuations predicted by quantum electrodynamics. The magnitude of the Lamb shift is much smaller than the splitting introduced by spin orbit coupling and is largest for the $n = 2$, $j = 1/2$ shells of the hydrogenic atom. In this case, the splitting introduced by the Lamb shift is approximately 10% of the magnitude of the energy separation of the $p_{1/2}$ and $p_{3/2}$ eigenfunctions.[21] It should not be too surprising that the predictions of the Dirac equation cannot entirely reproduce experimental observation, since it has its roots in special relativity. In order for any physical theory to definitively represent reality, it must at least be consistent with the general theory of relativity.

1.6 Dirac Fock Method

The Dirac-Coulomb Hamiltonian is one of the most widely used special-relativistic, many-electron Hamiltonians. This Hamiltonian may be utilized in conjunction with a Hartree-Fock-like wave-function in what is known as the Dirac-Hartree-Fock (DHF) method.[19,21,22] The DHF method has a special status in quantum chemistry as it often us utilized to benchmark relativistic effects in the absence of electron correlation. Such benchmarks can provide a gauge of the accuracy of more approximate methods which attempt to include relativistic effects as a perturbation of the non-relativistic Hartree-Fock case as well as methods which employ transformed, simplified versions of the Dirac-Coulomb Hamiltonian.

The Dirac equation has been shown to successfully treat the interactions of electrons with nuclei in a special-relativistic manner, and so represents a good starting point for a special-relativistic many-electron Hamiltonian. What is needed next is a description of the electron-electron interaction, and an associated quantum mechan-

ical operator, $\hat{g}_{ij}$. If the electron-electron interaction is not altered significantly by the introduction of special relativity, then the standard, non-relativistic coulomb operator, $\hat{g}_{ij} = \frac{1}{r_{ij}}$, might not be a bad guess. With the coulomb interaction, the Hamiltonian for an n electron system would be given by

$$\begin{aligned} \hat{H} &= \sum_{i=1}^{n} \hat{h}_D^i + \sum_{i>j}^{n} \frac{1}{r_{ij}} \\ &= \sum_{i=1}^{n} (\phi(\mathbf{r_i}) + c\hat{\alpha}^i \cdot \hat{p}^i + mc^2) + \sum_{i>j}^{n} \frac{1}{r_{ij}} \end{aligned} \tag{1.45}$$

This is known as the Dirac-Coulomb Hamiltonian, $\hat{H}_{DC}$. The associated wave equation, $\hat{H}_{DC}\Psi = E\Psi$, is not Lorentz invariant, and so $\hat{H}_{DC}$ does not represent a proper special relativistic Hamiltonian. In order to obtain a two-electron interaction term that is consistent with special relativity, it is necessary to turn to Quantum Electrodynamics. In order to cast the QED electron-electron interaction term into a reasonable form, it is necessary to expand it in perturbative series in orders of the fine structure constant, α. Retaining only the terms which contribute up to order α^2, gives the coulomb operator plus the Breit interaction term[19,20]

$$\hat{g}_{ij}^B = \frac{-1}{r_{ij}} \left(\alpha_i \cdot \alpha_j + \frac{(\alpha_i \cdot r_{ij})(\alpha_j \cdot r_{ij})}{r_{ij}^2} \right). \tag{1.46}$$

In practice, however, the full Breit magnetic interaction term is often cumbersome to implement, and so an approximation of the Breit opperator known as the Gaunt operator, may be used

$$\hat{g}_{ij}^G = \frac{-\alpha_i \cdot \alpha_j}{r_{ij}}. \tag{1.47}$$

The Gaunt operator is not gauge invariant, but it avoids having to solve integrals over operators more complicated than $\frac{1}{r_{ij}}$, and includes the largest contributions of the Breit interaction.

More rigorous forms of the molecular Hamiltonian have been suggested, but they are, at best, only approximately Lorentz covariant to some order in α. Because

the two-electron magnetic interaction terms are typically small, the contributions behind second order in α are typically chemically unimportant. Because of this the more rigorous Hamiltonians, which typically involve more complicated operators than even the Breit interaction, have received far less attention from quantum chemical investigators. The Dirac-Coulomb, Dirac-Coulomb-Gaunt, and Dirac-Coulomb-Breit Hamiltonians have become the most widely accepted four-component special relativistic molecular Hamiltonians.

1.6.1 Atomic Solutions

Atomic eigenfunctions of the D-C Hamiltonian may not be achieved analytically as were the hydrogenic solutions of the single particle Dirac equation. Instead, it is necessary, as it was in the non-relativistic theory, to appeal to approximate models such as the Dirac-Hartree-Fock (DHF) method. In a manner analogous to Hartree-Fock theory, DHF begins with the assumption that an n-electron atomic wavefunciton, Ψ, can be represented by an antisymmetrized product of n single particle functions, $\{$ ϕ_i $\}$. In contrast to the HF method and in accordance with the 4-component nature of the single particle operators, $\hat{h}_D^i$, the single particle functions ϕ_i are 4-component spinors. If we make the approximation that each electron experiences a central potential only, then the single particle functions may be separated into radial, angular, and spin parts analogous to the hydrogenic eigenfunctions. Anticipating the existence of electronic and positronic solutions, we may propose two separate forms for ϕ_i, analogous to the hydrogenic solutions **??**

$$\phi_i^{j,m_j}(+) = \frac{1}{r}\begin{pmatrix} p_i(r)\chi_i^{(+)} \\ iq_i(r)\chi_i^{(-)} \end{pmatrix} \qquad \text{and} \tag{1.48}$$

$$\phi_i^{j,m_j}(-) = \frac{1}{r}\begin{pmatrix} -p_i(r)\chi_i^{(-)} \\ iq_i(r)\chi_i^{(+)} \end{pmatrix} \tag{1.49}$$

The form of the radial functions has, again, been chosen such that the resultant wave equations and electronic energy expression are simplified. The total wavefunction formed by these one particle functions may be expressed as

$$\begin{aligned}\Psi &= \mathcal{A}\left(\prod_{i=1}^{n}\phi_i(r_i)\right) \\ &= \frac{1}{\sqrt{n!}}\begin{vmatrix} \phi_1(\mathrm{r}_1) & \phi_2(\mathrm{r}_1) & \cdots & \phi_n(\mathrm{r}_1) \\ \phi_1(\mathrm{r}_2) & \phi_2(\mathrm{r}_2) & \cdots & \phi_n(\mathrm{r}_2) \\ \vdots & \vdots & & \vdots \\ \phi_1(\mathrm{r}_\mathrm{n}) & \phi_2(\mathrm{r}_\mathrm{n}) & \cdots & \phi_n(\mathrm{r}_\mathrm{n}) \end{vmatrix}\end{aligned} \tag{1.50}$$

where $\mathcal{A}$ is the antisymetrizer operator. If this form of the atomic wavefunction is assumed, and the Dirac-Coulomb Hamiltonian is utilized, then the electronic energy is given by

$$\begin{aligned}E &= \langle\Psi|\hat{H}_{DC}|\Psi\rangle \\ &= \sum_{i}^{n}\phi_i\hat{h}_d\phi_i + \frac{1}{2}\sum_{i,j}^{n}\left(\phi_i\phi_j\frac{1}{r_{12}}\phi_i\phi_j - \phi_i\phi_j\frac{1}{r_{12}}\phi_j\phi_i\right) \\ &= \sum_{i}^{n} i\hat{h}_d i + \frac{1}{2}\sum_{i,j}^{n}\langle ij||ij\rangle.\end{aligned} \tag{1.51}$$

1.7 Breit-Pauli Hamiltonian and Scalar Relativistic Corrections

The similarity transformation, known as "Foldy-Wouthuysen transformation"

$$U = \frac{\beta H + |E|}{\sqrt{2|E|(|E| + m_0)}} \tag{1.52}$$

transforms the four-component Dirac wavefunction into two sets of two-component wavefunctions.[19,21] The transformation of four component wavefunction ψ with U yields

$$F = U\psi \tag{1.53}$$

Hence any operator O in the original four-component representation becomes O_F, given by

$$O_F = U^\dagger O U \tag{1.54}$$

where $U^\dagger$ is the hermetian adjoint of U. The hamiltonian and energy projection operators are transformed as

$$\lambda_F = U^\dagger \lambda U H_F = H a_U^\dagger H U \tag{1.55}$$

The transformation in a rigorous form can only be achieved only for a free-electron Hamiltonian, which produces

$$F = \begin{pmatrix} 1 \\ 0 \\ 0 \\ 0 \end{pmatrix} \frac{1}{2\pi^{2/3}} e^{ip_z z} \rightarrow m_s = \frac{1}{2} \tag{1.56}$$

and

$$F = \begin{pmatrix} 0 \\ 1 \\ 0 \\ 0 \end{pmatrix} \frac{1}{2\pi^{2/3}} e^{ip_z z} \rightarrow m_s = -\frac{1}{2} \tag{1.57}$$

for positive energy solution $E = E_+$. For the negative energy states

$$F = \begin{pmatrix} 0 \\ 0 \\ 1 \\ 0 \end{pmatrix} \frac{1}{2\pi^{2/3}} e^{ip_z z} \rightarrow m_s = \frac{1}{2} \tag{1.58}$$

and

$$F = \begin{pmatrix} 0 \\ 0 \\ 0 \\ 1 \end{pmatrix} \frac{1}{2\pi^{2/3}} e^{ip_z z} \rightarrow m_s = -\frac{1}{2} \tag{1.59}$$

These forms suggest the introduction of the following operators

$$\frac{1}{2}(1+\beta) \qquad \frac{1}{2}(1-\beta) \qquad F = \begin{pmatrix} f_1 \\ f_2 \\ f_3 \\ f_4 \end{pmatrix} \tag{1.60}$$

So the positive and negative solutions can be represented by the following two-component wave-function

$$\frac{1}{2}(1+\beta)F = \begin{pmatrix} f_1 \\ f_2 \\ 0 \\ 0 \end{pmatrix} = F_+ \tag{1.61}$$

$$\frac{1}{2}(1-\beta)F = \begin{pmatrix} 0 \\ 0 \\ f_3 \\ f_4 \end{pmatrix} = F_- \tag{1.62}$$

For an electron in a external field, as in a hydrogen atom, this separation is not possible, since the large and small components are coupled, as there is mixing between positive and negative energy states. Therefore, Pauli approximation seeks a simplified picture in which the small components, which make smaller contributions to the positive energy states, are neglected. Subsequently, one arrives at operator equations involving only the two large components. The two-components picture also unfolds the spin interpretation in that the first component corresponds to spin-up of the electron; the second component, spin-down.

The inclusion of the "somewhat" correct two-electron relativistic interaction (Breit Interaction Term)[19,21]

$$\hat{g}_{ij}^{B} = \frac{-1}{r_{ij}} \left(\alpha_i \cdot \alpha_j + \frac{(\alpha_i \cdot r_{ij})((\alpha_j \cdot r_{ij})}{r_{ij}^2} \right). \tag{1.63}$$

to the Pauli view produces "Breit-Pauli Equations". The much used simplified perturbational Breit-Pauli Hamiltonian for a multielectron atomic system includes the terms[19]

$$H_0 = \sum_i \left(\frac{1}{2m_0} p_i^2 - \frac{Ze^2}{r_i} \right) + \sum_{i<j} \frac{e^2}{r_{ij}} \tag{1.64}$$

$$H_1 = -\frac{1}{8m_0^3 c^2} \sum_i p_i^4 \tag{1.65}$$

$$H_2 = -\frac{e^2}{m_0^2 c^2} \sum_{i<j} \left[r_{ij}^{-1} p_i . p_j + \frac{(r_{ij}.p_i)(r_{ij}.p_j)}{r_{ij}^3} \right] \tag{1.66}$$

$$H_3 = \frac{\mu}{m_0 c} \sum_i s_i . \left(E_i \times p_i + \sum_{i<j} \frac{2e}{r_{ij}^3} [r_{ij} \times p_j] \right) \tag{1.67}$$

$$H_4 = \frac{ie\hbar}{(2m_0 c)^2} \sum_i (p_i . E_i) \tag{1.68}$$

$$H_5 = 4\mu^2 \left(\sum_{i<j} \left[\frac{s_i . s_j}{r_{ij}^3} - 3\frac{(s_i . r_{ij})(s_j . r_{ij})}{r_{ij}^5} - \frac{8\pi}{3} (s_i . s_j) \delta^3 (r_{ij}) \right] \right) \tag{1.69}$$

in which

$$\mu = \frac{e\hbar}{2m_0 c} \qquad E_i = \nabla_i V \qquad V = -Ze^2 \sum_i \frac{1}{r_i} + e^2 \sum_{i<j} \frac{1}{r_{ij}} \tag{1.70}$$

These terms in the Breit-Pauli Hamiltonian can be interpreted as

- H_0 is the non-relativistic hamiltonian
- H_1 is the mass-velocity term attributed to relativistic correction arising from the variation of the mass of the electron with its speed. It is a purely scalar term, and does not depend on the spin of the electrons.
- H_2 is the relativistic retardation due to the electron magnetic field generated by an electron.
- H_3 is the spin-orbit coupling term. This corresponds to the interaction between the spin magnetic moment and the orbital magnetic moment of the electron.

- H_4, the Darwin correction, is the relativistic correction characteristic of Dirac's theory and is attributed to the electron's "Zitterbewegung". It arises from the smearing of the charge of the electron due to its relativistic motion.

- H_5 arises from the interaction of the spin magnetic moments of two electrons, and constitutes a dipole-dipole interaction between the two spin magnetic moments, and a Fermi-contact-type interaction.

For molecular systems, the Breit-Pauli Hamiltonian is often written as the sum of four terms[19,22]

$$H_{BP} = H_0 + H_D + H_{MV} + H_{SO} \tag{1.71}$$

in which

$$H_D = \frac{\alpha^2}{8}(\nabla^2 V) \tag{1.72}$$

$$H_{MV} = -\frac{\alpha^2}{8}\sum_i p_i^4 \tag{1.73}$$

$$H_{SO} = \frac{\alpha^2}{2}\left[\sum_i \frac{Z}{r_i^3}(L_i.S_i) + \sum_{i,j}\frac{1}{r_{ij}^3}(r_{ij}\times P_i).(S_i + 2S_j)\right] \tag{1.74}$$

The H_{MV} and H_D are the major contributions to the total energy of the system. The *scalar relativistic corrections* refer to the calculations of these two terms, mass-velocity and Darwin terms, neglecting spin-orbit term which give rises to splitting in the potential energy surfaces. The Darwin term, is always positive, corrects the Coulomb attraction and the mass-velocity term, which is always negative, corrects the kinetic energy of the system. In this study, these two terms (scalar relativistic corrections) are evaluated using a first-order perturbation theory, suggested by R. D. Cowan and D. C. Griffin[23,24]

It has been shown that this perturbational treatment of the relativity gives very sufficient results, comparing to the calculation based on Drac-Hartree-Fock (DHF) and effective core potentials (ecp). In 1983, R. L. Martin[24] reported calculations

on Ag and AgH, and stated in the abstract of his paper that "The Cowan-Griffin relativistic operator, which retains only the mass-velocity and one-electron Darwin term of the Breit-Pauli Hamiltonian, has been shown to provide a remarkably good approximation to the more sophisticated Dirac-Hartree-Fock (DHF) approach for many atomic systems". In the same year, He also studied[25] Cu_2, and reported that the first-order perturbational approach is quite successful in the predictions of the excitation energies of Cu_2, as well as for first transition series atoms. In 1991, Dyall et. al.[26] studied the group IV tetrahydrides CH_4, SiH_4, GeH_4, SnH_4, and PbH_4. They employed DHF, ECP, and first order perturbational treatment where only mass-velocity and Darwin terms are calculated. They found that the first-order perturbational treatment show agreement to within 0.002 Å on the geometries, comparing to the DHF results. However, although this relativistic treatment is quite sufficient for the third and fourth row atoms, the large spin-orbit splitting for the atoms at the lower part of the periodic table makes the method insufficient for those molecules that contain very heavy atoms.

Chapter 2

The $\tilde{X}\ ^2\Pi$ and $\tilde{A}\ ^2\Sigma^+$ electronic states of the HCSi radical: Characterization of the Renner-Teller effect in the ground state *

*Levent Sari, Jason M. Gonzales, Yukio Yamaguchi, and Henry F. Schaefer III. Journal of Chemical Physics, 114, 4472 (2001). Reprinted by permission of the American Institue of Physics.

2.1 Abstract

The electronic structures of the ground and lowest lying excited state of the silicon methylidyne radical (HCSi) have been investigated at the SCF, CISD, CCSD, and CCSD(T) levels of theory with a wide range of basis sets. The total energies and physical properties including equilibrium geometries, dipole moments, harmonic vibrational frequencies, and Renner-Teller splitting are reported. At our highest level of theory [CCSD(T)/cc-pVQZ], the ground electronic state ($\tilde{X}\ ^2\Pi$) has a linear geometry with r_e(CH)=1.0781 Å and r_e(CSi)=1.6956 Å. This is in good agreement with the experimental values of r_0(CH)=1.0677 Å and r_0(CSi)=1.6925 Å, respectively. In the $\tilde{A}\ ^2\Sigma^+$ state, HCSi is also found to have a linear geometry with r_e(CH)=1.0737 Å and r_e(CSi)=1.6130 Å at the [CCSD(T)/cc-pVQZ] level, confirming experimental values of r_0(CH)=1.0625 Å, r_0(CSi)=1.6118 Å, and the observation of C-Si triple bond character. With the same method, the $\tilde{X}\ ^2\Pi$ and $\tilde{A}\ ^2\Sigma^+$ state C-H stretching vibrational frequencies are predicted to be 3271 cm^{-1} and 3319 cm^{-1}, respectively, for which experimental values are not available. The classical $\tilde{X}$-$\tilde{A}$ splitting (T_e value) was determined to be 32.6 kcal/mol (1.41 eV, 11400 cm^{-1}) and quantum mechanical splitting (T_0 value) to be 33.5 kcal/mol (1.45 eV, 11726 cm^{-1}) which are in excellent agreement with the experimental T_0 value of 11766.721 cm^{-1} (33.64 kcal/mol, 1.459 eV). The linear excited $\tilde{A}\ ^2\Sigma^+$ state of the molecule has a real degenerate bending vibrational frequency, whereas the ground state ($\tilde{X}\ ^2\Pi$) is subject to the Renner-Teller effect and presents two distinct real vibrational frequencies. The Renner parameter (ϵ) and average harmonic bending frequency (ω_2) of the $\tilde{X}\ ^2\Pi$ state are predicted to be ϵ=-0.114 and ω_2=518 at the CCSD(T)/cc-pVQZ level of theory. The electronic structure analysis of the ground state showed that the HCSi radical is an A-Type Renner-Teller molecule.

2.2 Introduction

Small hydrogen-containing carbon-silicon species are thought to be important in the interstellar medium due to the fact that carbon and silicon are the most abundant elements, after hydrogen and helium, in the universe. Several silicon and carbon based interstellar molecules have been observed, including SiC_2,[27] SiC_3,[28] SiC_4,[29] SiC,[30] and SiH_4.[31] Herbst, Miller, Wlodek, and Bohme[32] have reported model calculations of gas-phase chemistry of silicon coumpounds in interstellar clouds which suggest that silicon methylidyne (HCSi) and silylidene (H_2CSi) should be relatively aboundant. Therefore, it is probable that the HCSi radical is the precursor of SiC_n clusters found in stellar atmospheres. Also organosilicon radicals are important in the production of hydrogenated amorphous silicon carbide (a-SiCH) films. In the production process, organosilane precursors such as methyltrichlorosilane,[33,34] or a mixture of silane and some hydrocarbons[35,36] are decomposed in hydrogen atmospheres. Meanwhile, silicon atoms, silicon clusters, silylidenes, silylenes, and organosilicon radicals are most likely be formed, and their electronic structure and chemical reactions can influence the electronic properties of the final products, semiconductor films and carbides.

Srinivas, Sulzle, and Schwarz[37] reported that the HCSi radical is stable under collision-free conditions, detecting the radical in neutralization-reionization mass spectrometry. Han, Rittby, and Graham[38] conducted a Fourier transform infrared study of photolysis products of a mixture of silane and methane trapped in an argon matrix, and found a 1010 cm^{-1} value for the Si-C stretching fundamental of HCSi. At about the same time, Cireasa, Cossart and Vervleot[39] carried out a near-infrared emission experiment and they obtained 3_0^1, 0_0^0, and 3_1^0 bands as well as rotational constants for the 0_0^0 band. Recently, Smith, Li, and Clouthier[40,41] published experimental data on the electronic spectrum of HCSi from a study of laser-induced fluores-

cence in the 850-600 nm region, producing the radical by an electric discharge using tetramethylsilane as the precursor. They reported geometries for the ground $\tilde{X}\ ^2\Pi$ and first excited $\tilde{A}\ ^2\Sigma^+$ states, excited state Si-C stretching and bending frequencies as well as a detailed rotational analysis. While our work was in progress, Cireasa, Cossart, Vervloet, and Robbe[42] published an article on the Fourier transform emission spectrum of the HCSi radical, and they obtained (100)-(000), (000)-(000), and (000)-(100) $\tilde{A}\ ^2\Sigma^+$-$\tilde{X}\ ^2\Pi_i$ transitions. However, including their study, there are no experimental values for the ground state C-H stretching and bending vibrational frequencies, and the excited state C-H stretching vibrational frequency.

In 1997, Robbe, Lavendy, Flament, and Chambaud[43] investigated the electronic structure of this radical theoretically at the multi reference CI (MRCI)/cc-pVQZ* (cc-pVQZ for H and C, a modification of cc-pVQZ for Si) level of theory. They predicted a Si-C bond length of 1.702 Å and a C-H bond length of 1.078 Å for the ground $\tilde{X}\ ^2\Pi$ state, and 1.587 Å and 1.080 Å for the excited $\tilde{A}\ ^2\Sigma^+$ state, respectively. They also predicted the quartic force field in internal coordinates and vibrational frequencies for the ground state as 1012 cm^{-1}, and 3260 cm^{-1} for stretching modes, and 470 cm^{-1} and 539 cm^{-1} for the two components of the bending mode, and -0.137 for the Renner parameter. They carried out the same computations with the CASSCF level of theory and reported that the differences between the values determined with the two methods are typically 15 cm^{-1} for the harmonic frequency of the C-Si stretching mode, 50 cm^{-1} for the C-H stretching mode, 5 cm^{-1} for the lowest bending mode ($^2A'$ Renner-Teller component) and 20 cm^{-1} for the upper bending mode ($^2A''$). These differences suggest that it is necessary to perform more reliable higher level computations to provide definitive information for the energetics and spectroscopic properties of the radical.

In the present study, the electronic structure of both the ground and first excited states of HCSi are theoretically investigated using highly correlated coupled cluster

with single and double excitations (CCSD) and coupled cluster with singles and doubles including a perturbative expansion for connected triples [CCSD(T)] methods, as well as SCF and configuration interaction with single and double excitations (CISD) utilizing significantly large basis sets. Such a systematic study should provide a useful guideline in theoretically predicting physical properties of polyatomic molecules in a convincing manner with respect to correlation level and basis set size. During the bending motion, the excited $\tilde{A}\ ^2\Sigma^+$ state is subject to a variational collapse into the lower-lying $^2A'$ component of the $\tilde{X}\ ^2\Pi$ ground state. Therefore, the equation-of-motion (EOM) CCSD method has been employed to determine the bending frequency of the first excited electronic state. The EOM-CCSD wave function does not suffer from the orbital instability problem (vide infra) due to the fact that the excited state energies are determined as higher roots of the lowest energy state CCSD wave function in the same symmetry.

2.3 Electronic Structure Considerations

The lowest electronic state of the linear HCSi radical has the degenerate electronic configurations:

$$[core](5\sigma)^2(6\sigma)^2(7\sigma)^2(2\pi_i)^2(2\pi_0) \Rightarrow\ \tilde{X}\ ^2\Pi \tag{2.1}$$

and

$$[core](5\sigma)^2(6\sigma)^2(7\sigma)^2(2\pi_i)(2\pi_0)^2 \Rightarrow\ \tilde{X}\ ^2\Pi \tag{2.2}$$

where [core] donates the six core (Si: 1s-, 2s-, 2p-like and C: 1s-like) orbitals, and π_i and π_0 stand for the in-plane and out-of-plane π moleculer orbitals (MOs). The 5σ and 6σ MOs correspond to C-H and Si-C σ bonds. The 7σ MO is the lone pair orbital on the Si atom as shown in Figure 2.1, while the 2π molecular orbital is related to the C-Si π bond as depicted in Figure 2.2. This electronic state ($^2\Pi$) of the HCSi radical possesses two distinct real vibrational frequencies along the H-C-Si

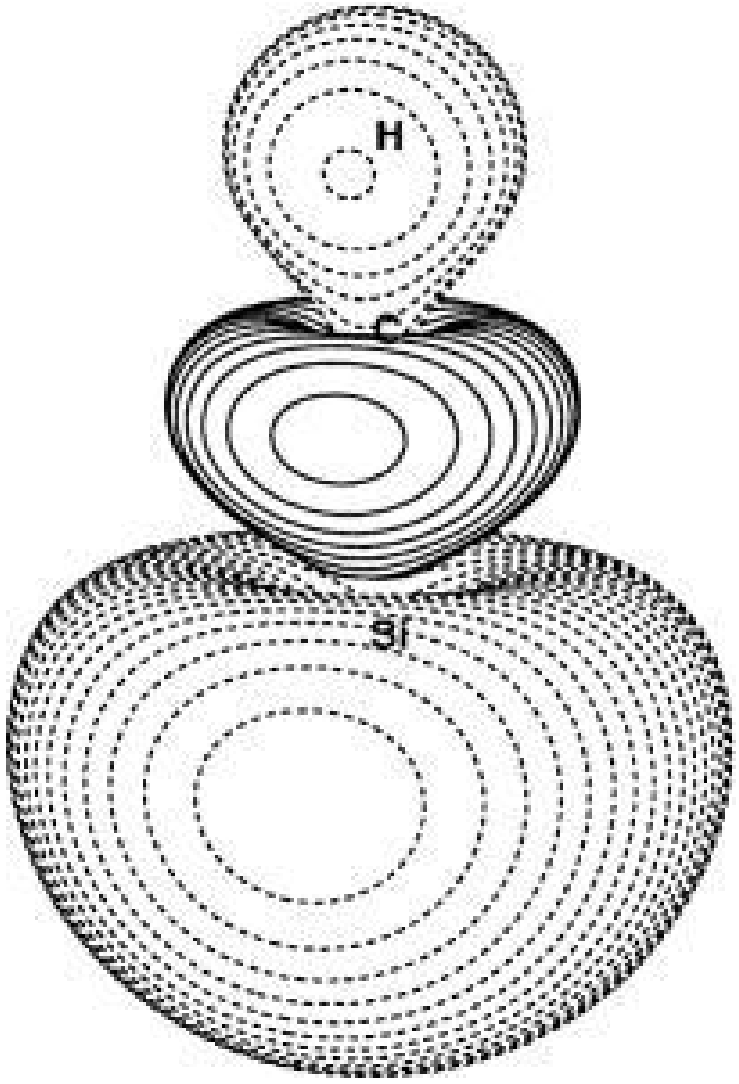

Figure 2.1: The 7σ molecular orbital of the $\tilde{X}\ ^2\Pi$ ground state of HCSi from the TZ2P(f,d)/SCF method.

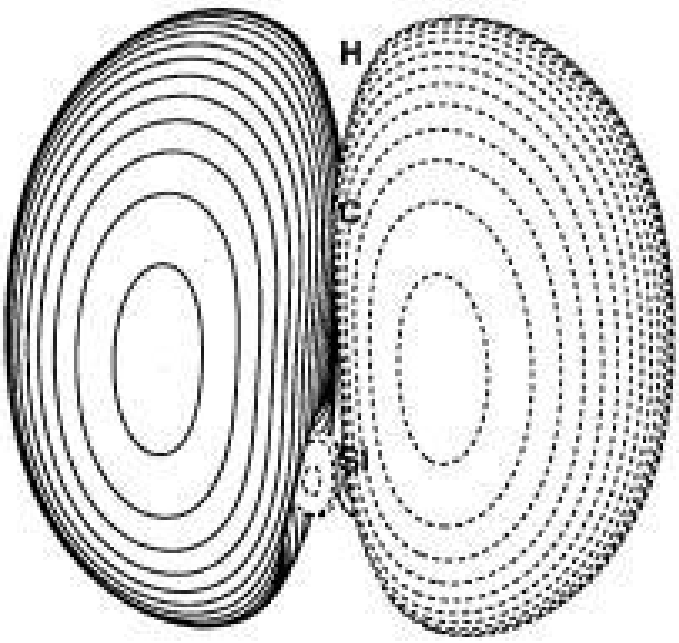

Figure 2.2: The 2π molecular orbital of the $\tilde{X}\ ^2\Pi$ ground state of HCSi from the TZ2P(f,d)/SCF method.

bending coordinate. Total energies of both components of the ground state increase upon bending, showing that this state is subject to the Renner-Teller effect [44–49] and is classified as a type A Renner-Teller molecule according to the nomenclature of Lee, Fox, Schaefer, and Pitzer. [50]

The first excited state of HCSi has the electron configuration:

$$[core](5\sigma)^2(6\sigma)^2(7\sigma)(2\pi_i)^2(2\pi_0)^2 \Rightarrow\ \tilde{A}\ ^2\Sigma^+ \tag{2.3}$$

which is a single electron excitation relative to the ground state;

$$(7\sigma)^2(2\pi)^3 \Rightarrow (7\sigma)(2\pi)^4 \tag{2.4}$$

The 2π MOs are occupied by four electrons in this state, giving rise to formal triple C-Si bond character. This first excited state of the molecule has a real degenerate bending frequency. However, because the state reduces to $^2A'$ symmetry on bending, it interacts with the lower Renner-Teller component of the ground state, which has the same symmetry $^2A'$. Therefore, the bending vibrational frequency of the $\tilde{A}\ ^2\Sigma^+$ excited electronic state cannot be determined as the first root of a correlated wave function.

At this point it may be useful to analyze the MO Hessian (the second derivatives of the SCF electronic energy with respect to MO rotations) of the reference SCF wave function.[51–53] For the linear $\tilde{X}\ ^2\Pi$ state, HCSi has one zero eigenvalue of the MO Hessian, related to the $2\pi_i$-$2\pi_0$ MO rotation, indicating that the SCF energy is not altered by exchanging the $2\pi_i$ and $2\pi_0$ orbitals. However, for the $\tilde{A}\ ^2\Sigma^+$ first excited state the MO Hessian has a doubly degenerate negative eigenvalue. The eigenvectors of this eigenvalue correspond to the 7σ-$2\pi_i$ and 7σ-$2\pi_0$ MO rotations. Therefore, the SCF wavefunction of the $\tilde{A}\ ^2\Sigma^+$ state is unstable and there is a lower-lying state, obtained by exchanging the 7σ-$2\pi_i$ or 7σ-$2\pi_0$ MOs, which is one of the Renner-Teller components of the ground state. The physical properties that involve the 7σ-2π MO rotation should be analyzed with great caution for the $\tilde{A}\ ^2\Sigma^+$ state. By the same token, the magnitudes of the eigenvalues of the MO Hessian may also be useful to analyze the instability of the SCF reference wave function.[51–53]

2.4 Renner-Teller Effects

Following Herzberg's arguments,[54] the Renner parameter (ϵ) and harmonic bending frequency (ω_2) are described in the following manner. In a degenerate electronic state, the potential function splits upon bending. This is because in the bent position of a linear molecule, there are no degenerate electronic state. The " upper" (inner)

potential function is denoted as V^+, while the "lower" (outer) one as V^-, for the Π and Δ states. The parity of the potential refers to its symmetry with respect to the singly occupied MOs. The zero-order bending potential function can be written as;

$$V^0 = aq^2 + bq^4 + ... \tag{2.5}$$

and the splitting of the potential function in Π, Δ, ...states must have the same form;

$$V^+ - V^- = \alpha q^2 + \beta q^4 + ... \tag{2.6}$$

where α and a are quadratic force constants, β and b are quartic force constants, and q is the bending displacement coordinate. Neglecting anharmonicity, the Renner parameter (ϵ) is defined as

$$\epsilon = \frac{\alpha}{2a} \tag{2.7}$$

It may be shown that eq. 2.7 is equivalent to

$$\epsilon = \frac{f^+ - f^-}{f^+ + f^-} = \frac{(\omega^+)^2 - (\omega^-)^2}{(\omega^+)^2 + (\omega^-)^2} \tag{2.8}$$

where f^+ and f^-, ω^+ and ω^- are the force constants and harmonic frequencies associated with the "upper" and "lower" bending potentials, respectively. If we denote the kinetic energy contribution to the bending motion as μ, the harmonic bending frequency (ω_2) may be determined by using the equation;

$$\omega_2 = \frac{1}{2\pi c}\sqrt{\frac{a}{\mu}} = \frac{1}{2\pi c}\sqrt{\frac{f^+ + f^-}{2\mu}} \tag{2.9}$$

which may be rewritten as;

$$\omega_2 = \sqrt{\frac{1}{2}\left[(\omega^+)^2 + (\omega^-)^2\right]} \tag{2.10}$$

The ϵ and ω_2 are experimentally observable quantities.[44–49,54] In this study, eqs.(2.5)-(2.10) will be used to theoretically determine the ϵ and ω_2 values.

2.5 Theoretical Methods

Eight basis sets were employed in this study. The basis set of triple-ζ (TZ) qualities for silicon is derived from McLean and Chandler's contraction[55] of Huzinaga's primitive Gaussian sets[56] with contraction scheme (13s9p/6s5p) for TZ. The TZ basis sets for carbon and hydrogen were obtained from Dunning's contractions[57] of Huzinaga's primitive Gaussian set[58] and are designated, (11s6p/5s3p)⇒ TZ for carbon, and (5s/3s)⇒ TZ for hydrogen. The TZ quality basis sets were augmented with a double and triple sets of polarization functions. The orbital exponents of the polarization functions are: α_d(Si)=1.00, 0.25, α_d(C)=1.50, 0.375, α_p(H)=1.50, 0.375 for double plarization (TZ2P); and α_d(Si)=1.00, 0.50, 0.25, α_d(C)=1.50, 0.75, 0.375, α_p(H)=1.50,0.75, 0.375 for triple polarization (TZ3P). The orbital exponents of the higher angular momentum functions are: α_f(Si)=0.32, α_f(C)=0.80, α_f(H)=1.00 for one set of higher angular momentum functions [TZ2P(f,d)]; and α_f(Si)=0.64, 0.16, α_f(C)=1.60, 0.40, α_d(H)=2.00, 0.50 for the two sets of higher angular momentum functions [TZ3P(2f,2d)]. The orbital exponents of diffuse functions are: α_p(Si)=0.02354 and α_s(Si)=0.02567, α_p(C)=0.03389 and α_s(C)=0.04812, and α_s(H)=0.03016 for single sets of diffuse functions [TZ2P+diff and TZ2P(f,d)+diff]. Two sets of diffuse functions were appended to the [TZ3P(2f,2d)] basis set, with the orbital exponents α_p(Si)=0.02354 and 0.008368, α_s(Si)=0.02567 and 0.008218, α_p(C)=0.03389 and 0.01253, α_s(C)=0.04812 and 0.01669, α_s(H)=0.03016 and 0.009246 to construct the basis set TZ3P(2f,2d)+2diff. Pure angular momentum d and f functions were used throughout.

The largest TZ derived basis set [TZ3P(2f,2d)+2diff] comprises 133 contracted Gausssian functions with a contraction scheme of Si (15s11p3d2f/8s7p3d2f), C (13s8p3d2f/7s5p3d2f), and H (7s3p2d/5s3p2d). Two correlation consistent polarized valence basis sets developed by Dunning and coworkers,[59] cc-pVTZ and cc-

pVQZ, have also been employed. The cc-pVQZ basis set consists of 144 contracted Gaussian functions with a contraction scheme of Si (16s11p3d2f1g/6s5p3d2f1g), C (12s6p3d2f1g/5s4p3d2f1g), and H (6s3p2d1f/4s3p2d1f).

The zeroth order descriptions of the $\tilde{X}\ ^2\Pi$ and $\tilde{A}\ ^2\Sigma^+$ states of HCSi were obtained using a one-configuration SCF (restricted open shell) wave function. Correlation effects were included using configuration interaction with single and double excitations (CISD), coupled cluster with single and double excitations (CCSD)[60] and CCSD with perturbative triple excitations [CCSD(T)][61] levels of theory. The six lowest-lying MOs (Si 1s-, 2s-, 2p-like and C 1s-like) were frozen and two highest-lying virtual MOs (Si and C 1s*-like) were deleted in all correlated procedures with the valence TZ plus quality basis sets. For the two correlation consistent basis sets, we froze only the six core MOs.

Using all eight basis sets, we optimized the geometries of both $\tilde{X}\ ^2\Pi$ and $\tilde{A}\ ^2\Sigma^+$ states of HCSi via analytic derivative methods[62,63] at the SCF and CISD levels. Harmonic vibrational frequencies at the SCF level were evaluated analytically, while at the CISD level of theory they were obtained by finite differences of analytic gradients. The CCSD, CCSD(T), and EOM-CCSD geometries and vibrational frequencies were determined via five-point numerical differentiation of the total energies. Throughout our study, cartesian forces at optimized geometries were required to be less than 10^{-6} hartree/bohr. All computations were carried out using the PSI 2.0.8 program package,[64] except the EOM-CCSD calculations, which were performed using the ACES II package[65] on IBM RS/6000 workstations.

2.6 Results and Discussion

Total energies, equilibrium geometries, dipole moments, and harmonic vibrational frequencies of the $\tilde{X}\ ^2\Pi$ state of HCSi are presented in Table 2.1 at four different

level of theories, SCF, CISD, CCSD, and CCSD(T) with the two largest basis sets, [TZ3P(2f,2d)+2diff] and cc-pVQZ. In Table 2.2 the corresponding properties for the $\tilde{A}\ ^2\Sigma^+$ state are reported at five different levels of theory, SCF, CISD, EOM-CCSD, CCSD, and CCSD(T), with the same two basis sets. As explained earlier, bending vibrational frequencies for the $\tilde{A}\ ^2\Sigma^+$ state were not obtained at the CISD, CCSD, and CCSD(T) level of theories, but they were determined at the SCF and EOM-CCSD levels. The bending vibrational frequencies for the two Renner-Teller components of the $\tilde{X}\ ^2\Pi$ state and the corresponding Renner parameters are given in Table 2.3 at four levels of theory. Other theoretical results may be obtained from the authors upon request. Relative energies of the two lowest-lying electronic states are presented in Table 2.4.

2.6.1 Geometries

The optimized geometries of the $\tilde{X}\ ^2\Pi$ state are given in Table 2.1 at eight representative levels of theory. Given a basis set, the two bond lengths increase with the inclusion of correlation effects. At our highest level of theory, CCSD(T)/cc-pVQZ, we predicted the C-H bond length as r_e(CH)=1.0781 Å and the C-Si bond length as r_e(CSi)=1.6956 Å. These two r_e values are consistent with the experimental values [41] of r_0(CH)=1.0677 Å and r_0(CSi)=1.6925 Å, respectively. Han *et al.*[38] studied the ground state of the radical at the CCSD(T)/6-31G** level of theory and predicted the C-H bond length to be r_e(CH)=1.077 Å and r_e(CSi)=1.699 Å. This prediction is similar to our CCSD(T)/TZ2P(f,d) result of 1.0770 Å and 1.6982 Å as expected.

For the $\tilde{A}\ ^2\Sigma^+$ state, r_e(CH) was predicted to be 1.0737 Å and r_e(CSi) to be 1.6130 Å at our most reliable level, CCSD(T)/cc-pVQZ. The experimental values for the $\tilde{A}\ ^2\Sigma^+$ state C-H and C-Si bond lengths were reported by Smith *et al.*[41] as r_0(CH)=1.0625 Å and r_0(CSi)=1.6118 Å. Our results show that the C-H bond length decreases 0.0044 Å upon excitation, which is in good agreement with the

Table 2.1: Total energies (in hartree), bond distances (in Å), harmonic vibrational frequencies (in cm^{-1}), and dipole moments (in debye) for the $\tilde{X}\ ^2\Pi$ state of HCSi.

	SCF TZ3P(2f,2d) +2diff	SCF cc-pVQZ	CISD TZ3P(2f,2d) +2diff	CISD cc-pVQZ	CCSD TZ3P(2f,2d) +2diff	CCSD cc-pVQZ	CCSD(T) TZ3P(2f,2d) +2diff	CCSD(T) cc-pVQZ
Energy	-327.271611	-327.278620	-327.508977	-327.523368	-327.529423	-327.544428	-327.543530	-327.559372
r_e(HC)	1.0655	1.0652	1.0709	1.0716	1.0746	1.0755	1.0770	1.0781
r_e(CSi)	1.6592	1.6600	1.6775	1.6765	1.6865	1.6854	1.6965	1.6956
ω_1(C-H Str.)	3452	3451	3353	3350	3305	3302	3276	3271
ω_2^- (π^-,$^2A''$)	653	658	570	597	550	573	529	547
ω_2^+ (π^+,$^2A'$)	645	650	566	590	487	515	467	488
ω_3(C-Si Str.)	1155	1155	1090	1095	1058	1062	1025	1028
μ_e	0.095		0.024					

Available experimental values:

r_0(HC)= 1.069 Å from Ref. 40, 1.0677 Å from Ref. 41.
r_0(CSi)= 1.6913 Å from Ref. 40, 1.6925 Å from Ref. 41.
ν_3= 1010.4 cm^{-1} from Ref. 38, 1013 cm^{-1} from Ref. 39.

experimental decrease of 0.0052 Å. Achieving this level of agreement is very important, because the previous theoretical study[43] predicted an increase in C-H bond length on excitation. At the same CCSD(T)/cc-pVQZ level of theory, we predict a decrease in C-Si bond length of 0.0826 Å on excitation, although a recent theoretical study[43] suggests a 0.115 Å decrease. Our prediction is in very close agreement with the recent experimental[41] C-Si bond length decrease of 0.0807 Å. The 7σ MO in Figure 2.1 mainly consists of the nonbonding lone pair on the Si atom (3s atomic orbital), while the 2π MO has C-Si π-bonding character as shown in Figure 2.2. Therefore, a single excitation from the 7σ MO to the 2π MO in eq. (4) decreases the C-Si bond length. With the cc-pVQZ basis set, the difference in the SCF and CCSD(T) bond lengths for the ground state is 0.0129 Å for the C-H bond and 0.0355 Å for the Si-C bond. It is observed that the Si-C bond is more sensitive to correlation effects, due to the multiple bond character of the silicon-carbon linkage.

2.6.2 Harmonic vibrational frequencies

The C-H stretching (ω_1) and C-Si stretching (ω_3) vibrational frequencies of both the $\tilde{X}\ ^2\Pi$ and $\tilde{A}\ ^2\Sigma^+$ states are lowered when correlation effects are included, reflecting the longer bond distances. Similarly, the two stretching modes of the ground state have lower frequencies than the corresponding values for the first excited state. The C-Si stretching fundamental frequency of the $\tilde{X}\ ^2\Pi$ state of HCSi was experimentally determined to be 1010 cm^{-1} from the matrix infrared absorption spectrum [38] and 1013 cm^{-1} from the gas phase emission spectrum.[39] Cireasa *et al.*[42] more recently reported $\tilde{X}\ ^2\Pi_{1/2}$ and $\tilde{X}\ ^2\Pi_{3/2}$ C-Si stretching vibrational frequencies as 1084.866 cm^{-1} and 1014.693 cm^{-1}, respectively. The corresponding harmonic vibrational frequency was predicted to be 1028 cm^{-1} with our most reliable method CCSD(T)/cc-pVQZ, and 1025 cm^{-1} with CCSD(T)/TZ3P(2f,2d) level of theory. The C-H stretching harmonic vibrational frequency was determined to be 3271 cm^{-1} for

Table 2.2: Total energies (in hartree), bond distances (in Å), harmonic vibrational frequencies (in cm^{-1}), and dipole moments (in debye) for the $\tilde{A}\ ^2\Sigma^+$ state of HCSi.

	SCF cc-pVQZ	CISD TZ3P(2f,2d) +2diff	CISD cc-pVQZ	CCSD TZ3P(2f,2d) +2diff	CCSD cc-pVQZ	EOM-CCSD TZ3P(2f,2d) +2diff	EOM-CCSD cc-pVQZ	CCSD(T) TZ3P(2f,2d) +2diff	CCSD(T) cc-pVQZ
Energy	-327.19853	-327.44532	-327.45981	-327.47085	-327.48594	-327.47030	-327.48552	-327.49135	-327.50748
r_e(HC)	1.0605	1.0656	1.0663	1.0697	1.0706	1.0697	1.0706	1.0725	1.0737
r_e(CSi)	1.5662	1.5878	1.5868	1.6015	1.6002	1.6015	1.6001	1.6141	1.6130
ω_1(C-H Str.)	3509	3412	3414	3357	3357	3357	3357	3321	3319
ω_2(bend)						741	762		
ω_3(C-Si Str.)	1372	1280	1284	1227	1232	1226	1232	1180	1184
μ_e		2.080				1.326	1.313		

Available experimental values:

r_0(HC)= 1.0625 Å from Ref. 41, 1.044 Å (for ν_3'= 3 vibrational level in the excited state) from Ref. 40.
r_0(CSi)= 1.6118 Å from Ref. 41, 1.6316 Å (for ν_3'= 3 vibrational level in the excited state) from Ref. 40.
ν_3= 1168 cm^{-1} from Ref. 41, 1171 cm^{-1} from Ref. 40.
ν_2= 715 cm^{-1} from Ref. 41.

Table 2.3: Bending vibrational frequencies,(in cm^{-1}), [ω_2^-, (π^-,$^2A''$)], [ω_2^+, (π^+,$^2A'$)], the suitably averaged ω_2, and Renner parameter (ϵ) for the $\tilde{X}$ $^2\Pi$ state of HCSi.

	TZ3P(2f,2d)	TZ3P(2f,2d) +2diff	cc-pVTZ	cc-pVQZ
SCF-$\omega_2^-/\omega_2^+/\omega_2$	664/651/657	652/644/648	654/645/649	657/650/653
(ϵ)	-0.0197	-0.0123	-0.0138	-0.0107
CISD-$\omega_2^-/\omega_2^+/\omega_2$	582/572/577	569/565/567	588/581/584	596/589/592
(ϵ)	-0.0173	-0.0070	-0.0119	-0.0118
CCSD-$\omega_2^-/\omega_2^+/\omega_2$	559/493/527	549/486/518	568/504/536	573/514/544
(ϵ)	-0.1249	-0.1212	-0.1189	-0.1082
CCSD(T)-$\omega_2^-/\omega_2^+/\omega_2$	538/473/506	528/466/498	544/485/515	547/488/518
(ϵ)	-0.1280	-0.1242	-0.1143	-0.1136

the ground state and 3319 cm^{-1} for the first excited state, at the CCSD(T)/cc-pVQZ level. There is no experimental value available for the C-H mode of HCSi for either the $\tilde{X}$ $^2\Pi$ or $\tilde{A}$ $^2\Sigma^+$ states in the literature. However there are two previous theoretical studies. Robbe *et al.*,[43] reported the harmonic vibrational frequencies of the $\tilde{X}$ $^2\Pi$ state to be ω_1=3260 cm^{-1} (C-H stretching) and ω_3=1012 cm^{-1} (C-Si stretching), at the MRCI/cc-pVQZ level of theory. These predictions are in close agreement with our results. Secondly, Han *et al.*[38] predicted the values of 3337 cm^{-1} and 1033 cm^{-1}, for the C-H and C-Si stretching modes respectively, at the CCSD(T)/6-31G** level. Although the prediction on the C-Si stretching mode is close to our CCSD(T)/cc-PVQZ result, the value of 3337 cm^{-1} for the C-H stretching vibrational frequency is 67 cm^{-1} higher than our CCSD(T)/cc-pVQZ result. Vibrational frequencies given by Han *et al.*[38] are close to our TZ2P/CCSD predictions of 3310 cm^{-1} for the C-H mode and 1035 cm^{-1} for the C-Si mode. For the $\tilde{A}$ $^2\Sigma^+$ state C-H stretching, Lavendy *et al.*[66] predicted 3249 cm^{-1} at a multiconfiguration self-consistent filed-configuration interaction (MCSCF-CI) level of theory, which is 70 cm^{-1} lower than our value. As

discussed in the Introduction, the $\tilde{X}\ ^2\Pi$ state of the HCSi radical is subject to the Renner-Teller effect and presents two distinct bending frequencies. Because there are no experimental data for the ground state bending mode, the bending vibrational frequencies for both components, $^2A''$ and $^2A'$, as well as the average ω_2 frequency of the ground state are presented at representative levels of theory in Table 2.3. Both frequencies decrease with inclusion of correlation effects. At the CCSD(T)/cc-pVQZ level, the $\tilde{X}\ ^2\Pi$ state bending vibrational frequencies were predicted to be 547 cm^{-1} and 488 cm^{-1}, respectively, for the upper and lower Renner-Teller components, which is consistent with the previous theoretical values of 538.8 cm^{-1} and 469.9 cm^{-1}, at the MRCI/cc-pVQZ level.[43] We found a difference of 59 cm^{-1} between in-plane and out-of-plane bending vibrations at the CCSD(T)/cc-pVQZ level. The Renner parameter, (ϵ), which is used to describe the splitting of the potential energy surface, is on the order of -0.01 at the SCF and CISD levels, which is almost ten times smaller than the values from the CCSD and CCSD(T) levels. Robbe *et al.*[43] predicted ϵ to be -0.137 which is reasonably close to our CCSD(T)/cc-pVQZ result of -0.114. The $\tilde{A}\ ^2\Sigma^+$ state bending mode has a degenerate frequency which is determined to be 762 cm^{-1} with the EOM-CCSD/cc-pVQZ method, while Lavendy *et al.* predicted it to be 849 cm^{-1} at the MCSCF-CI level. Our EOM-CCSD/cc-pVQZ value is in good agreement with the experimental fundamental bending frequency of 715 cm^{-1} for the $\tilde{A}\ ^2\Sigma^+$ state.[40]

2.6.3 Energetics

With the cc-pVQZ basis set, the classical $\tilde{X}$-$\tilde{A}$ splitting was predicted to be 50.3 (SCF), 39.9 (CISD), 36.7 (CCSD), and 32.6 kcal/mol [CCSD(T)], respectively. It is seen that advanced treatments of correlation effects decrease the energy separation, while we find that this energy separation is almost independent of the basis sets used. Recently, Cireasa *et al.*[42] have studied the emission spectrum of the HCSi radical

and observed three bands whose origins appeared at 12934.406 cm^{-1}, 11766.721 cm^{-1}, and 10752.430 cm^{-1}. They analyzed and assigned these bands as (100)-(000), (000)-(000), and (000)-(001) $\tilde{A}\ ^2\Sigma^+$-$\tilde{X}\ ^2\Pi_i$ transitions. Our cc-pVQZ/CCSD(T) T_e result of 11400 cm^{-1} (32.6 kcal/mol), and TZ3P(2f,2d)/CCSD(T) result of 11500 cm^{-1} (32.7 kcal/mol) are in very good agreement with the above (000)-(000) $\tilde{A}\ ^2\Sigma^+$-$\tilde{X}\ ^2\Pi_i$ transion, 11766.721 cm^{-1}. Robbe *et al.*[43] predicted the T_e value as 12200 cm^{-1} at the MRCI level of theory. As seen in Table 2.4, the SCF, CISD, CCSD, and also MRCI[43] results, all overestimate the energy gap. It is observed that only the CCSD(T) results are in good agreement with the experimental value. Also, we included (ZPVE) corrections for all level of theories. In determining the ZPVE, the average w_2 values for bending mode of $\tilde{X}\ ^2\Pi$ state, and the EOM-CCSD bending vibrational frequencies of $\tilde{A}\ ^2\Sigma^+$ state are used. The T_0 value at the CCSD(T)/cc-pVQZ level was thus determined to be 11726 cm^{-1} which is only 41 cm^{-1} smaller than the experimental value of 11766.721 cm^{-1}.

2.7 Concluding Remarks

The two lowest-lying electronic states of the methylidyne molecule, (HCSi), have been studied systematically employing *ab initio* SCF, CISD, CCSD, EOM-CCSD, and CCSD(T) levels of theory with a wide range of basis sets. Both the $\tilde{X}\ ^2\Pi$ and $\tilde{A}\ ^2\Sigma^+$ states are found to have linear structures. The Renner-Teller effect in the ground state has been investigated, and a value of -0.114 is predicted for the Renner parameter (ϵ) at the CCSD(T)/cc-pVQZ level. With the same method, the ground state C-H stretching, the ground state bending, and the excited state C-H stretching vibrational frequencies are predicted to be 3270 cm^{-1}, 518 cm^{-1}, and 3319 cm^{-1}, respectively. The classical $\tilde{X}$-$\tilde{A}$ splitting (T_e value) was determined to be 32.6 kcal/mol (1.41 eV, 11390 cm^{-1}) and quantum mechanical splitting (T_0 value)

Table 2.4: Energy separations, T_e, (kcal/mol), between $\tilde{X}\ ^2\Pi$-$\tilde{A}\ ^2\Sigma^+$ states (T_0 values in parentheses).

	TZ2P	TZ2P+diff	TZ2P(f,d)	TZ2P(f,d)+diff	TZ3P(2f,2d)	TZ3P(2f,2d)+2diff	cc-pVTZ	cc-pVQZ
SCF	50.26	50.43	50.03	50.19	49.94	50.09	50.73	50.25
	(50.85)	(51.00)	(50.68)	(50.85)	(50.60)	(50.75)	(51.39)	(50.93)
CISD	40.24	40.47	39.95	40.11	39.79	39.94	40.43	39.88
	(41.02)	(41.24)	(40.77)	(40.93)	(40.65)	(40.83)	(41.25)	(40.69)
CCSD	36.95	37.23	36.76	36.92	36.61	36.75	37.18	36.70
	(37.84)	(38.10)	(37.68)	(37.84)	(37.58)	(37.75)	(38.10)	(37.62)
CCSD(T)	33.04	33.27	32.76	32.92	32.60	32.74	33.08	32.56
	(33.96)	(34.17)	(33.70)	(33.82)	(33.59)	(33.76)	(34.04)	(33.53)

Experimental value:

T_0=33.64 kcal/mol (11766.721 cm^{-1}, 1.459 ev) from Ref. 42.

to be 33.5 kcal/mol (1.45 eV, 11720 cm^{-1}) at the cc-pVQZ/CCSD(T) level, which is in excellent agreement with the experimental T_0 value of 11766.721 cm^{-1} (1.459 eV, 33.64 kcal/mol). The present study demonstrates that the CCSD(T) method in conjunction with large basis sets is able to achieve a chemical accuracy of less than one kcal/mol in critical energetic quantities.

Chapter 3

Coupled cluster study of the $\tilde{X}\ ^2\Pi$ and $\tilde{A}\ ^2\Sigma^+$ electronic states of the HCGe radical: Renner-Teller splitting and the effects of relativistic corrections *

*Levent Sari, Yukio Yamaguchi, and Henry F. Schaefer III. Journal of Chemical Physics, 115, 5932 (2001). Reprinted by permission of the American Institue of Physics.

3.1 Abstract

The $\tilde{X}\ ^2\Pi$ and $\tilde{A}\ ^2\Sigma^+$ states of the germanium methylidyne radical (HCGe) have been investigated at the SCF, CISD, CCSD, and CCSD(T) levels of theory. The total energies, equilibrium geometries, dipole moments, harmonic vibrational frequencies, infrared intensities, and Renner-Teller splitting are reported. The relativistic one-electron Darwin and mass-velocity terms are calculated using first-order perturbation theory and the effects of these corrections on energetics, harmonic vibrational frequencies, and Renner-Teller splitting are discussed. At our highest level of theory [CCSD(T)/cc-pVQZ], the ground electronic state ($\tilde{X}\ ^2\Pi$) has a linear geometry with r_e(CH)=1.079 Å and r_e(CGe)=1.769 Å in good agreement with the experimental values of r_0(CH)=1.067 Å and r_0(CGe)=1.776 Å. In the electronically excited $\tilde{A}\ ^2\Sigma^+$ state, HCGe is also found to have a linear geometry with r_e(CH)=1.074 Å and a much shorter r_e(CGe)=1.669 Å at the [CCSD(T)/cc-pVQZ] level, in agreement with experimental values of r_0(CH)=1.059 Å, r_0(CGe)=1.674 Å, and the observation of C-Ge triple bond character. The $\tilde{A}\ ^2\Sigma^+$ state C-Ge stretching vibrational frequency is determined to be ω_3=990.2 cm^{-1} at the CCSD(T)/cc-pVTZ level with the inclusion of relativistic effects, which is in essentially perfect agreement with the experimental value of ν_3=990 cm^{-1}. With the same method, the $\tilde{X}\ ^2\Pi$ state harmonic vibrational frequencies are predicted to be 846 cm^{-1} for the C-Ge stretching, 443 and 506 cm^{-1} for the two nondegenerate bending Renner-Teller components, and 3249 cm^{-1} for the C-H stretching modes for which experimental values are not available. The quantum mechanical splitting (T_0 value) was determined to be 38.0 kcal/mol at the non-relativistic CCSD(T)/TZ3P(2f,2d)+2diff level, while it is found to be 39.9 kcal/mol with the inclusion of relativity, in very good agreement with the experimental value of 39.8 kcal/mol. The Renner parameter (ϵ) is determined to be

-0.1386, and effects of relativity were seen to produce a smaller Renner parameter of -0.1329.

3.2 Introduction

In 1997 Harper, Ferrall, Hilliard, Stogner, Grev, and Clouthier[67] reported the first observation of 1-germavinylidene or germylidene (H_2C=Ge), the simplest unsaturated germylene. The discovery of the high-resolution spectrum of this molecule has been a fundamental interest due to the observation of quantum beats in their fluorescence decay curves.[67–69] In 1998 Stogner et al.[68] carried out good quality ab initio calculations (CISD,CCSD and CCSD(T) with TZ quality basis sets) on H_2C=Ge and HCGeH, and they predicted geometries and harmonic vibrational frequencies in close agreement with the existing experimental data.

The first observation of the germanium methylidyne radical (HCGe) was reported by Smith, Li, Clouthier,[70] in 1999, by a short communication paper on both HCSi and HCGe radicals. One year later, Smith, Li, Clouthier, Kingston, and Merer[71] published a detail study on HCGe radical. The radical was produced in a pulsed electric discharge using tetramethylgermane as the precursor. They recorded $\tilde{A}\ ^2\Sigma^+$-$\tilde{X}\ ^2\Pi$ electronic transition of jet-cooled HCGe in the 730-555nm region by laser-induced fluorescence techniques. The ground $\tilde{X}\ ^2\Pi$ and the first excited $\tilde{A}\ ^2\Sigma^+$ state geometries and the excited state Ge-C stretching and bending vibrational frequencies were determined experimentally. They used B3LYP/6-311G** level of theory to predict ground state vibrational frequencies without characterization of the Renner-Teller effect in $\tilde{X}\ ^2\Pi$ state, which causes the bending potential to split into two non-degenerate surface. At this level of theory, values of 865 cm^{-1}, 3235 cm^{-1}, and 492 cm^{-1} were predicted for the ground $\tilde{X}\ ^2\Pi$ state Ge-C stretching, C-H stretching, and bending vibrational frequencies, respectively. They also used the same level of theory

to predict values for the excited $\tilde{A}\ ^2\Sigma^+$ state harmonic vibrational frequencies for which experimental results were already found. The differences between their theoretical predictions at the B3LYP/6-311G** level and their experimental results are 50 cm^{-1} for the Ge-C stretching and 75 cm^{-1} for the bending vibrational frequencies. They also reported that the excitation energy determined at the B3LYP/6-311G** level of theory is about 1800 cm^{-1} higher than the experimental value, and the B3P86 density functional, SCF, and UMP2 levels of theory show considerable variations. All of these results, along with the fact that there is no any other study in literature, suggest that it is desirable to perform more reliable high level quantum mechanical computations to provide dependable predictions of the energetics and spectroscopic properties of the HCGe radical.

In the present study, the highly correlated coupled cluster with single and double excitations (CCSD) method and coupled cluster with singles and doubles including a perturbative expansion for connected triples [CCSD(T)] methods have been employed to study the electronic structure of both the ground and first excited states of HCGe radical. The SCF and configuration interaction with single and double excitations (CISD) methods have also been used. Relativistic corrections, Darwin and mass-velocity terms, are evaluated for both the ground and excited states, and the effects of these corrections on several physical properties including the Renner-Teller splitting are discussed. The excited $\tilde{A}\ ^2\Sigma^+$ state is subject to a variational collapse, during the bending motion, into the lower-lying $^2A'$ component of the $\tilde{X}\ ^2\Pi$ ground state. Therefore, the equation-of-motion (EOM) CCSD method, which does not suffer from the orbital instability problem (vide infra), has been employed to determine the bending frequency of the first excited electronic state of HCGe.

3.3 Electronic Structure Considerations

The degenerate ground electron configurations of HCGe are

$$[core](8\sigma)^2(9\sigma)^2(10\sigma)^2(4\pi_i)^2(4\pi_o) \Rightarrow \tilde{X}\ ^2\Pi \tag{3.1}$$

and

$$[core](8\sigma)^2(9\sigma)^2(10\sigma)^2(4\pi_i)(4\pi_o)^2 \Rightarrow \tilde{X}\ ^2\Pi \tag{3.2}$$

In (1) and (2), [core] denotes the fifteen core (Ge: 1s-, 2s-, 2p-, 3s-, 3p-, and 3d-like and C: 1s-like) orbitals, and π_i and π_o stand for the in-plane and out-of-plane π moleculer orbitals (MOs). The 8σ and 9σ molecular orbitals correspond to the σ_{CH}+σ_{CGe} and σ_{CH}-σ_{CGe} bonds.

The 10σ MO is the lone pair orbital on the Ge atom as shown in Figure 3.1, while the 4π molecular orbital is related to the Ge-C π bond as depicted in Figure 3.2. This ground electronic state ($^2\Pi$) of the HCGe radical possesses two distinct real vibrational frequencies along the H-C-Ge bending coordinate. Total energies of two components of the ground state increase upon bending. This shows that this state is subject to the Renner-Teller effect[44–49] and is classified as a type A Renner-Teller molecule.[50]

The electron configuration for the first excited doublet state of HCGe is

$$[core](8\sigma)^2(9\sigma)^2(10\sigma)(4\pi)^4 \Rightarrow \tilde{A}\ ^2\Sigma^+ \tag{3.3}$$

representing a single excitation relative to the ground state:

$$(10\sigma)^2(4\pi)^3 \Rightarrow (10\sigma)(4\pi)^4 \tag{3.4}$$

The 4π MO is fully occupied in the $\tilde{A}\ ^2\Sigma^+$ state, resulting in formal triple C-Ge bond character. Because the $\tilde{A}\ ^2\Sigma^+$ state collapses to $^2A'$ symmetry on bending, it interacts with the lower Renner-Teller component of the ground $\tilde{X}\ ^2\Pi$ state,

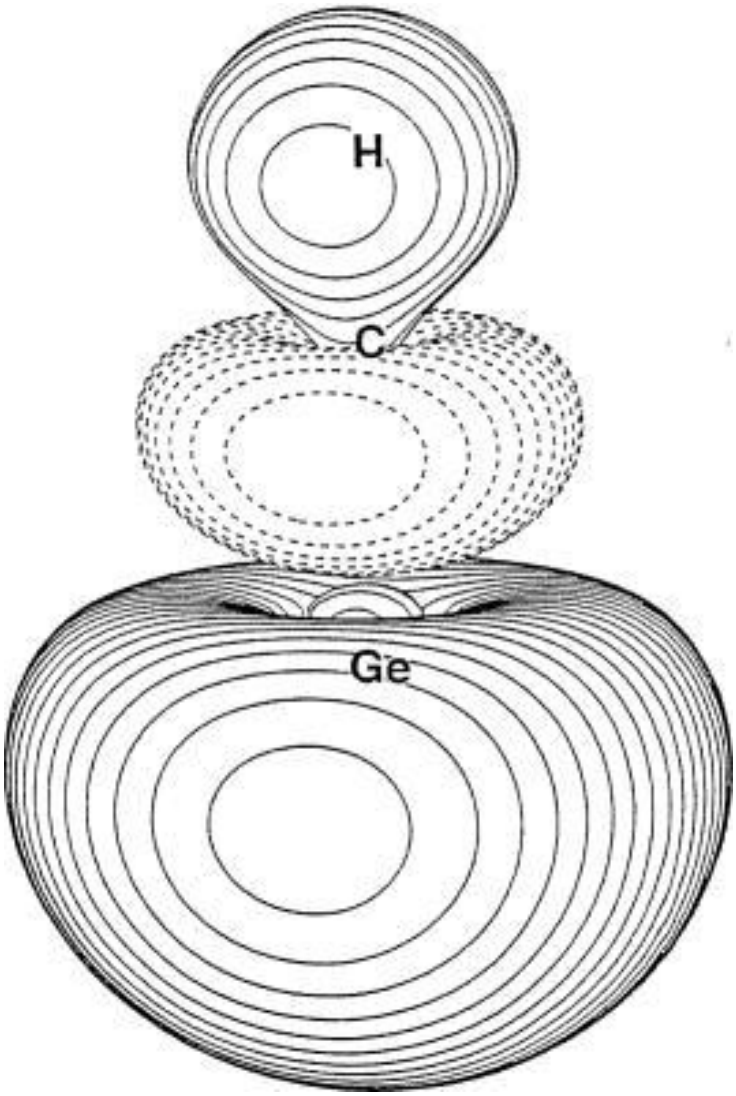

Figure 3.1: The 10σ molecular orbital for the $\tilde{X}\ ^2\Pi$ ground state of HCGe from the TZ2P(f,d)/SCF method

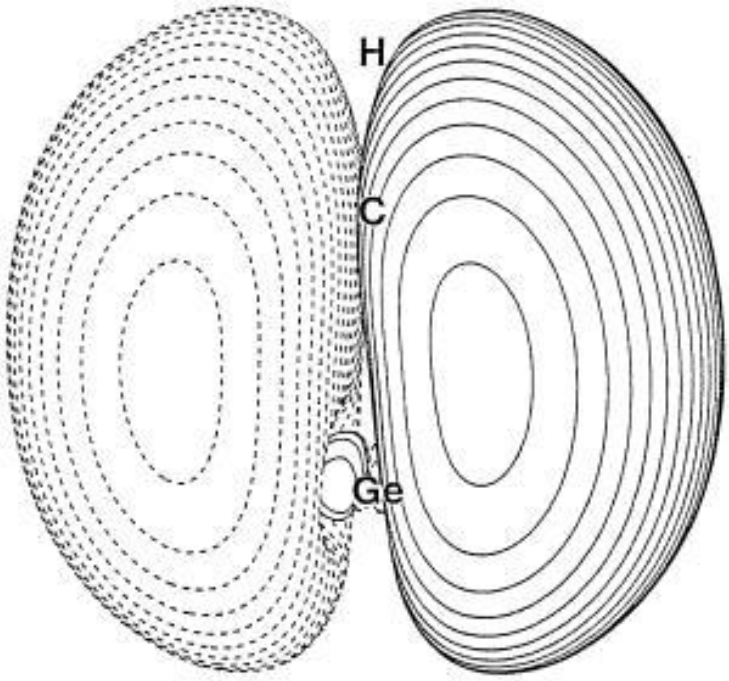

Figure 3.2: The 4π molecular orbital of the $\tilde{X}\ ^2\Pi$ ground state of HCGe from the TZ2P(f,d)/SCF method.

which has the same symmetry $^2A'$. Therefore, the bending vibrational frequency of the $\tilde{A}\ ^2\Sigma^+$ electronic state cannot be calculated from the lowest eigenvalue of the appropriate secular equation.

It may be useful to analyze the MO Hessian (the second derivatives of the SCF electronic energy with respect to MO rotations) of the reference SCF wave function.[51–53] For the $\tilde{X}\ ^2\Pi$ state, the SCF wave function has one zero eigenvalue of the MO Hessian related to the $4\pi_i$-$4\pi_0$ MO rotation. This is an indication of the fact that the SCF energy is not changed by exchanging the $4\pi_i$ and $4\pi_0$ orbitals. However, for the $\tilde{A}\ ^2\Sigma^+$ state, the MO Hessian has a doubly degenerate negative eigenvalue. The corresponding eigenvectors are the 10σ-$4\pi_i$ and 10σ-$4\pi_0$ MO rotations. Therefore, the SCF wavefunction for the $\tilde{A}\ ^2\Sigma^+$ state is unstable and there is a lower-lying state. We can obtain the lower-lying state by exchanging the 10σ-$4\pi_i$ or 10σ-$4\pi_0$ moleculer orbitals, which is one of the Renner-Teller components of the ground state. The excited state properties that involve the 10σ-4π MO rotation should be interpreted with great caution. Also, the magnitudes of the eigenvalues of the MO Hessian may also be useful to study the instability of the SCF reference wave function.[51–53]

As shown in Chapter 1, the Renner parameter[44–49,54] (ϵ) and the averaged harmonic bending frequency (ω_2) may be determined using the equations

$$\epsilon = \frac{f^+ - f^-}{f^+ + f^-} = \frac{(\omega^+)^2 - (\omega^-)^2}{(\omega^+)^2 + (\omega^-)^2} \tag{3.5}$$

$$\omega_2 = \sqrt{\frac{1}{2}\left[(\omega^+)^2 + (\omega^-)^2\right]} \tag{3.6}$$

where f^+ and f^-, ω^+ and ω^- are the force constants and harmonic frequencies associated with the "plus" and "minus" bending potentials, respectively.

3.4 Theoretical Methods

The zeroth order descriptions of the $\tilde{X}\ ^2\Pi$ and $\tilde{A}\ ^2\Sigma^+$ states of HCGe were obtained using single configuration SCF (restricted open shell) wave functions. Correlation effects were included using configuration interaction with single and double excitations (CISD), coupled cluster with single and double excitations (CCSD)[60] and CCSD with perturbative triple excitations [CCSD(T)][61] levels of theory. The ten lowest-lying MOs (Ge 1s-, 2s-, 2p-, 3s-, 3p-like and C 1s-like) were frozen and the highest-lying virtual MO was deleted in all correlated procedures with the valence TZ plus quality basis sets. For the two correlation consistent basis sets, only the ten core MOs were frozen. All MOs were included into relativistic calculations.

A total of six basis sets were employed in this study. The basis set of triple-ζ (TZ) qualities for germanium is derived from Schäfer, Horn, and Ahlrichs[72] with the contraction scheme (17s12p6d/6s5p2d). The TZ basis sets for carbon and hydrogen were obtained from Dunning's contractions[57] of Huzinaga's primitive Gaussian set[58] and are designated (10s6p/5s3p)⇒ TZ for carbon, and (5s/3s)⇒ TZ for hydrogen. The TZ quality basis sets were augmented with double and triple sets of polarization functions. The orbital exponents of the polarization functions are: α_d(Ge)=0.3549, 0.1316, α_d(C)=1.50, 0.375, α_p(H)=1.50, 0.375 for double plarization (TZ2P); and α_d(Ge)=0.7098, 0.24325, 0.0658, α_d(C)=3.00, 0.75, 0.1875, α_p(H)=1.50, 0.75, 0.375 for triple polarization (TZ3P). The orbital exponents of the higher angular momentum functions are: α_f(Ge)=0.362, α_f(C)=0.80, α_d(H)=1.00 for one set of higher angular momentum functions [TZ2P(f,d)]; and α_f(Ge)=0.724, 0.181, α_f(C)=1.60, 0.40, α_d(H)=2.00, 0.50 for the two sets of higher angular momentum functions [TZ3P(2f,2d)]. The orbital exponents of diffuse functions are: α_p(Ge)=0.02269 and α_s(Ge)=0.02633, α_p(C)=0.03389 and α_s(C)=0.04812, and α_s(H)=0.03016 for single sets of diffuse functions [TZ2P(f,d)+diff]. Two sets of

diffuse functions were appended to the [TZ3P(2f,2d)] basis set, with the orbital exponents α_p(Ge)=0.02269 and 0.006358, α_s(Ge)=0.02633 and 0.008465, α_p(C)=0.03389 and 0.01253, α_s(C)=0.04812 and 0.01669, α_s(H)=0.03016 and 0.009246 to construct the basis set TZ3P(2f,2d)+2diff. Pure angular momentum d and f functions were used throughout.

The basis set [TZ3P(2f,2d)+2diff] is the largest TZ derived basis set which comprises 143 contracted Gausssian functions with a contraction scheme of Ge (19s14p9d2f/8s7p5d2f), C (13s8p3d2f/7s5p3d2f), and H (7s3p2d/5s3p2d). Two of Dunning's correlation consistent polarized valence basis sets,[73] cc-pVTZ and cc-pVQZ, have also been employed. The cc-pVQZ basis set consists of 153 contracted Gaussian functions with a contraction scheme of Ge (21s16p12d2f1g/7s6p4d2f1g), C (12s6p3d2f1g/5s4p3d2f1g), and H (6s3p2d1f/4s3p2d1f).

The geometries of both $\tilde{X}\ ^2\Pi$ and $\tilde{A}\ ^2\Sigma^+$ states of HCGe were optimized via analytic derivative methods[62,63] at the SCF and CISD levels. Harmonic vibrational frequencies at the SCF level were evaluated analytically, while at the CISD level of theory they were obtained by finite differences of analytic gradients. The CCSD, CCSD(T), and EOM-CCSD geometries and vibrational frequencies were determined via five-point numerical differentiation of the total energies.

The one-electron Darwin term, which is always positive and corrects the Coulomb attraction, and the mass-velocity term, which is always negative and corrects the kinetic energy of the system, were evaluated using first-order perturbation theory.[23?] This method gives consistent results for germanium compounds compared to methods such as Dirac-Hartree-Fock (DHF) and the use of relativistic effective core potentials (RECP).[26] The two-electron Darwin correction, which reduces the repulsion between electrons, is very small due to the fact that it depends on the probability of two electrons being at the same point in space. In all of the calculations for the relativistic effects, non-relativistic optimized geometries were used. Relativistic cor-

rections to the harmonic vibrational frequencies are determined by evaluating the Darwin and mass-velocity terms at each displaced geometry and adding them to the total non-relativistic energy in the numerical differentiation procedure.

Throughout our study, cartesian forces at optimized geometries were required to be less than 10^{-8} hartree/bohr. All computations were carried out using the PSI 2.0.8 program package,[64] except the calculations for EOM-CCSD and for relativistic effects which were performed using the ACES II package,[65] on IBM RS/6000 workstations.

3.5 Results and Discussion

In Table 3.1, the equilibrium geometries, total energies and dipole moments for the $\tilde{X}$ $^2\Pi$ state of HCGe are presented. In Table 3.2, the ground state harmonic vibrational frequencies including two non-degenerate bending vibrational frequencies, ω_2^+ and ω_2^-, infrared intensities, and Renner parameters are given. Total energies, and physical properties for the $\tilde{A}$ $^2\Sigma^+$ state are reported at five different levels of theory, SCF, CISD, EOM-CCSD, CCSD, and CCSD(T) in Table 3.3. As explained earlier, bending vibrational frequencies for the $\tilde{A}$ $^2\Sigma^+$ were not obtained at the CISD, CCSD, and CCSD(T) level of theories, but they were predicted with the SCF and EOM-CCSD methods. The effects of isotopic substitutions on the C-Ge stretching vibrational frequency were predicted at the CCSD(T)/TZ3P(2f,2d)+2diff and CCSD(T)/cc-pVQZ level of theories and results are given in Table 3.4. Relative energies of the two lowest-lying electronic states are presented in Table 3.5. Relativistic corrections to total energies and to the T_0 values are predicted at the CCSD and CCSD(T) levels with two different basis sets, and the results are given in Table 3.6. Effects of relativistic corrections on the Renner parameter (ϵ) were investigated and are tabulated in Table 3.7. Also, effects of relativity on the stretching harmonic frequencies

Table 3.1: Total energies (in hartree), bond distances (in Å), and dipole moments (in debye) for the $\tilde{X}\ ^2\Pi$ state of HCGe.

	Total energy	μ_e	r_e(HC)	r_e(CGe)
TZ3P(2f,2d) SCF	-2113.711019	0.402	1.0673	1.7457
TZ3P(2f,2d)+2diff SCF	-2113.711537	0.361	1.0673	1.7459
cc-pVTZ SCF	-2113.748058	0.229	1.0676	1.7456
cc-pVQZ SCF	-2113.753650		1.0670	1.7444
TZ3P(2f,2d) CISD	-2114.094117	0.237	1.0712	1.7529
TZ3P(2f,2d)+2diff CISD	-2114.095066	0.202	1.0713	1.7527
cc-pVTZ CISD	-2114.040544	0.024	1.0728	1.7553
cc-pVQZ CISD	-2114.104589		1.0709	1.7451
TZ3P(2f,2d) CCSD	-2114.136929		1.0773	1.7690
TZ3P(2f,2d)+2diff CCSD	-2114.137993		1.0775	1.7689
cc-pVTZ CCSD	-2114.069990	0.046	1.0776	1.7681
cc-pVQZ CCSD	-2114.141877	0.036	1.0762	1.7581
TZ3P(2f,2d) CCSD(T)	-2114.157130		1.0800	1.7808
TZ3P(2f,2d)+2diff CCSD(T)	-2114.158252		1.0802	1.7807
cc-pVTZ CCSD(T)	-2114.088351	0.138	1.0802	1.7794
cc-pVQZ CCSD(T)	-2114.162992	0.053	1.0790	1.7692
B3LYP/6-311G** from Reference 71.			1.082	1.775
B3LYP/6-311++G(d,p) from Reference 74.			1.082	1.774

Available experimental values:
r_0(HC)= 1.0671 Å and r_0(CGe)= 1.7758 Å from Reference 71.

were studied at the CCSD(T) level with two basis sets, and values included in Table 3.8.

3.5.1 Geometries

In Table 2.1, the optimized geometries of the $\tilde{X}\ ^2\Pi$ state are given at sixteen representative levels of theory. The two bond lengths increase with the inclusion of

Table 3.2: Harmonic vibrational frequencies (in cm^{-1}), infrared (IR) intensities (in parentheses in km mol^{-1}), and Renner parameter (ϵ) for the $\tilde{X}\ ^2\Pi$ state of HCGe.

	ω_1 (C-H Str.)	ω_3 (C-Ge Str.)	ω_2^+ (π^+,$^2A'$)	ω_2^- (π^-,$^2A''$)	ω_2^a	ϵ
TZ2P(f,d) SCF	3434(8.7)	968(58.5)	583(37.9)	589(161.1)	586	-0.0102
TZ2P(f,d)+diff SCF	3434(10.5)	966(62.9)	581(42.8)	588(188.8)	584	-0.0120
TZ3P(2f,2d) SCF	3430(8.3)	969(58.6)	584(35.6)	588(154.0)	586	-0.0070
TZ3P(2f,2d)+2diff SCF	3429(9.7)	967(62.5)	585(37.6)	590(172.3)	587	-0.0097
cc-pVTZ SCF	3427(7.6)	970(53.8)	579(38.6)	584(173.9)	581	-0.0091
cc-pVQZ SCF	3429	969	577	581	579	-0.0059
TZ2P(f,d) CISD	3360(4.8)	929(42.9)	543(26.7)	540(132.3)	541	0.0052
TZ2P(f,d)+diff CISD	3360(5.8)	928(46.4)	550(30.1)	545(151.9)	548	0.0080
TZ3P(2f,2d) CISD	3350(5.2)	935(45.9)	545(25.0)	536(126.8)	541	0.0159
TZ3P(2f,2d)+2diff CISD	3349(5.9)	935(49.3)	551(26.5)	541(140.8)	546	0.0180
cc-pVTZ CISD	3345(4.2)	930(39.4)	544(26.6)	540(141.0)	542	0.0074
cc-pVQZ CISD	3361	947	575	568	572	0.0115
TZ2P(f,d) CCSD	3290	883	437	515	477	-0.1614
TZ2P(f,d)+diff CCSD	3289	882	448	521	486	-0.1519
TZ3P(2f,2d) CCSD	3271	887	439	511	476	-0.1524
TZ3P(2f,2d)+2diff CCSD	3271	886	447	517	483	-0.1438
cc-pVTZ CCSD	3283	891	446	519	484	-0.1521
cc-pVQZ CCSD	3291	905	482	549	517	-0.1299
TZ2P(f,d) CCSD(T)	3258	853	419	495	459	-0.1656
TZ2P(f,d)+diff CCSD(T)	3257	853	455	498	477	-0.0905
TZ3P(2f,2d) CCSD(T)	3238	856	426	490	459	-0.1391
TZ3P(2f,2d)+2diff CCSD(T)	3237	855	431	496	465	-0.1386
cc-pVTZ CCSD(T)	3251	861	443	509	477	-0.1386
cc-pVQZ CCSD(T)	3258	874	474	526	500	-0.1046
B3LYP/6-311G** from Reference 71.	3235	865			492	

[a]The suitably averaged bending vibrational frequency.

correlation effects, at given a basis set. At our highest level of theory, CCSD(T)/cc-pVQZ, the C-H bond length is predicted as r_e(CH)=1.0790 Å and the C-Ge bond length as r_e(CGe)=1.7692 Å. These two r_e values are consistent with the experimental values[71] of r_0(CH)=1.0671 Å and r_0(CGe)=1.7758 Å, respectively. At this level, our prediction of r_e(CH) is 0.0119 Å longer and that of r_e(CGe) is 0.0066 Å shorter than the experimental r_0 values. The discrepancy between r_e(CH) and r_0(CH), may be atributed to relatively large zero-point vibrational correction to the C-H bond length. Smith *et al.*[71] studied the ground state of the radical with a DFT method, B3LYP/6-311G**, and predicted the bond lengths to be r_e(CH)=1.0822 Å and r_e(CGe)=1.7753 Å. Also Jackson *et al.*[74] found almost the same geometry with the values of r_e(CH)= 1.082 Å and r_e(CGe)=1.774 Å at the B3LYP/6-311++G(d,p) level. For the $\tilde{A}\ ^2\Sigma^+$ state, r_e(CH) was predicted to be 1.0737 Å and r_e(CGe) to be 1.6687 Å at the our highest level of theory, CCSD(T)/cc-pVQZ, as seen in Table 3.3. The experimental values for the $\tilde{A}\ ^2\Sigma^+$ state C-H and C-Ge bond lengths were reported by Smith *et al.*[71] as r_0(CH)=1.0588 Å and r_0(CGe)=1.6736 Å. The B3LYP/6-311G** predictions[71] of bond lengths at the excited state are r_e(CH)=1.0776 Å and r_e(CGe)=1.6655 Å and the B3LYP/6-311++G(d,p) predictions[74] are r_e(CH)=1.078 Å and r_e(CGe)=1.667 Å. Our results show that the C-H bond length decreases 0.0053 Å upon excitation, which is in good agreement with the experimental decrease of 0.0083 Å. At the same CCSD(T)/cc-pVQZ level of theory, we predict a decrease in C-Ge bond length of 0.1005 Å upon excitation, while B3LYP/6-311G** suggests a 0.110 Å decrease.[71] Our prediction is in very close agreement with the experimental[71] C-Ge bond length decrease of 0.1022 Å. As seen in Figure 3.1, the 10σ MO mainly consists of the nonbonding 4s atomic orbital on the Ge atom, while the 4π MO has the C-Ge π-bonding character shown in Figure 3.2. Therefore, a single excitation from the 10σ MO to the 4π MO in equation (4) decreases the C-Ge bond length. With the cc-pVQZ basis set, the difference in the

SCF and CCSD(T) bond lengths for the ground state is 0.012 Å for the C-H bond and 0.0248 Å for the C-Ge bond. It is observed that the C-Ge bond is more sensitive to correlation effects, due to the multiple bond character of the carbon-germanium linkage.

3.5.2 Dipole Moments

The dipole moments were determined as first derivatives of the total energies with respect to external electric fields. As seen in Table 3.1, dipole moment predictions for the ground $\tilde{X}\ ^2\Pi$ state are small. At our highest level of theory, CCSD(T)/cc-pVQZ, a value of 0.053 debye is predicted for the ground state. For the $\tilde{A}\ ^2\Sigma^+$ state, our prediction is 1.530 debye at the same level of theory. A single electron excitation from the 10σ MO to 4π MO in eq.(4) appears to increase the charge separation between the carbon and germanium atoms. For both states, CCSD and CCSD(T) predicitons are consistent with each other while SCF predictions are higher than CCSD and CCSD(T) results by amounts 0.2-0.9 debye. The CISD predictions for the dipole moments are between SCF and CCSD results. In all levels of theory and for the both states, carbon atom is negatively charged, around 0.35-0.45, and germanium atom is positively charged, around 0.25-0.35, i.e. HC^-Ge^+. The hydrogen atom is almost neutral, having a positive charge around 0.08-0.15.

3.5.3 Harmonic vibrational frequencies

When correlation effects are included, the C-H stretching (ω_1) and C-Ge stretching (ω_3) vibrational frequencies of both the $\tilde{X}\ ^2\Pi$ and $\tilde{A}\ ^2\Sigma^+$ states are lowered, which reflects the longer bond distances. The two stretching modes of the excited state have higher frequencies than the corresponding values for the ground state. Experimental values for the vibrational frequencies of the ground $\tilde{X}\ ^2\Pi$ state have not yet been reported. On the other hand, in May 2000, Smith *et al.*[71] reported the $\tilde{A}\ ^2\Sigma^+$

Table 3.3: Total energies (in hartree), bond distances (in Å), dipole moments (in debye), harmonic vibrational frequencies (in cm^{-1}), and infrared (IR) intensities (in parentheses in km mol^{-1}) for the $\tilde{A}\ ^2\Sigma^+$ state of HCGe.

	Energy	μ_e	r_e(HC)	r_e(CGe)	ω_1	ω_2	ω_3
TZ3P(2f,2d) SCF	-2113.621743	2.487	1.0619	1.6338	3497(52.4)	1037(434.2)	1179(1.6)
TZ3P(2f,2d)+2diff SCF	-2113.622268	2.494	1.0619	1.6344	3497(53.7)	1035(481.6)	1177(1.8)
cc-pVTZ SCF	-2113.658779	2.346	1.0620	1.6344	3498(50.5)	1032(482.3)	1179(0.6)
cc-pVQZ SCF	-2113.664907		1.0615	1.6331	3498		1180
TZ3P(2f,2d) CISD	-2114.021918	2.036	1.0654	1.6450	3417(61.2)		1116(0.5)
TZ3P(2f,2d)+2diff CISD	-2114.022762	2.037	1.0655	1.6453	3417(61.5)		1116(0.6)
cc-pVTZ CISD	-2113.969859	1.872	1.0663	1.6485	3421(60.0)		1107(0.1)
cc-pVQZ CISD	-2114.033947		1.0649	1.6397	3431		1131
TZ3P(2f,2d) CCSD	-2114.072212		1.0716	1.6639	3333		1056
TZ3P(2f,2d)+2diff CCSD	-2114.073159		1.0718	1.6641	3333		1056
cc-pVTZ CCSD	-2114.005954	1.623	1.0714	1.6644	3353		1055
cc-pVQZ CCSD	-2114.078351	1.725	1.0705	1.6557	3357		1078
cc-pVTZ EOM-CCSD	-2114.006210	1.220	1.0714	1.6644	3350	722	1047
cc-pVQZ EOM-CCSD	-2114.078429	1.258	1.0705	1.6557	3354	743	1070
TZ3P(2f,2d) CCSD(T)	-2114.098308		1.0748	1.6776	3293		1011
TZ3P(2f,2d)+2diff CCSD(T)	-2114.099322		1.0750	1.6779	3294		1011
cc-pVTZ CCSD(T)	-2114.030266	1.428	1.0744	1.6778	3314		1012
cc-pVQZ CCSD(T)	-2114.105434	1.530	1.0737	1.6687	3316		1034
B3LYP/6-311G** Ref. 71.			1.078	1.665	3282	713	1040
B3LYP/6-311++G(d,p) Ref. 74			1.078	1.667			

Available experimental values:

r_0(HC)= 1.0588 Å, r_0(CGe)= 1.6736 Å, ν_2=638 cm^{-1}, ν_3=990 cm^{-1} from Reference 71.

state C-Ge stretching and bending vibrational frequencies, studying the electronic transition of the radical by laser-induced fluorescence techniques. They found the C-Ge stretching vibrational frequency to be 990 cm^{-1}. We predict the corresponding frequency to be 1034 cm^{-1} with the CCSD(T)/cc-pVQZ method, and 1011 cm^{-1} with CCSD(T)/TZ2P(2f,2d)+2diff level. Smith *et al.*[71] carried out computations with the B3LYP/6-311G** method, and they found a frequency of ω_3=1040 cm^{-1}. Although CCSD(T) predicts slightly better values with all basis sets, compared to the DFT value, it is clear from Table 3.3 that CCSD(T)/cc-pVQZ result is about 20 cm^{-1} larger than the other CCSD(T) results. In fact, the cc-pVQZ basis set predicts the C-Ge stretching (ω_3) vibrational frequency of the both $\tilde{X}\ ^2\Pi$ and $\tilde{A}\ ^2\Sigma^+$ states about 15-25 cm^{-1} higher than the other basis sets, at all levels of theory except at the SCF level. This may be due to the presence of a g-function in the basis set. It is unlikely to be a result of the lack of diffuse functions, because the TZ3P(2f,2d), TZ3P(2f,2d)+2diff, and cc-pVTZ basis sets predict very similar vibrational frequencies. Therefore, we think that the results with our second largest basis set TZ3P(2f,2d)+2diff (which comprises 143 contracted Gausssian functions, 10 less than cc-pVQZ) for the harmonic vibrational frequencies may be considered more reliable. The excited state C-H stretching vibrational frequency was determined to be 3294 cm^{-1}, at the CCSD(T)/TZ2P(2f,2d)+2diff level, for which there is no experimental value. The B3LYP/6-311G** prediction[71] for this mode is 12 cm^{-1} less than our prediction.

For the excited state bending mode, the EOM-CCSD method was employed to avoid variatonal collapse due to the identical symmetry of the excited state with the $^2A'$ component of the ground $\tilde{X}\ ^2\Pi$ state in the bent structures. We determined values of 743 cm^{-1} and 722 cm^{-1} at the EOM-CCSD/cc-pVQZ and EOM-CCSD/cc-pVTZ levels of theory. Although the EOM-CCSD/cc-pVTZ result is better, it deviates from the experimental result[71] of 638 cm^{-1} by 84 cm^{-1}. Such deviations are

probably caused by the fact that EOM calculations were performed on geometries which were optimized at the CCSD level. For the same mode, Smith *et al.*[71] predict 713 cm^{-1} at the B3LYP/6-311G** level, which is close to our predictions, and is 75 cm^{-1} larger than the experimental value.

As mentioned before, there are no experimental values for the ground state vibrational frequencies. Therefore, we present all of our results for these vibrational frequencies in Table 3.2. The ground state C-H stretching (ω_1) vibrational frequency is predicted to be 3237 cm^{-1}, and the C-Ge stretching (ω_3) to be 855 cm^{-1} at the CCSD(T)/TZ3P(2f,2d)+2diff level. Again, the cc-pVQZ basis set produce higher vibrational frequencies by 10-15 cm^{-1} in all correlated methods. The B3LYP/6-311G** results[71] are 3235 cm^{-1} and 865 cm^{-1}, which are close to our predictions.

The effects of isotopic substitution of germanium on the C-Ge stretching harmonic vibrational frequency were determined at the two highest levels of theory, CCSD(T)/TZ3P(2f,2d)+2diff and CCSD(T)/cc-pVQZ. As seen in Table 3.4, at the CCSD(T)/cc-pVQZ level, the difference between the smallest vibrational frequency (for $HC^{76}Ge$) and the largest one (for $HC^{70}Ge$) is 5.4 cm^{-1} for the ground $\tilde{X}\ ^2\Pi$ state and 6.5 cm^{-1} for the excited $\tilde{A}\ ^2\Sigma^+$ state. Because the C-H stretching and bending vibrational frequencies do not change very much (on the order of 0.1 cm^{-1} for the bending and 0.01 cm^{-1} for the C-H stretching), they were not included in the table. Smith *et al.*[71] experimentally investigated the effects of germanium isotopes on the excitation energies between $\tilde{A}\ ^2\Sigma^+$-$\tilde{X}\ ^2\Pi$ states. They determined $HC^{72}Ge$-$HC^{74}Ge$ isotope splittings as 2.2 cm^{-1} for the 3_0^1, 4.2 cm^{-1} for the 3_0^2, and 6.0 cm^{-1} for the 3_0^3 bands. We evaluated the same splittings as 2.25 cm^{-1} for the 3_0^1, 4.35 cm^{-1} for the 3_0^2, and 6.45 cm^{-1} for the 3_0^3 bands, using the values of the predicted C-Ge stretching vibrational frequencies for the $HC^{72}Ge$ and $HC^{74}Ge$ at the CCSD(T)/TZ3P(2f,2d)+2diff level. This excellent agreement between experiment and theory supports the reliability of the CCSD(T)/TZ3P(2f,2d)+2diff predictions

Table 3.4: Theoretical predictions of the C-Ge stretching harmonic vibrational frequency (ω_3) for the isotopomers of HCGe.

	$HC^{70}Ge$	$HC^{72}Ge$	$HC^{73}Ge$	$HC^{74}Ge$	$HC^{76}Ge$
$\tilde{X}\ ^2\Pi$ state					
TZ2P(2f,2d)+2diff CCSD(T)	858.9	857.0	856.0	855.2	853.5
cc-pVQZ CCSD(T)	877.2	875.3	874.4	873.5	871.8
$\tilde{A}\ ^2\Sigma^+$ state					
TZ2P(2f,2d)+2diff CCSD(T)	1015.7	1013.5	1012.4	1011.4	1009.4
cc-pVQZ CCSD(T)	1038.8	1036.5	1035.4	1034.3	1032.3

of the physical properties. Specifically, the theoretically predicted ground state vibrational frequencies will be useful in determining experimental (unknown) frequencies. As we will discuss later, CCSD(T)/TZ3P(2f,2d)+2diff level of theory predicts the best value for the quantum mechanical splitting (T_0) which is only 0.14 kcal/mol (49.0 cm^{-1}) larger than the experimental value, after including relativistic effects.

3.5.4 Renner-Teller splitting in the $\tilde{X}\ ^2\Pi$ state

As discussed previously, the ground state of the HCGe radical has two distinct real bending vibrational frequencies. One of them corresponds to the bending motion of the $^2A'$ state, where the single electron in the 4π MO is in the plane which transforms as a' in point group C_s. The other vibrational frequency corresponds to the bending motion of the $^2A''$ state, where the singly-occupied orbital is in the plane and transforms as a''. As seen in Table 3.2, the Renner parameter (ϵ) has a magnitude of the order of 0.01 at the SCF and CISD levels, about 10 times smaller than the values from CCSD and CCSD(T) levels. Another important point is that the CISD method predicts positive values for the Renner parameter, while SCF,

CCSD, and CCSD(T) predict negative values. Negative values mean that the $^2A'$ (=V^+) surface, which corresponds to the electronic state that is symmetric under reflection in the plane of the bent molecule, lies below the $^2A''$ surface (=V^-).

This feature is illustrated in Figure 3.3, where the energy difference between the two surfaces is plotted using 24 different levels of theory. As seen in the figure, the difference ($^2A'$ - $^2A''$) is positive for the CISD levels, whereas it is negative with the SCF, CCSD and CCSD(T) methods. The sign change in CISD cannot be readily attributed to the treatment of correlation effects in CISD compared to CCSD and CCSD(T), because SCF predicts the same sign as CCSD and CCSD(T). For the $^2A'$ state energy calculations, we suspect that the CISD somehow overestimates the energy contribution from the configurations formed by the single excitations. However, higher order excitations in CCSD and CCSD(T) can reduce the effects of single excitations, because of the huge number of different excitations formed, compared to the CI expansion. The *magnitude* of the splitting, the absolute value of the Renner parameter, can be attributed to the incomplete treatment of electron correlation in CISD, because the SCF method also predicts very small splittings.

The Renner parameter for the $\tilde{X}$ $^2\Pi$ state was determined as -0.1046 at the CCSD(T)/cc-pVQZ level, and -0.1386 at the CCSD(T)/TZ3P(2f,2d)+2diff level. There is no available experimental value for the ϵ, as well as no previous theoretical prediction. Our CCSD(T)/TZ3P(2f,2d)+2diff result should be more reliable, inasmuch as it is very consistent with the other basis set results. We recently investigated the Renner-Teller effect in HCSi and reported the Renner parameter as -0.1136 at the CCSD(T)/cc-pVQZ level and -0.1242 at the CCSD(T)/TZ3P(2f,2d)+2diff level,[75] which are close to the ϵ values for HCGe. It is important to note that the CCSD(T)/cc-pVQZ method predicts smaller ϵ values (in absolute magnitudes) than the CCSD(T)/TZ3P(2f,2d)+2diff level by 0.02, for both radicals HCSi and HCGe.

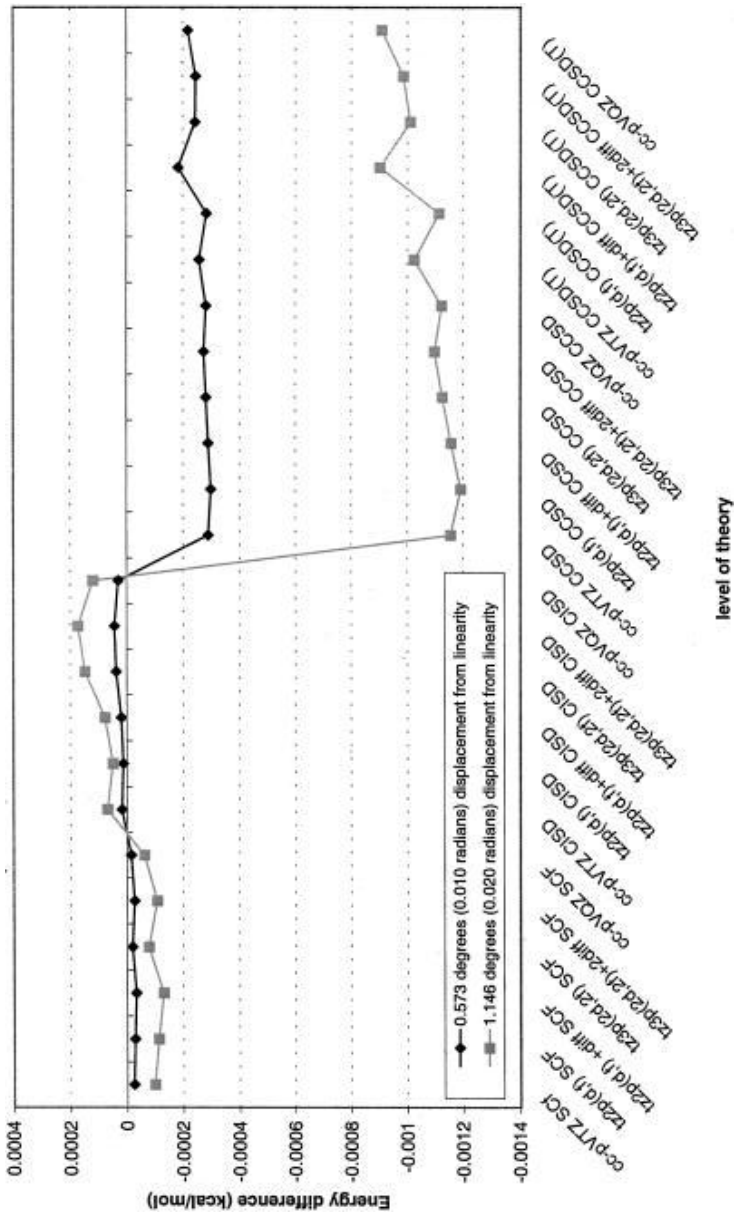

Figure 3.3: The energy difference between the $^2A'$ and $^2A''$ Renner-Teller components of the $\tilde{X}\ ^2\Pi$ state

3.5.5 Infrared (IR) intensities

The most intense IR mode for the ground $\tilde{X}\ ^2\Pi$ state is found for the ω_2^- vibrational frequency, which corresponds to the $^2A''$ Renner-Teller component. As seen in Table 3.2, this mode has an intensity of 140.8 km mol^{-1} whereas the other mode ω_2^+, which corresponds to the $^2A'$ component, has only a 26.5 km mol^{-1} intensity at the CISD/TZ3P(2f,2d)+2diff level. The C-Ge stretching vibrational mode is much more intense for the ground $\tilde{X}\ ^2\Pi$ state comparing to the excited $\tilde{A}\ ^2\Sigma^+$ state. The situation is the reverse for the C-H stretching mode, which has 5.9 km mol^{-1} intensity for the ground state whereas the intensity for the excited state is 61.5 km mol^{-1}. For the excited state bending mode, we could not determine the intensity due to the variational collapse. Although we present SCF results for the intensity of this mode, they may not be too reliable for the reason just mentioned.

3.5.6 Energetics

The classical $\tilde{X}$-$\tilde{A}$ splitting was predicted to be 56.0 (SCF), 45.4 (CISD), 40.7 (CCSD), and 37.0 kcal/mol [CCSD(T)], with the TZ3P(2f,2d)+2diff basis set. This basis set provides better energetics than the cc-pVQZ basis set which predicts 0.7-0.9 kcal/mol smaller energy separations than the TZ3P(2f,2d)+2diff values. It is seen that advanced treatments of correlation effects decrease the energy seperation, while increase of the basis set size provides larger separations. At the CCSD(T) level, the difference between result of TZ2P(f,d) and that of TZ3P(2f,2d)+2diff is 0.4 kcal/mol. We include zero-point corrections for all basis sets, using the EOM-CCSD/cc-pVTZ value for the $\tilde{A}\ ^2\Sigma^+$ state bending mode. As seen in Table 3.5, the T_0 value was predicted to be 38.0 kcal/mol at the CCSD(T)/TZ3P(2f,2d)+2diff level. The experimental value was determined by Smith *et al.*[71] to be T_0=39.75 kcal/mol (13901.8297 cm^{-1}). Comparing with the experimental value, the SCF, CISD, and

CCSD methods overestimate the energy gap in all basis sets, whereas the CCSD(T) energy separations are in good agreement with the experimental value. Although our CCSD(T)/TZ3P(2f,2d)+2diff result of 38.0 kcal/mol is much better than B3LYP/6-311G** result of 45.4 kcal/mol (15875 cm^{-1}),[71] we still see a 1.7 kcal/mol deviation from the experiment. Considering the fact that we recently predicted[75] the $\tilde{X}$-$\tilde{A}$ energy gap for HCSi within 0.12 kcal/mol error at the CCSD(T)/TZ3P(2f,2d)+2diff level of theory, we think that the 1.7 kcal/mol deviation for the HCGe molecule is not satisfactory. As seen in Table 3.5, after addition of relativistic effects, Darwin and mass-velocity terms determined at the CCSD(T)/cc-pVQZ level, we predicted a value of 39.9 kcal/mol at the CCSD(T)/TZ3P(2f,2d)+2diff level which is only 0.14 kcal/mol (=49 cm^{-1}) larger than the experimental value. In the next section, effects of relativistic corrections on several physical properties as well as the energy gap will be discussed in detail.

3.5.7 Effects of relativistic corrections

The power series expansion of the exact solution of the Dirac equation for hypothetical relativistic atoms without any electron correlation produces very simple equations for estimating the relativistic corrections.[20,76] Especially, the second term in the expansion in powers of c^{-1};

$$e^{(2)} = (\frac{3}{8n^4} - \frac{1}{2n^3|\kappa|})Z^4 \tag{3.7}$$

where n and κ ($|\kappa|$=j+1/2) are quantum numbers, produces more than 96 percent of the total relativistic corrections for atoms up to Kr(Z=36)[76] (note that the first term in this expansion is just the non-relativistic energy). This term gives a value of around -21 hartree for germanium, considering it as a hypothetical relativistic atom without any electron correlation. All of our predictions about the relativistic corrections for the HCGe radical are in good agreement with this simple model.

Table 3.5: Energy separations, T_e, (kcal/mol), between $\tilde{X}\ ^2\Pi$ and $\tilde{A}\ ^2\Sigma^+$ states (T_0 values in parentheses).

	TZ2P(f,d)	TZ2P(f,d)+diff	TZ3P(2f,2d)	TZ3P(2f,2d)+2diff	cc-pVTZ	cc-pVQZ
SCF	56.06(56.87)	56.11(56.92)	56.02(56.83)	56.02(56.82)	56.03(56.85)	55.69(56.51)
CISD	44.78(45.68)	44.89(45.78)	45.31(46.20)	45.37(46.25)	44.36(45.25)	44.33(45.15)
CCSD	40.28(41.34)	40.40(41.43)	40.61(41.67)	40.68(41.72)	40.18(41.22)	39.86(40.81)
CCSD(T)	36.58(37.66)	36.69(37.73)	36.91(37.99)	36.98(38.04)	36.45(37.48)	36.12(37.08)
[a]CCSD	42.13(43.19)	42.25(43.29)	42.47(43.52)	42.54(43.57)	42.04(43.07)	41.72(42.67)
[a]CCSD(T)	38.44(39.52)	38.55(39.58)	38.77(39.84)	38.84(39.89)	38.31(39.33)	37.98(38.94)

[a]Includes relativistic effects determined at the CCSD(T)/cc-pVQZ level.

T_0=39.75 kcal/mol [13901.8297(6) cm^{-1}, 1.724 ev] from experiment, Reference 71.
B3LYP/6-311G** T_e=45.39 kcal/mol (15875 cm^{-1}) from Reference 71.
B3LYP/6-311++G(d,p) T_e=35.2 kcal/mol from Reference 74.

Table 3.6: Relativistic corrections, sum of Darwin and mass-velocity terms, to total energies (in hartree), and to T_0 values (in kcal/mole).

	Correction to $\tilde{X}\ ^2\Pi$ state	Correction to $\tilde{A}\ ^2\Sigma^+$ states	$\Delta\ T_0$*
cc-pVTZ CCSD	-21.238956	-21.236911	+1.277
cc-pVQZ CCSD	-21.240123	-21.237223	+1.813
cc-pVTZ CCSD(T)	-21.239117	-21.236958	+1.348
cc-pVQZ CCSD(T)	-21.240343	-21.237382	+1.852

*The contribution from the relativistic ZPVE changes was estimated to be -0.0066 kcal/mol at the CCSD(T)/cc-pVQZ level, and included into all $\Delta\ T_0$ values.

The most important effect of relativity was seen to be on the energetics of the system. As we mentioned before, the best non-relativistic T_0 value predicted is 38.0 kcal/mol which is 1.7 kcal/mol smaller than the experimental value of 39.7 kcal/mol. The relativistic corrections to total energies and to T_0 values are presented in Table 3.6. As seen in the table, the cc-pVQZ basis set predicts larger corrections than the cc-pVTZ basis set. When the CCSD(T)/cc-pVQZ result is taken into account, the corrected T_0 values are in very good agreement with experiment, as seen in Table 3.5. The T_0 value is predicted to be 39.9 kcal/mol at the CCSD(T)/TZ3P(2f,2d)+2diff level of theory which is only 0.14 kcal/mol larger than the experimental result. The effects of relativity on the non-degenerate bending harmonic vibrational frequencies of the two components of the $\tilde{X}\ ^2\Pi$ state are small. The results of four different level of theory are presented in Table 3.7. The two bending vibrational frequencies decrease by amounts of 2-3 cm^{-1} when the relativistic corrections are included. Dyall *et al.*[26] investigated relativistic effects on the several spectroscopic constants for the XH_4 and XH_2 (X=Si, Ge, Sn, and Pb) systems, and they reported that the effects of relativity were seen in the shorter bond lengths and higher frequencies

for XH_4, but lower stretching frequencies for the XH_2 systems. They reported 0.004 Å and 0.003 Å bond length decreases for GeH_2 by perturbation theory and Dirac-Hartree-Fock calculations, respectively, which in turn result in 3-4 cm^{-1} increases in the bending vibrational frequency. Therefore, it is desirable that geometry re-optimization including the relativistic effects should be done in order to predict the changes in the bending modes. The relativistic corrections also decrease the Renner-Teller splitting, and again, the cc-pVQZ basis set predicts larger effects than the cc-pVTZ basis. The resultant relativistic correction to the Renner parameter ϵ is +0.0079 at the CCSD(T)/cc-pVQZ level of theory. The effects can be larger for the stretching vibrational frequencies. It is observed that relativistic corrections decrease the C-Ge stretching frequency by amounts of 15-20 cm^{-1} while its effects are on the order of 3-4 cm^{-1} for the C-H stretching mode, as seen in Table 3.8. Dyall *et al.*[26] reported that the symmetric stretching vibrational frequency [$\omega_1(a_1)$] of GeH_2 decrease 11 cm^{-1} (PT) and 12 cm^{-1} (DHF) with inclusion of relativity, consistent with our results. With the inclusion of the relativistic effects, the excited state C-Ge stretching frequency is determined to be 1014 cm^{-1} and 990 cm^{-1} at the CCSD(T)/cc-pVQZ and CCSD(T)/cc-pVTZ levels, respectively. As we mentioned before, the TZ3P(2f,2d)+2diff basis set predicts more reliable values than the cc-pVQZ basis set, and for the C-Ge mode, the cc-pVTZ predictions are very close to TZ3P(2f,2d)+2diff. Our relativistic CCSD(T)/cc-pVTZ result for the $\tilde{A}\ ^2\Sigma^+$ state C-Ge harmonic vibrational frequency (ω_3) is almost the same as the experimental[71] fundamental of ν_3=990 cm^{-1}. Therefore, perhaps the relativistic CCSD(T)/cc-pVTZ result of 846.4 cm^{-1} should be a more reliable value for the ground $\tilde{X}\ ^2\Pi$ state C-Ge stretching mode, for which experimental value is not available.

We investigated the change of the relativistic corrections at each displacement of the C-H and C-Ge internal coordinates. When one of the two internal coordinates

Table 3.7: Effects of relativistic corrections on two-non degenerate bending vibrational frequencies, $\omega_2^+(\pi^+,^2A')$ and $\omega_2^-(\pi^-,^2A'')$, and on the Renner parameter, for the $\tilde{X}\ ^2\Pi$ state (non-relativistic/with the inclusion of Darwin and Mass-velocity terms).

	$\omega_2^+(\pi^+,^2A')$	$\omega_2^-(\pi^-,^2A'')$	ω_2(averaged)	ϵ	$\Delta\ \epsilon$ (x10^{-3})
cc-pVTZ CCSD	445.6/443.1	519.4/514.5	483.9/480.1	-0.1521/-0.1483	+3.8
cc-pVQZ CCSD	482.1/483.8	549.4/547.8	516.8/516.7	-0.1299/-0.1236	+6.3
cc-pVTZ CCSD(T)	443.0/442.7	509.3/506.0	477.3/475.4	-0.1386/-0.1329	+6.0
cc-pVQZ CCSD(T)	473.5/476.9	526.0/525.5	500.4/501.8	-0.1046/-0.0967	+7.9

Table 3.8: Effects of relativistic corrections on stretching harmonic vibrational frequencies (in cm^{-1}), and on the zero point vibrational energy (non-relativistic/with the inclusion of Darwin and mass-velocity terms).

	CCSD(T)/cc-pVTZ	CCSD(T)/cc-pVQZ	Experiment
$\tilde{X}\ ^2\Pi$ state			
ω_1(C-H Str.)	3251.4/3248.6	3257.8/3263.2	
ω_3(C-Ge Str.)	860.8/846.4	873.5/851.9	
ZPVE	2533/2523	2566/2559	
$\tilde{A}\ ^2\Sigma^+$ states			
ω_1(C-H Str.)	3314.0/3310.7	3316.2/3313.5	
ω_3(C-Ge Str.)	1012.2/990.2	1034.3/1014.4	ν_3=990
ZPVE*	2885/2872	2897/2886	

*For the $\tilde{A}\ ^2\Sigma^+$ state bending mode (ω_2), the non-relativistic EOM-CCSD/cc-pVTZ value is used for both relativistic and non-relativistic ZPVEs.

is changed, the other one is fixed. Figure 3.4 shows the variations of the relativistic effects in terms of the two internal coordinates.

The displacements along the C-H and C-Ge internal coordinates produce the similar effect in the one electron Darwin term, which corrects the Coulomb attraction. In both cases, the Darwin term increases with the positive displacements, and decreases (gets more negative) with the negative displacements. However, the variation in mass-velocity term is in the opposite directions for the two internal coordinates, as seen in Figure 3.4.a The variation for the total correction, the sum of the two terms, is again in opposite directions. For the C-H displacements, variations in the total correction are very small as expected because almost all of the relativistic corrections come from the germanium atom. However, displacements along the C-Ge internal coordinate cause significant variations in the total energy correction. As seen in Figure 3.4.c and 3.4.d, positive displacements from the equilibrium

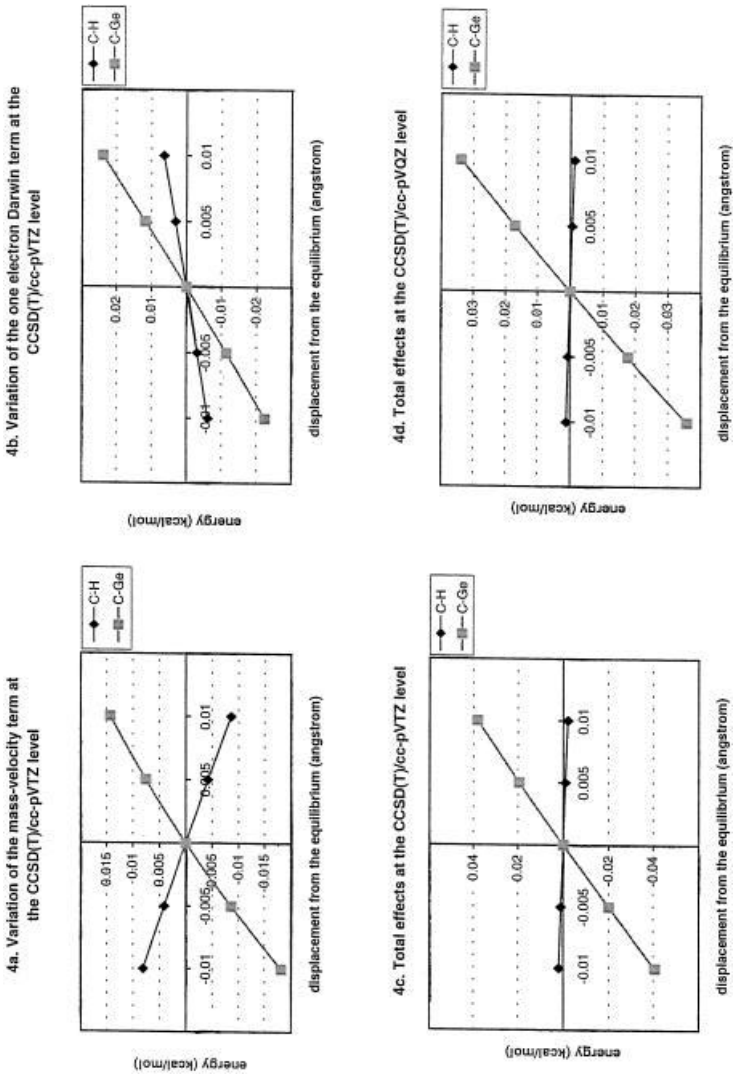

Figure 3.4: Variations of the mass-velocity term, one electron Darwin term, and the total relativistic energy corrections with the displacements along the C-H and C-Ge internal coordinates, for the $\tilde{X}\ ^2\Pi$ state (energies are relative to the equilibrium energy).

distance produce higher energies, while negative displacements produce negative energy corrections. In other words, the shorter C-Ge bond distance minimizes the total relativistic energy correction, which result in the common term 'relativistic bond contraction'. For some systems where three or more heavy atoms are adjacent, this kind of analysis of the total relativistic energy correction calculated on the non-relativistic geometries may be helpful in deciding whether a specific bond contracts or elongates with the inclusion of the total relativistic effects of the system. In all physical systems, it is expected that the geometry changes in a way that the total relativistic energy correction is minimized, the same as the total energy of the system. Using this argument for our system, the C-H bond should elongate slightly and the C-Ge bond should contract with the inclusion of relativity, a result of the fact that slope of the C-Ge lines is positive, whereas that of the C-H lines is negative, as seen in Figure 3.4.c and 3.4.d.

3.6 Concluding Remarks

The germanium methylidyne molecule (HCGe) is valence isoelectronic with the C_2H radical, well known in combustion chemistry. In the present study, the properties of HCGe have been investigated with a variety of theoretical methods. As was found for the HCSi radical, both the $\tilde{X}\ ^2\Pi$ and $\tilde{A}\ ^2\Sigma^+$ states of HCGe are found to have linear structures. It is observed that the CCSD(T) method in conjunction with large basis sets is able to predict very reliable values for many physical properties. The relativistic one-electron Darwin and mass-velocity terms are calculated using first-order perturbation theory and effects of these corrections on energetics, harmonic vibrational frequencies, and Renner-Teller splitting are discussed. The relativistic effects were seen to produce lower stretching vibrational frequencies and larger energy gaps between the ground $\tilde{X}\ ^2\Pi$ and first excited $\tilde{A}\ ^2\Sigma^+$ states. Although non-relativistic

estimations of the quantum mechanical splitting (T_0 value) and harmonic vibrational frequencies agree reasonably well with the available experimental values, inclusion of the relativistic corrections produces excellent agreement between the theory and the experiment. This feature indicates that it may be necessary for germanium compounds to take relativistic considerations into account to make quantitative spectroscopic predictions.

Chapter 4

An L-Shaped Equilibrium Geometry for Germanium Dicarbide(GeC_2)? Interesting Effects of Zero-Point Vibration, Scalar Relativity, and Core-Valence Correlation *

*Levent Sari, Kirk A. Peterson, Yukio Yamaguchi, and Henry F. Schaefer III. Journal of Chemical Physics, 117, 10008 (2002). Reprinted by permission of the American Institue of Physics.

4.1 Abstract

The ground state potential energy surface of the GeC_2 molecule has been investigated at highly correlated coupled cluster levels of theory. Large basis sets including diffuse functions and functions to describe core correlation effects were employed in order to predict the true equilibrium geometry for GeC_2. Like the much-studied valence isoelectronic SiC_2, the linear ($^1\Sigma^+$), L-Shaped ($^1A'$), and T-Shaped structures ($^1A_1$) must be investigated. The L-Shaped C_s geometry is found to have real harmonic vibrational frequencies along every internal coordinate, and the linear stationary point has an imaginary vibrational frequency along the bending mode at every level of theory employed. The T-Shaped geometry is found to have an imaginary vibrational frequency along the asymmetric stretching mode. At the coupled cluster with single and double excitations and perturbative triple excitations [CCSD(T)]/correlation consistent polarized valence quadruple-ζ (cc-pVQZ) level, the non-relativistic classical relative energies of the T-Shaped and linear structures with respect to the L-Shaped minimum are 0.1 kcal/mol and 2.8 kcal/mol, respectively. Including zero-point vibrational energy (ZPVE), scalar relativistic, and core-valence corrections, the T-L energy separation is shifted to 0.4 kcal/mol and the relative energy between the L-Shaped and linear structures is still 2.8 kcal/mol. All non-relativistic and relativistic computations predict that the L-Shaped ($^1A'$) structure is most favored for the ground state. The linear structure is predicted to be a transition state, as the case of SiC_2.

4.2 Introduction

The group IV diatomics and triatomics such as CSi, CSi_2, SiC_2, GeC, Ge_2C, GeC_2, and SnC have held a growing interest for both experimental and theoretical researchers, mainly due to the their extraordinary electronic structures and potential

usages in optoelectronic and semiconductor applications.[77–82] The inconsistency in the electronic structures of these periodically related species gave rise to incorrect conclusions about the ground state structures, some of which had been held for many years. One reason for encountering these surprising results is that C, Si, Ge, and Sn have different core sizes, which play a significant role in the minimum energy geometries and in the extent of relativistic energy corrections. Also, the absence of occupied d-electrons for C and Si causes an unbalanced competition for the valence electrons compared to Ge or Sn. There have been many cases reported in the literature showing this inconsistency. For instance, the ground state of C_2[83] is $^1\Sigma_g^+$, that of CSi[81] is $^3\Pi$, and for Ge_2[84] it is $^3\Sigma_g^-$. Further, C_3 has a linear structure [85] in its ground state ($^1\Sigma_g^+$), Si_3 has a triangular structure[86] ($^1A_1$), while $GeSi_2$ is predicted[80] to have a triplet ($^3B_2$) rather than singlet ground state.

The most discussed molecule of this kind is SiC_2. Once evidences were found for SiC_2 in carbon rich stars[87] in 1926, it became a focus of interest. However until 1982, experimental and theoretical studies seemed to show that SiC_2 has a linear structure in its ground state ($^1\Sigma^+$). In 1982, Bondybey[88] carried out a time-resolved laser-induced fluorescence spectroscopy experiment, and he concluded that linear ground state structure is not *a priori* obvious. The first *ab initio* study of SiC_2 was published by Green[89] in 1983. They excluded the possibility of the CSiC isomer, and concluded that the linear $^1\Sigma^+$ state is the ground state. However, in 1984, Grev and Schaefer[90] carried out CISD/DZP studies and reported that the T-Shaped $^1A_1$ state is in fact lower in energy than the linear structure by 0.4 kcal/mol. Simultaneously, Smalley and coworkers[91] concluded that the linear $^1\Sigma^+$ structure is not consistent with the observed rotational spectra. In 1988, Shepherd and Graham[92] performed fourier transform infrared spectroscopy (FTIR) experiments and confirmed the cyclic T-Shaped geometry for the ground state ($^1A_1$).

The analogous GeC_2 molecule was detected by Schmude, Gingerich, and Kingcade[82] in a mass spectrometry experiment in 1995. They reported enthalpies of formation for GeC_2 as well as Ge_2C, Ge_2C_2, and Ge_3C. However, they assumed the structure of GeC_2 to be T-Shaped, considering the Si analog. Of course, the mass spectroscopic experiments did not provide any information concerning the geometry of the global minimum and the electronic structure. The only theoretical study to date was reported by Li et al.[80] in 2001. They performed DFT calculations on A_mB_n (A,B = Si,Ge,C and m+n $<$ 10). For GeC_2, they excluded the possibility of a linear structure, stating that AB_2 binary clusters of group IV elements have extremely low stabilities for linear geometries. Li and coworkers reported that GeC_2, Ge_2C, SiC_2, Si_2C, and $SiGe_2$ all have T-Shaped geometries in their ground states.

Because there is no experimental data pertinent to the structure and energetics of the GeC_2 system, as well as no high level theoretical study, we aimed to study the ground state electronic structure of this elusive molecule by employing highly correlated coupled-cluster theories in conjunction with substantial basis sets. Especially, we wanted to see the effects of relativistic and core-valence correlations on the structure and energetics of the system due to the existence of the Ge atom. The primary motivation here is that the ground state potential energy surface is extremely flat, like SiC_2, and even 2-3 kcal/mol energy is sufficient to invert the Ge atom around the molecule. Secondly, the main differences between the Si and Ge atoms are (a) the relatively large core of Ge, which makes relativity more important; and (b) the 3d electrons of Ge which gives rise to additional core-valence correlations with the 4s and 4p electrons. Therefore, the Ge atom sometimes behave differently from the Si atom, and in turn, the ground state potential energy surface of GeC_2 might be different from that of SiC_2, due to the fact that very small energy differences determine the shape of the surface.

4.3 Electronic Structure Considerations

The three different geometries that have been studied in this work are given in Figure 4.1 The ground electronic state of GeC_2 has accordingly the following electronic configurations:

Linear $C_{\infty v}$ symmetry,

$$[core](10\sigma)^2(11\sigma)^2(12\sigma)^2(13\sigma)^2(4\pi)^4 \Rightarrow \quad {}^1\Sigma^+ \tag{4.1}$$

Cyclic C_{2v} symmetry (T-Shaped geometry),

$$[core](9a_1)^2(10a_1)^2(5b_2)^2(4b_1)^2(11a_1)^2(12a_1)^2 \Rightarrow \quad {}^1A_1 \tag{4.2}$$

Bent C_s symmetry (L-Shaped geometry),

$$[core](13a')^2(14a')^2(15a')^2(5a'')^2(16a')^2(17a')^2 \Rightarrow \quad {}^1A' \tag{4.3}$$

In the above equations, [core] denotes the sixteen core (Ge: 1s-, 2s-, 2p-, 3s-, 3p-, and 3d-like and C: 1s-like) orbitals. One of the 4π molecular orbitals (MOs) of linear GeC_2 becomes the $4b_1$ MO for the T-Shaped structure and represents the π bonding. The $5a''$ MO of the L-Shaped structure corresponds to the π molecular orbital. The in-plane π MO in the L-Shaped structure is mixed with other MOs of the same symmetry. The 10σ and 11σ MOs of the linear structure, $9a_1$, $10a_1$, and $5b_2$ MOs of the T-Shaped, and $13a'$ and $14a'$ MOs of the L-Shaped arrangement correspond to the σ(C-C) + σ(C-Ge) and σ(C-C) - σ(C-Ge) bonds. The 12σ and 13σ orbitals of the linear structure, $11a_1$ and $12a_1$ orbitals for T-Shaped, and $16a'$ and $17a'$ orbitals for L-Shaped are associated with the lone pairs of the C and Ge atoms, respectively.

4.4 Theoretical Methods

SCF (restricted open shell) wave functions have been used for the zeroth order descriptions of the ground state for each geometry (T-Shaped, linear, and L-Shaped).

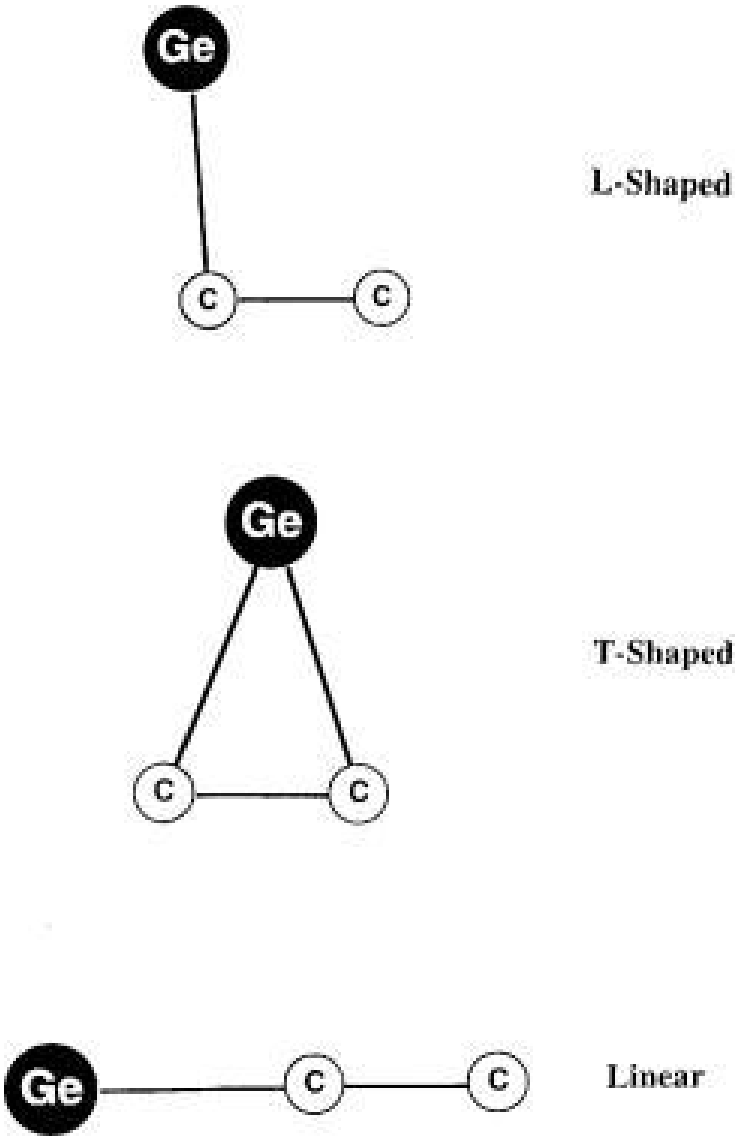

Figure 4.1: The three different geometries of GeC_2 studied in this work.

The configuration interaction with single and double excitations (CISD), the coupled cluster with single and double excitations (CCSD),[60] and CCSD with perturbative triple excitations [CCSD(T)][61] methods have been employed to include correlation effects. The eleven lowest-lying MOs (Ge: 1s-, 2s-, 2p-, 3s-, 3p-like and C: 1s-like) were frozen and the two highest-lying virtual MOs were deleted with all correlated levels with the TZ2P+diff and TZ3P(2f) basis sets. Only the eleven lowest-lying MOs were frozen for the correlation consistent basis sets (cc-pVXZ). In the correlated relativistic calculations, core and core-valence correlation effects were explicitly included.

Four basis sets, TZ2P+diff, TZ3P(2f), cc-pVTZ, and cc-pVQZ, were used at the SCF, CISD, and CCSD levels, for all three structures. The triple-ζ (TZ) valence basis for germanium is obtained from Schäfer, Huber, and Ahlrichs[72] with the contraction scheme (17s12p6d/6s5p2d). The TZ basis set for carbon is from Dunning's contraction[57] of Huzinaga's primitive Gaussian set[58] with the contraction scheme (10s6p/5s3p). The detailed descriptions of these basis sets were given in our recent study of HCGe.[93] To obtain more reliable results for the L-Shaped and T-Shaped geometries, which are the main candidates for the ground state, an aug-cc-pVTZ basis set was also included at the CCSD(T) level. All correlation consistent basis sets were obtained from the EMSL basis set library.[73]

The cc-pwCVTZ basis set for germanium is constructed here from the cc-pVTZ set by adding two s-functions with orbital exponents 5.6565 and 0.9693, two p-functions with orbital exponents 3.1638 and 1.4818, two d-functions with α= 2.9448 and 1.0686, two f-functions (5.2610 and 1.3303), and one g-function (1.5394). This new basis set, designated correlation consistent polarized weighted core-valence triple-ζ (cc-pwCVTZ), is weighted so that core-valence correlation effects are stressed. This choice is due to the fact that we employ the mass-velocity and Darwin (MVD) contributions for recovering the relativistic effects. This per-

turbative method for recovering relativistic effects couples with the correlation treatment (especially correlation effects involving electrons near the nuclei) because it is based on the Breit-Pauli relativistic Hamiltonian.[19,20] Therefore, we tried to avoid overemphasizing the core-core correlation when employing the cc-pwCVTZ basis set. Pure angular momentum d and f functions were used throughout.

The geometry optimizations and harmonic vibrational frequency evaluations for all three structures were performed using analytic first and second derivative methods[62,63] at the SCF level. At the CISD level, optimizations were performed using gradients, whereas for the frequency calculations five-point numerical differentiation of the total energies was used. At all coupled-cluster levels, both geometry optimizations and harmonic vibrational frequency evaluations were carried out using five-point numerical differentiation of the total energies. In the relativistic optimizations and frequency calculations, the same five-point procedure was used with the total relativistic energies (non-relativistic + MVD correction). Cartesian forces at optimized geometries were required to be less than 10^{-7} hartree/bohr in all geometry optimizations.

In the evaluation of the relativistic energy corrections, the one-electron Darwin term, which is always positive, and the mass-velocity term, which is always negative, were evaluated using first-order perturbation theory.[23,24] The Darwin term corrects the Coulomb attraction, and the mass-velocity term corrects the kinetic energy of the system. This level of relativistic treatment gives adequate results for germanium compounds (and other atoms up to Z=40) compared to methods such as Dirac-Hartree-Fock (DHF) and the use of relativistic effective core potentials (RECP).[26,76]

Throughout our study, all computations were carried out using the PSI 2.0.8 program package,[64] except the evaluation for relativistic effects which was performed

using the ACES II package.[65] IBM RS/6000 workstations, an IBM SP2, and PCs were used.

4.5 Results and Discussion

4.5.1 Non-Relativistic Results

We present the equilibrium geometries, total energies, dipole moments evaluated at some levels, and harmonic vibrational frequencies for the T-Shaped geometry ($^1A_1$) in Table 4.1. Similar properties for the linear structure ($^1\Sigma^+$) are given in Table 4.2, and those for the L-Shaped geometry ($^1A'$) may be seen in Table 4.3.

Geometries

Table 4.1 indicates that the T-Shaped geometry was optimized at every level of theory. The C-C bond length r_e(CC) systematically increases with the inclusion of correlation effects. At the SCF level it is $\sim$ 1.25 Å, at the CISD level $\sim$ 1.26 Å, at the CCSD level $\sim$ 1.27 Å, and at the CCSD(T) level $\sim$ 1.28 Å. However, the same trend is not observed for the Ge-C bond distance. As seen in Table 4.1, the basis set dependence is more apparent than the effects of correlation for r_e(GeC). This distance changes between 1.96 Å and 1.92 Å depending on the basis set choice. For instance, with the TZ2P+diff basis set r_e(GeC) is 1.943 Å at the SCF level, 1.938 Å at the CISD level, 1.947 Å at the CCSD level, and 1.956 Å at the CCSD(T) level, which distances are reasonably close to each other. At the highest non-relativistic level of theory, CCSD(T)/cc-pVQZ, r_e(CC) is predicted to be 1.279 Å and r_e(GeC) is 1.929 Å. The linear geometry ($^1\Sigma^+$) has similar C-C bond distances to the T-Shaped structure. As presented in Table 4.2, the trend in r_e(CC) with the inclusion of correlation effects parallels that for the T-Shaped geometry. However, the linear Ge-C bond length is about 0.15-0.20 Å shorter than that of the T-Shaped structure

Table 4.1: Total non-relativistic energies (in hartree), bond distances (in Å), dipole moments (in debye), and harmonic vibrational frequencies (in cm^{-1}) for the T-Shaped geometry ($^1A_1$ symmetry).

	Total energy	μ_e	r_e(CC)	r_e(GeC)	Θ	$\omega_1(a_1)$	$\omega_2(a_1)$	$\omega_3(b_2)$
TZ2P+diff SCF	-2150.974221	3.70	1.2536	1.9431	37.64	1938	665	$283i$
TZ3P(2f) SCF	-2150.979296	3.67	1.2525	1.9354	37.75	1943	667	$259i$
cc-pVTZ SCF	-2151.015394	3.60	1.2539	1.9375	37.76	1938	669	$264i$
cc-pVQZ SCF	-2151.023467		1.2519	1.9350	37.75	1943	667	$257i$
TZ2P+diff CISD	-2151.385477	3.48	1.2641	1.9379	38.07	1850	665	$215i$
TZ3P(2f) CISD	-2151.464142		1.2609	1.9212	38.31	1878	677	$166i$
cc-pVTZ CISD	-2151.412295	3.28	1.2658	1.9237	38.41	1855	679	$144i$
cc-pVQZ CISD	-2151.482824		1.2600	1.9150	38.41	1874	678	$154i$
TZ2P+diff CCSD	-2151.442661		1.2743	1.9467	38.21	1781	650	$172i$
TZ3P(2f) CCSD	-2151.532887	3.25	1.2718	1.9289	38.50	1802	662	$95i$
cc-pVTZ CCSD	-2151.465256		1.2755	1.9296	38.60	1793	668	$43i$
cc-pVQZ CCSD	-2151.545978		1.2702	1.9211	38.61	1808	665	$73i$
TZ2P+diff CCSD(T)	-2151.470570		1.2825	1.9555	38.29	1725	633	$170i$
TZ3P(2f) CCSD(T)	-2151.564938		1.2804	1.9373	38.59	1744	646	$80i$
cc-pVTZ CCSD(T)	-2151.495462		1.2842	1.9375	38.70	1735	652	36
aug-cc-pVTZ CCSD(T)	-2151.506748		1.2834	1.9371	38.69	1739	649	38
cc-pVQZ CCSD(T)	-2151.579612		1.2789	1.9291	38.72	1750	649	$38i$
cc-pwCVTZ CCSD(T)	-2151.843234		1.2842	1.9363	38.73	1738	644	$105i$

at every level of theory. Our most reliable non-relativistic values for the r_e(CC) and r_e(GeC) distances at the linear stationary point geometry are 1.287 Å and 1.769 Å, respectively.

The L-Shaped ($^1A'$) equilibrium geometry has a slightly longer C-C bond distance than the T-Shaped and linear structures, by about 0.01 Å. On the other hand, the L-Shaped Ge-C bond distance falls between that of the T-Shaped and linear geometries. The effects of electron correlation on the L-Shaped geometry are similar to those found for the T-Shaped structure. The primary difference is an increase in the C-C bond distance. An important point is that the bond angle in the L-Shaped geometry is very much dependent on both theoretical method and basis set. As shown in Table 4.3, larger basis sets produce smaller bond angles. However, as we include electron correlation no regular trend was observed. Although the CISD and CCSD Ge-C-C angles are smaller than the SCF values, the CCSD(T) angles are larger than both CISD and CCSD. This is not very surprising because, as will be discussed later, the potential energy surface is extremely flat, and even 2-3 kcal/mol of energy is enough to invert the Ge atom with respect to the C-C bond.

Nielsen et al.[94] published a significant theoretical (*ab initio*) paper on SiC_2 in 1997. Their predictions for the C-C bond distances in the T-Shaped, linear, and L-Shaped structures are very similar to our predictions for GeC_2. The Ge-C bond distance is about 0.10 Å, 0.06 Å, and 0.10 Å longer than the analogous Si-C distances in the T-Shaped, linear, and L-Shaped geometries, respectively. Nielsen and coworkers reported that they could not locate an L-Shaped stationary point at several levels of theory. Here we find an L-Shaped GeC_2 stationary point at every level of theory. As is now well known, the true ground state geometry of SiC_2 is T-Shaped, and the experimental structural parameters[95] are r_0(CC) = 1.269 Å, r_0(SiC) = 1.832 Å, while the C-Si-C bond angle is 40.4 degrees. The predicted geometrical parameters for the T-Shaped GeC_2 are r_e(CC) = 1.279 Å, r_e(GeC)=1.929 Å, and Θ_e(CGeC)

Table 4.2: Total non-relativistic energies (in hartree), bond distances (in Å), dipole moments (in debye), and harmonic vibrational frequencies (in cm^{-1}) for the linear geometry ($^1\Sigma^+$ symmetry).

	Total energy	μ_e	r_e(CC)	r_e(GeC)	$\omega_1(\sigma)$	$\omega_2(\pi)$	$\omega_3(\sigma)$
TZ2P+diff SCF	-2150.972623	5.41	1.2596	1.7592	2033	$92i$	699
TZ3P(2f) SCF	-2150.978020	5.38	1.2594	1.7549	2040	$72i$	702
cc-pVTZ SCF	-2151.013818		1.2608	1.7547	2039	$68i$	703
cc-pVQZ SCF	-2151.021455		1.2589	1.7543	2037	$83i$	702
TZ2P+diff CISD	-2151.380541	5.35	1.2690	1.7652	1968	$92i$	675
TZ3P(2f) CISD	-2151.459335	5.32	1.2667	1.7548	1993	$57i$	687
cc-pVTZ CISD	-2151.406247	5.12	1.2712	1.7559	1988	$54i$	685
cc-pVQZ CISD	-2151.476538		1.2658	1.7483	1996	$26i$	693
TZ2P+diff CCSD	-2151.437311		1.2786	1.7757	1911	$102i$	654
TZ3P(2f) CCSD	-2151.527896		1.2771	1.7648	1932	$72i$	665
cc-pVTZ CCSD	-2151.458566		1.2801	1.7644	1933	$73i$	667
cc-pVQZ CCSD	-2151.539271		1.2754	1.7562	1942	$41i$	674
TZ2P+diff CCSD(T)	-2151.467811		1.2901	1.7901	1839	$93i$	622
TZ3P(2f) CCSD(T)	-2151.562810		1.2885	1.7784	1863	$50i$	634
cc-pVTZ CCSD(T)	-2151.491380		1.2916	1.7780	1864	$60i$	636
cc-pVQZ CCSD(T)	-2151.575353		1.2866	1.7692	1873	$12i$	643
cc-pwCVTZ CCSD(T)	-2151.839143		1.2925	1.7749	1857	$79i$	633

Table 4.3: Total non-relativistic energies (in hartree), bond distances (in Å), dipole moments (in debye), and harmonic vibrational frequencies (in cm^{-1}) for the L-Shaped geometry ($^1A'$ symmetry).

	Total energy	μ_e	r_e(CC)	r_e(GeC)	Θ	$\omega_1(a')$	$\omega_2(a')$	$\omega_3(a')$
TZ2P+diff SCF	-2150.977849	4.40	1.2615	1.7822	100.53	1916	878	162
TZ3P(2f) SCF	-2150.982279	4.37	1.2609	1.7796	99.49	1919	877	159
cc-pVTZ SCF	-2151.018486	4.27	1.2622	1.7807	99.31	1914	877	165
cc-pVQZ SCF	-2151.026371		1.2602	1.7795	99.20	1915	875	160
TZ2P+diff CISD	-2151.386991	4.01	1.2710	1.7988	93.19	1823	836	162
TZ3P(2f) CISD	-2151.464941	4.00	1.2677	1.7920	90.86	1845	838	143
cc-pVTZ CISD	-2151.412824	3.80	1.2718	1.8006	88.87	1828	824	136
cc-pVQZ CISD	-2151.483414		1.2664	1.7918	89.11	1843	829	143
TZ2P+diff CCSD	-2151.443616		1.2812	1.8116	92.14	1754	810	141
TZ3P(2f) CCSD	-2151.533135		1.2780	1.8085	88.41	1775	800	103
cc-pVTZ CCSD	-2151.465276	3.41	1.2783	1.8422	80.95	1774	735	59
cc-pVQZ CCSD	-2151.546061		1.2748	1.8167	84.37	1782	769	85
TZ2P+diff CCSD(T)	-2151.472036		1.2924	1.8107	98.15	1695	813	121
TZ3P(2f) CCSD(T)	-2151.565544		1.2909	1.7978	97.76	1718	830	100
cc-pVTZ CCSD(T)	-2151.495586	3.70	1.2927	1.8087	92.28	1703	813	86
aug-cc-pVTZ CCSD(T)	-2151.506847		1.2922	1.8071	93.04	1704	813	81
cc-pVQZ CCSD(T)	-2151.579785		1.2874	1.8024	91.43	1713	809	96
cc-pwCVTZ CCSD(T)	-2151.843890		1.2941	1.7995	95.18	1703	819	116

= 38.7 degrees at the CCSD(T)/cc-pVQZ level of theory. However, as we will discuss in the next section, unlike SiC_2 the T-Shaped geometry of GeC_2 is found to be a transition state rather than the global minimum.

Harmonic Vibrational Frequencies

The T-Shaped geometry ($^1A_1$), which is the true global minimum for SiC_2, is found to be a stationary point having an imaginary harmonic vibrational frequency, for the asymmetric stretching mode $\omega_3(b_2)$. As presented in Table 4.1, although the imaginary value is getting smaller as correlation effects are included, our CCSD(T) GeC_2 $\omega_3(b_2)$ predictions are still imaginary except with the cc-pVTZ and aug-cc-pVTZ basis sets, for which real frequencies of 36 cm^{-1} and 38 cm^{-1} were obtained, respectively. However, the cc-pVQZ CCSD(T) method yields an imaginary $\omega_3(b_2)$ of $38i$ cm^{-1}, and the core-valence correlation consistent basis set (cc-pwCVTZ) produced an imaginary frequency of $105i$ cm^{-1}. Interestingly, as discussed later, relativistic corrections turn the real $\omega_3(b_2)$ values for the cc-pVTZ and aug-cc-pVTZ basis sets into imaginary values. Therefore, considering that almost all non-relativistic levels (except the two as just mentioned), the core-valence correlated correlation consistent basis set at the CCSD(T) level, and all relativistic computations produce imaginary values for the asymmetric stretching $\omega_3(b_2)$ mode, the T-Shaped GeC_2 is predicted to be a transition state between the two L-Shaped geometries. Although our theoretical results support this conclusion, we realize that new experiments are necessary in this respect, because the system is elusive and the surface is extraordinarily flat.

The C-C $\omega_1(a_1)$ stretching vibrational frequency of the T-Shaped structure decreases with more sophisticated treatments of correlation effects, whereas the Ge-C stretching $\omega_2(a_1)$ frequency is mainly dependent on the basis set choice, similar to the Ge-C bond length. At the highest non-relativistic level of theory,

CCSD(T)/cc-pVQZ, T-Shaped frequencies of 1750 cm^{-1}, 649 cm^{-1}, and $38i$ cm^{-1} are predicted for the $\omega_1(a_1)$, $\omega_2(a_1)$, and $\omega_3(b_2)$ modes, respectively.

The linear structure has an imaginary harmonic vibrational frequency for the degenerate bending mode $\omega_2(\pi)$. This imaginary frequency, as well as the C-C stretching frequency $\omega_1(\sigma)$, decreases as we improve the level of theory. The linear Ge-C stretching harmonic vibrational frequency $\omega_3(\sigma)$ is slightly higher at the SCF, CISD, and CCSD levels than the values for the corresponding mode of the T-Shaped $\omega_2(a_1)$, whereas at the CCSD(T) level $\omega_3(\sigma)$ is slightly lower than $\omega_2(a_1)$. Although some *ab initio* and DFT methods[94,96] give a spurious real vibrational frequency for the bending mode of SiC_2 in the linear structure, it has been concluded both from experiment and theory[90–92,94] that the linear geometry of SiC_2 is a transition state to the cyclic T-Shaped structure. In contrast, we have obtained imaginary frequencies for the bending $\omega_2(\pi)$ mode of GeC_2 at all levels of theory (Table 4.2). Therefore, the linear geometry of GeC_2 is a transition state. However, as mentioned above, this transition state cannot connect two T-Shaped structures because the T-Shaped geometry is also predicted to be a transition state. Consequently, the linear geometry of GeC_2 should be a transition state between the two equivalent L-Shaped geometries.

The L-Shaped geometry was successfully optimized at every level of theory, and real values are obtained for all harmonic vibrational frequencies, as may be observed in Table 4.3. All three vibrational frequencies decrease with higher level treatments of electron correlation, with the exception that the CCSD(T) values for the Ge-C stretching mode (ω_2) and Ge-C-C bending mode (ω_3) are slightly higher than those predicted by CCSD. At the highest non-relativistic level, CCSD(T)/cc-pVQZ, frequencies of 1713, 809, and 96 cm^{-1} are predicted for the C-C stretching (ω_1), Ge-C stretching (ω_2), and Ge-C-C bending (ω_3) modes, respectively. Because we did not encounter any imaginary vibrational frequencies, and found this L-Shaped geometry

to lie energetically lowest, the L-shaped geometry is predicted to be the ground state equilibrium geometry. As will be discussed later, the inclusion of core-valence correlation and relativistic corrections supports this conclusion.

Dipole Moments

Some predicted dipole moments are presented in Tables 4.1-4.3. For all three geometries, the molecule has a significant dipole moment. At the CISD/cc-pVTZ level of theory, values of 3.28, 5.12, and 3.80 debye are predicted for the T-Shaped, linear, and L-Shaped geometries, respectively. At the T-Shaped geometry, the Ge atom has a positive Mulliken charge of 0.50, and each C atom has a negative charge of -0.25. For the linear geometry, the Ge atom has a positive Mulliken charge of 0.46 and the adjacent C atom has a negative charge of -0.45. The second C atom in the linear geometry is essentially neutral in this oversimplified picture. At the L-Shaped geometry, the Ge atom again is predicted to have a positive charge of 0.34, the neighboring C atom has a negative charge of -0.20, and the other C atom has the remaining negative charge of -0.14. These Mulliken atomic population were predicted at the CISD/cc-pVTZ level of theory.

Energetics

At all non-relativistic levels of theory, the L-Shaped geometry is found to be lower in energy than the T-Shaped and linear structures. This supports our earlier conclusion from the vibrational analysis that the L-Shaped structure is the global minimum for the ground state of GeC_2. The relative energies of the T-Shaped and linear geometries with respect to the L-Shaped structure are plotted in Figure 4.2. The relative energy of the T-Shaped geometry decreases as we increase the level of theory. At the CCSD(T)/cc-pVQZ level, the T-L energy difference is only 0.11 kcal/mol.

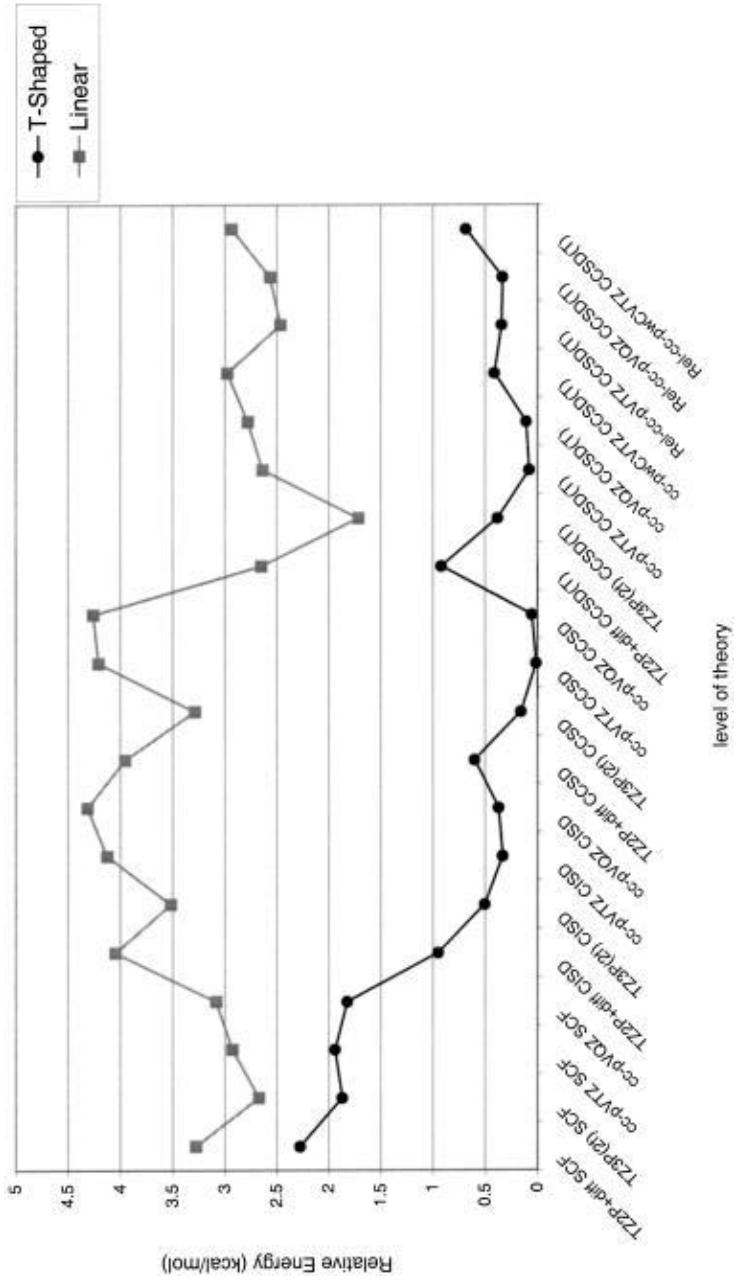

Figure 4.2: The relative energies of the T-shaped ($^1A_1$) and linear ($^1\Sigma^+$) geometries with respect to the L-shaped ($^1A^{'}$) geometry.

It is necessary to include the zero-point vibrational energy (ZPVE) correction to obtain a quantum mechanical energy separation. However, due to the extremely flat and sensitive potential energy surface of the GeC_2 system, the ZPVE corrections should be evaluated cautiously. According to the study by Grev, Janssen, and Schaefer,[97] the ZPVE estimated from SCF harmonic vibrational frequencies is usually overestimated by few tenths of a kcal/mol. Thus, they recommended a scaling factor of 0.91 for determinations of ZPVEs. With the CCSD(T) method, a scaling factor of 0.95 would be a reasonable estimate to obtain the ZPVE correction from CCSD(T) harmonic vibrational frequencies. At the CCSD(T)/cc-pVQZ level, the T-shaped isomer is predicted to be a transition state, the ZPVE correction for the T-L energy difference being -0.31 (-0.30) kcal/mol. However, the T-Shaped isomer is predicted to be a minimum at the CCSD(T)/cc-pVTZ and CCSD(T)/aug-cc-pVTZ levels. The ZPVE corrections for the T-L energy difference at these two levels are -0.26 (-0.24) kcal/mol and -0.25 (-0.23) kcal/mol, respectively. The above ZPVE corrections in parentheses are the scaled values. Since the T-Shaped structure is a reasonable candidate for the global minimum, it should be treated as if it were a minimum. Thus, employing the scaled ZPVE correction of -0.23 kcal/mol and classical relative energy of 0.11 kcal/mol at the CCSD(T)/cc-pVQZ level, the non-relativistic quantum mechanical T-L energy separation becomes -0.12 kcal/mol.

An energy difference this small suggests the need for highly precise experimental work or more advanced theoretical methods (perhaps some kind of extrapolation technique to the full CI limit). The basis set convergence at the CISD, CCSD, and CCSD(T) levels does not absolutely guarantee our assignment of the L-Shaped geometry to the equilibrium geometry (see Figure 4.2). However, the basis set convergence appears satisfactory, and the convergence seems to be approached near the cc-pVQZ basis set. The cc-pVQZ T-L energy differences are very slightly greater than the cc-pVTZ results at the correlated levels [by 0.038 kcal/mol higher with CISD, 0.039

kcal/mol with CCSD, and 0.031 kcal/mol with CCSD(T)]. This observation may suggest that larger basis sets will not significantly lower the relative energy. As a result, although all of our non-relativistic and relativistic (see below) calculations put the T-Shaped geometry above the L-Shaped structure, we are concerned that a definitive conclusion about the energetics of these two geometries is difficult due to the extremely flat nature of the ground state potential energy surface.

The energy relative to the global minimum is more evident for the linear structure. As displayed in Figure 4.2, the SCF method puts the linear geometry about 3 kcal/mol, CISD and CCSD about 4 kcal/mol, and CCSD(T) 2.5-3.0 kcal/mol above the L-Shaped structure. At the CCSD(T) level, except for one basis set, TZ3P(2f), the other seven basis sets produced values between 2.5 and 3.0 kcal/mol for the relative energy of the linear geometry. The best non-relativistic classical energy separation is predicted to be 2.78 kcal/mol at the CCSD(T)/cc-pVQZ level and the quantum mechanical energy difference (with the scaled ZPVE correction) to be 2.64 kcal/mol. Therefore, the linear structure is certainly not the true global minimum.

4.5.2 Effects of Core-Valence Correlations

As described in the theoretical section, the cc-pwCVTZ basis set documented here for Ge was used at the CCSD(T) level to consider core-valence electron correlation effects. The results for this level of theory, CCSD(T)/cc-pwCVTZ, are included in Tables 4.1-4.3. The predictions with this basis set should be compared with those for the cc-pVTZ basis set in order to deduce the differential effects of Ge core-valence correlations. This is because the only difference between the two basis sets is the usage of core-valence correlated version of the normal cc-pVTZ basis sets for the Ge atom (see above theoretical procedures for more information).

The most obvious effect of the inclusion of Ge core-valence correlation was seen to be on the asymmetric stretching mode $\omega_3(b_2)$ of the T-Shaped geometry and on

the bending harmonic vibrational frequencies of the linear and L-Shaped geometries. This is expected because movement of the Ge atom in the molecular plane requires very little energy, and all these harmonic vibrations are associated with the motion of the Ge atom. As noted above, the CCSD(T)/cc-pVTZ level of theory predicts a real harmonic vibrational frequency of 36 cm^{-1} for the asymmetric stretching mode $\omega_3(b_2)$ of the T-Shaped geometry, although most other methods predict imaginary values. As seen in Table 4.1, inclusion of the core-valence correlation replaces the real frequency with an imaginary value of $105i$ cm^{-1}. This is quite important because this core-valence correlation effect very much supports our earlier finding that the T-Shaped geometry of GeC_2 is a transition state. The situation is similar in the linear case. As presented in Table 4.2, our result for the bending harmonic vibration $\omega_2(\pi)$ with the normal cc-pVTZ basis set [at the CCSD(T) level] is $60i$ cm^{-1} and inclusion of core-valence correlation produces a larger imaginary value of $79i$ cm^{-1}. This confirms our earlier prediction that the linear geometry is a transition state. The inverse effect is seen for the L-Shaped geometry (see Table 4.3). The Ge-C-C bending harmonic vibrational frequency (ω_3) becomes more real, 116 cm^{-1} (the cc-pVTZ prediction is 86 cm^{-1}). In other words, the core-valence correlation effects associated with the Ge atom in the L-Shaped geometry decrease the likelihood that the L-Shaped structure is a transition state.

The effects of core-valence correlation on the energetics of the GeC_2 system are also important. The relative energy of the T-Shaped geometry with the cc-pwCVTZ basis set is 0.41 kcal/mol, and it is larger by 0.33 kcal/mol relative to that (0.078 kcal/mol) with the cc-pVTZ basis set. This stabilization of the L-Shaped geometry with respect to the T-Shaped structure also suggests the L-Shaped to be the favored choice for the ground state geometry. On the other had, the energy difference between the linear and L-Shaped geometries is 2.98 kcal/mol with the cc-pwCTZ basis set and 2.64 kcal/mol with the cc-pVTZ basis set. Therefore, the relative energy of the

linear structure increases with the inclusion of core-valence correction as well, by a similar amount of 0.34 kcal/mol with respect to the L-Shaped geometry.

4.5.3 Effects of Relativistic Corrections.

The relativistic optimizations are computationally demanding. They require nine single point and nine numerical first derivative CCSD(T) calculations for the T-Shaped and linear geometries, and 13 single points and 13 numerical first derivative CCSD(T) calculations for the L-Shaped geometry just for *one* optimization cycle. Therefore, we focused more attention on the T-Shaped geometry. This is also because the non-relativistic results for the L-Shaped and linear geometries are definitive, whereas those for the L-Shaped and T-Shaped geometries are not. As discussed earlier, the T-L energy difference is small, and two of our non-relativistic levels of theory gave real frequencies for the asymmetric stretching vibration $\omega_3(b_2)$ of the T-Shaped geometry (see Table 4.1). Therefore, we carried out relativistic optimizations and frequency evaluations for the T-Shaped geometry with four different basis sets at the CCSD(T) level. For the linear geometry we employed three different basis sets, whereas only one basis set was used for the L-Shaped geometry, due to the high computational cost [a total of 52 single point and 52 numerical first derivative CCSD(T) calculations in C_s symmetry were performed for the relativistic optimization of the L-Shaped geometry with one basis set]. We present the effects of relativistic corrections in Table 4.4 for the T-Shaped, in Table 4.5 for the linear, and in Table 4.6 for the L-Shaped geometries. The effects of relativity on the geometries are somewhat different among the three structures. The Ge-C bond shortens by ~ 0.003 Å in the T-Shaped geometry, by ~ 0.005 Å in the linear case, and by ~ 0.013 Å in the L-Shaped geometry. The C-C bond distance decreases very slightly for the T-Shaped and linear geometries, whereas it elongates by ~ 0.001 Å for the L-Shaped geometry.

Table 4.4: The effects of relativistic corrections, namely mass-velocity and one electron Darwin terms, on the geometry, energetics, and harmonic vibrational frequencies of the T-Shaped geometry ($^1A_1$ symmetry).

	Non-Relativistic	Relativistic	Δ
——CCSD(T)/cc-pVTZ——			
Total Energy	-2151.495462	-2172.748839	-21.253377
r_e(CC)	1.2842	1.2841	-0.0001
r_e(GeC)	1.9375	1.9341	-0.0034
Θ	38.70	38.78	+0.08
$\omega_1(a_1)$	1735.1	1734.4	-0.7
$\omega_2(a_1)$	652.2	649.3	-2.9
$\omega_3(b_2)$	35.5	$75.7i$	$35.5 \rightarrow 75.7i$
——CCSD(T)/aug-cc-pVTZ——			
Total Energy	-2151.506748	-2172.760546	-21.253798
r_e(CC)	1.2834	1.2833	-0.0001
r_e(GeC)	1.9371	1.9335	-0.0036
Θ	38.69	38.76	+0.07
$\omega_1(a_1)$	1739.0	1736.1	-2.9
$\omega_2(a_1)$	648.9	646.3	-2.6
$\omega_3(b_2)$	37.8	$82.4i$	$37.8 \rightarrow 82.4i$
——CCSD(T)/cc-pVQZ——			
Total Energy	-2151.579612	-2172.834445	-21.254833
r_e(CC)	1.2789	1.2790	-0.0001
r_e(GeC)	1.9291	1.9261	-0.0030
Θ	38.72	38.78	+0.06
$\omega_1(a_1)$	1750.1	1747.8	-2.3
$\omega_2(a_1)$	648.7	647.7	-1.0
$\omega_3(b_2)$	$38.0i$	$74.7i$	$38.0i \rightarrow 74.7i$
——CCSD(T)/cc-pwCVTZ——			
Total Energy	-2151.843234	-2173.098334	-21.255100
r_e(CC)	1.2842	1.2841	-0.0001
r_e(GeC)	1.9363	1.9336	-0.0027
Θ	38.73	38.79	+0.06
$\omega_1(a_1)$	1737.5	1734.1	-3.4
$\omega_2(a_1)$	644.3	640.4	-3.9
$\omega_3(b_2)$	$105.0i$	$131.1i$	$105.0i \rightarrow 131.1i$

The relativistic effects on the L-Shaped geometry are considerably larger than those for the other two structures.

For the T-Shaped geometry, the asymmetric stretching vibrational frequency $\omega_3(b_2)$ becomes *more imaginary* when relativity is considered. The two real frequencies, 36 cm^{-1} and 38 cm^{-1} obtained at the CCSD(T)/cc-pVTZ and CCSD(T)/aug-cc-pVTZ levels, shifted to imaginary values of $76i$ cm^{-1} and $82i$ cm^{-1}, respectively, as presented in Table 4.4. At the highest level of theory, CCSD(T)/cc-pVQZ, the imaginary value of $38i$ cm^{-1} becomes $75i$ cm^{-1} for the same mode. This shift is in the same direction as the effects of core-valence correlation (see the previous section). Therefore, depending on the relativistic and core-valence correlated results, we can say that both of these corrections tend to move the Ge atom in the T-Shaped geometry toward the L-Shaped geometry. This interesting effect of relativity may be attributed to the fact that the valence electrons, which mainly contribute to the chemical bonding, also display direct relativistic effects due to their core-penetrating natures as well as indirect relativistic effects. The main relativistic effects for the linear structure are observed for the bending harmonic vibrational frequency $\omega_2(\pi)$, as shown in Table 4.5. The CCSD(T)/cc-pVTZ basis set produces a lower imaginary frequency, whereas the CCSD(T)/cc-pwCVTZ generates a higher imaginary value compared to the corresponding non-relativistic imaginary bending $\omega_2(\pi)$ frequencies. The CCSD(T)/cc-pVQZ basis set shifts the small imaginary value of $12i$ cm^{-1} to a real value of 34 cm^{-1} when relativity is included. This shift should not be taken too seriously because the relativistic CCSD(T)/cc-pwCVTZ level, which has core-valence correlation, presents a larger imaginary bending frequency, as mentioned above. For the L-Shaped structure, the GeC stretching (ω_2) and Ge-C-C bending (ω_3) frequencies increase by 15 cm^{-1} and 21 cm^{-1}, respectively, upon the inclusion of the relativity. The relativistic effects on the energetics of the system are significant. The relative energy of the T-Shaped geometry increases by 0.27

Table 4.5: The effects of relativistic corrections, namely mass-velocity and one electron Darwin terms, on the geometry, energetics, and harmonic vibrational frequencies of the linear geometry ($^1\Sigma^+$ symmetry).

	Non-Relativistic	Relativistic	Δ
——CCSD(T)/cc-pVTZ——			
Total Energy	-2151.491380	-2172.745452	-21.254072
r_e(CC)	1.2916	1.2914	-0.0002
r_e(GeC)	1.7780	1.7723	-0.0057
$\omega_1(\sigma)$	1864.1	1863.0	-1.1
$\omega_2(\pi)$	$60.4i$	$52.7i$	$60.4i \rightarrow 52.7i$
$\omega_3(\sigma)$	635.8	634.2	-1.6
——CCSD(T)/cc-pVQZ——			
Total Energy	-2151.575353	-2172.830886	-21.255533
r_e(CC)	1.2866	1.2864	-0.0002
r_e(GeC)	1.7692	1.7643	-0.0049
$\omega_1(\sigma)$	1873.3	1872.9	-0.4
$\omega_2(\pi)$	$11.8i$	34.3	$11.8i \rightarrow 34.3$
$\omega_3(\sigma)$	643.4	642.7	-0.7
——CCSD(T)/cc-pwCVTZ——			
Total Energy	-2151.839143	-2173.094758	-21.255627
r_e(CC)	1.2925	1.2923	-0.0002
r_e(GeC)	1.7749	1.7703	-0.0046
$\omega_1(\sigma)$	1856.9	1854.8	-2.1
$\omega_2(\pi)$	$79.2i$	$88.4i$	$79.2i \rightarrow 88.4i$
$\omega_3(\sigma)$	632.6	630.2	-2.4

Table 4.6: The effects of relativistic corrections, namely mass-velocity and one electron Darwin terms, on the geometry, energetics, and harmonic vibrational frequencies of the L-Shaped geometry ($^1A'$ symmetry).

	Non-Relativistic	Relativistic	Δ
——CCSD(T)/cc-pVTZ——			
Total Energy	-2151.495586	-2172.749386	-21.253800
r_e(CC)	1.2927	1.2937	+0.0010
r_e(GeC)	1.8087	1.7960	-0.0127
Θ	92.28	96.38	+4.1
ω_1	1703.0	1705.9	+2.9
ω_2	812.7	827.4	+14.7
ω_3	86.1	106.7	+20.6

kcal/mol at the CCSD(T)/cc-pVTZ, 0.23 kcal/mol at the CCSD(T)/cc-pVQZ, and 0.27 kcal/mol at the CCSD(T)/cc-pwCVTZ levels of theory. These energy shifts are important because the non-relativistic energy T-L differences at the CCSD(T) levels are very close to zero (see Figure 4.2). Unlike the T-Shaped geometry the linear geometry is stabilized with respect to the L-Shaped structure, by 0.17 kcal/mol, 0.21 kcal/mol, and 0.07 kcal/mol, at the CCSD(T)/cc-pVTZ, CCSD(T)/cc-pVQZ, and CCSD(T)/cc-pwCVTZ levels, respectively. These relativistic effects on the energetics of the system are plotted in Figure 4.3.

In Section I-d. the non-relativistic classical and ZPVE-corrected T-L energy separations at the CCSD(T)/cc-pCVQZ level of theory were determined to be 0.11 kcal/mol and -0.12 kcal/mol, respectively. Assuming the additivity of core-valence correlation effects of +0.33 kcal/mol in Section II and relativistic effects of +0.23 kcal/mol, the relativistic quantum mechanical T-L energy difference is predicted to be +0.44 kcal/mol. On the other hand, the non-relativistic classical and quantum mechanical energy separations between the linear and L-Shaped structures at the CCSD(T)/cc-pCVQZ level of theory were found to be 2.78 kcal/mol and 2.64 kcal/mol, respectively. Including core-valence correlation effects of +0.34 kcal/mol and relativistic effects of -0.21 kcal/mol, the relativistic quantum mechanical energy difference between the linear and L-Shaped structures is predicted to be +2.77 kcal/mol. The final predicted shape of the ground state potential energy surface at the relativistic CCSD(T)/cc-pVQZ level of theory is depicted in Figure 4.4.

4.6 Concluding Remarks

The ground state potential energy surface of the experimentally observed GeC_2 molecule reflects the same kind of elusive structure as that of the much discussed SiC_2. Although the T-Shaped and L-Shaped geometries are very close in energy, and

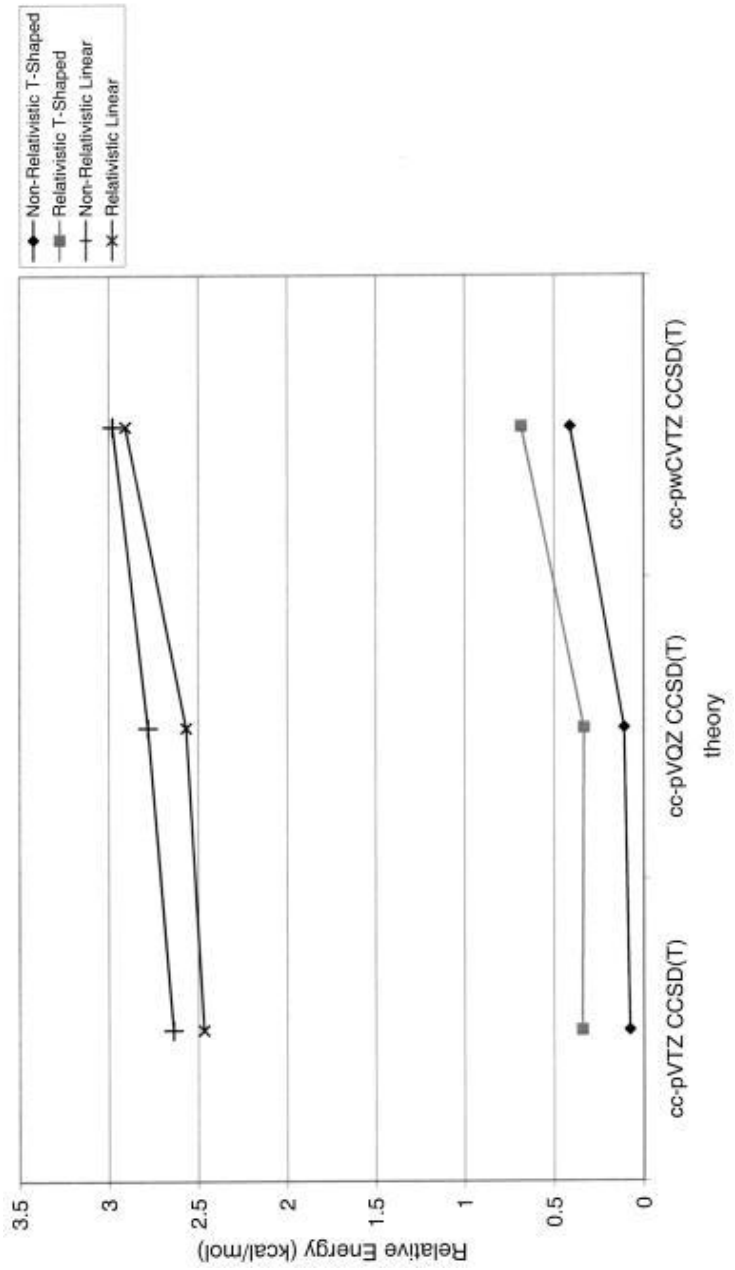

Figure 4.3: The effects of relativistic corrections on the relative energies of the T-shaped ($^1A_1$) and linear ($^1\Sigma^+$) geometries with respect to the L-shaped ($^1A^{'}$) geometry.

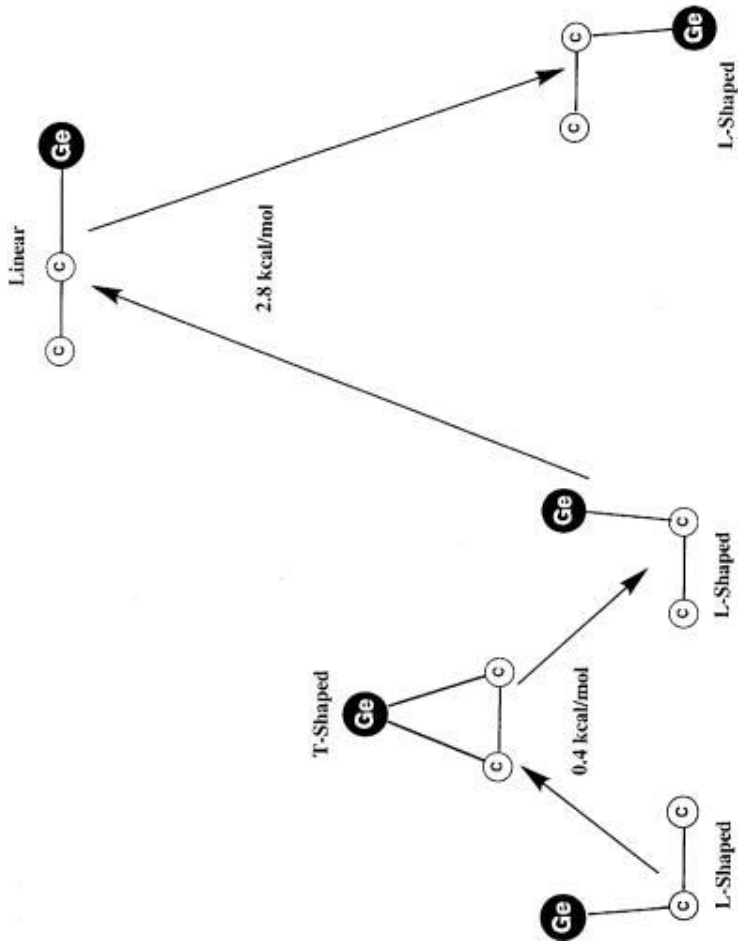

Figure 4.4: The proposed potential energy surface for the ground state of GeC_2 at the CCSD(T)/cc-pVQZ level with the inclusion of zero-point vibrational energy, scalar relativistic, and core-valence corrections.

a conclusive result is difficult to reach due to the very flat nature of the potential energy surface, the L-Shaped structure is predicted to be the global minimum. The scalar relativistic corrections (mass-velocity and one-electron Darwin terms) and core-valence corrections are found to stabilize the L-Shaped geometry over the T-Shaped structure. All of our non-relativistic and relativistic computations predict the L-Shaped structure to be lower in energy than the T-Shaped geometry, which is the equilibrium geometry for SiC_2. The linear structure is predicted to be a transition state, as is the case with SiC_2. However, this transition state connects the two L-Shaped geometries, not the two T-Shaped structures. The predicted shape of the ground state potential energy surface is given in Figure 4.4. Finally, it is important to note that new experimental work will be necessary to come to definitive conclusions.

Chapter 5

Mono- and Di-bridged Isomers of Si_2H_3 and Si_2H_4: the True Ground State Global Minima. Theory and Experiment in Concert.

5.1 Abstract

Highly correlated ab initio coupled-cluster theories (e.g. CCSD(T), CCSDT) were applied on the ground electronic states of Si_2H_3 and Si_2H_4, with substantive basis sets. A total of ten isomers, which include mono- and di-bridged structures, were investigated. Scalar relativistic corrections and zero-point vibrational energy corrections were included to predict reliable energetics. For Si_2H_3, we predict an unanticipated monobridged H_2Si-H-Si like structure (C_s, $^2A''$) to be the lowest energy isomer, in constrast to previous studies which concluded that either H_3Si-Si (C_s, $^2A''$) or near-planar H_2Si-SiH (C_1, ^2A) is the global minimum. Our results confirm that the disilene isomer, H_2Si-SiH_2 is the lowest energy isomer for Si_2H_4, and that it has a trans-bent structure (C_{2h}, ^1A_g). In addition to the much studied silylsilylene, H_3Si-SiH, we also find that a new monobridged isomer H_2Si-H-SiH (C_1, ^1A, designated **2c**) is a minimum on the potential energy surface and that it has comparable stability; both isomers are predicted to lie about 7 kcal/mol above disilene. By means of Fourier transform microwave spectroscopy of a supersonic molecular beam, the rotational spectrum of this novel Si_2H_4 isomer has recently been measured in the laboratory, as has that of the planar H_2Si-SiH radical. Harmonic vibrational frequencies as well as infrared intensities of all ten isomers were determined at the cc-pVTZ CCSD(T) level.

5.2 Introduction

Small silicon hydrides are of interest because of their potential applications in semiconductors and optoelectronics, in surface growth processes, and their possible existence in the circumstellar atmospheres of evolved carbon stars.[75,98–105] They play key roles in the plasma-enhanced chemical vapor deposition of thin-films and nanomaterials, which is an important but a poorly understood process.[99,103,106,107] Unsat-

urated silicon hydrides such as SiH, SiH_2, and Si_2H_2 have been the subject of numerous experimental investigations because silicon molecules are readily observed in space: nearly 10 % of the presently identified astronomical molecules are silicon bearing, and the silicon is central to the photochemistry of the carbon rich star IRC+10216.

The ability of silicon to form mono- and di-bridged hydrides and existence of Si-Si multiple bonds make the silicon hydrides very attractive systems for both experimental and theoretical study. This is especially true for unsaturated silicon hydrides, where determination of the ground state geometries and relative energies of the different isomers are quite challenging because the potential energy surfaces are often flat and because of the existence of many possible isomeric arrangements. Therefore, predictions of the equilibrium geometries requires careful, advanced quantum mechanical investigations. Among Si_2H_n family, the Si_2H has been found to be mono-bridged and Si_2H_2 to be di-bridged in their ground states on the basis of many theoretical and experimental studies.[102,108–116] These somewhat surprising findings added a new dimension to the silicon chemistry, which had been widely assumed to be similar to that of carbon.[94,112,113,115,116]

The equilibrium geometries for Si_2H_3 and Si_2H_4 are still not fully determined. In 1991, Sax and Kalcher[117] reported a study of many silicon hydrides including Si_2H_3 and Si_2H_4. They used the MRCI technique with double and triple-ζ quality basis sets, and investigated H_3Si-Si ($^2A''$) and the near-planar H_2Si-SiH like isomers of the Si_2H_3 molecule. They found H_3Si-Si ($^2A''$) to be 1.1 kcal/mol more stable than the near-planar H_2Si-SiH. In 1991, Curtiss, Raghavachari, Deutsch, and Pople[118] reported that the lowest energy structure for the Si_2H_3 molecule is the H_3Si-Si ($^2A''$) isomer, with near-planar H_2Si-SiH lying 1.3 kcal/mol higher in energy. They also reported that all bridged structures were found to be significantly higher in energy. In 1997, Gong, Guenzburger, and Saitovitch[107] studied six different isomers of Si_2H_3: silylsi-

lylidyne H_3Si-Si (C_s); the near-planar H_2Si-SiH (C_1); two mono-bridged isomers, HSi-H-SiH (C_2) and H_2Si-H-Si (C_s); a di-bridged; and a tri-bridged isomer. They concluded that the lowest energy structure is the mono-bridged structure (HSi-H-SiH, C_2), while the other mono-bridged structure (H_2Si-H-Si, C_s) is only 0.9 kcal/mol (0.04 eV) higher in energy. They also reported that the H_3Si-Si (C_s) like structure, which was predicted to be the lowest energy isomer by both Kalcher[117] and Pople[118], is 9.0 kcal/mol (0.39 eV) higher in energy. The tri-bridged isomer was found to be significantly higher in energy (0.64 eV). In 2001, Pak, Rienstra-Kiracofe, and one of us[104] studied the H_3Si-Si (C_s), the near-planar H_2Si-SiH (C_1), and the mono-bridged (HSi-H-SiH, C_2) isomers at the DFT level (B3LYP/DZP+). They reported that the H_3Si-Si (C_s) isomer and the near-planar H_2Si-SiH (C_1) isomer are isoenergetics, and that the employed level of theory (B3LYP/DZP+) was not adequate to decide which is more stable (only 0.02 kcal/mol energy difference was found between two structures). The mono-bridged (HSi-H-SiH, C_2) isomer, which was predicted to be the ground state geometry by Saitovitch et al.[107], was predicted to be 4.1 kcal/mol higher in energy.

The shape of the minimum energy structure of the Si_2H_4 molecule has been studied for almost twenty years. When isolated and characterized in 1981, by Michl, West and co-workers[119], the first disilene (Si_2R_4) was thought to be planar, like ethylene. The ab initio studies have focused primarily on the two isomers of Si_2H_4, disilene (H_2Si-SiH_2) and silylsilylene (H_3Si-SiH). Although all of the theoretical studies found that disilene (H_2Si-SiH_2) is the lowest energy isomer, they predict significantly different structures. In 1986, Olbrich[120] carried out SCF/TZP calculations and collected the previous estimates about the minimum energy structure of disilene (H_2Si-SiH_2). According to Table 1 of his paper, six of the eleven previous theoretical studies found disilene (H_2Si-SiH_2) to be planar, like ethylene, and five of them found it to be trans-bent structure. His SCF/TZP calculations predicted the

trans-bent structure to be of minimum energy. Recent theoretical predictions are still not entirely in agreement whether the disilene (H_2Si-SiH_2) is planar or trans-bent. In 1990, Trinquier[121] favored the planar form, in 1991 Pople and co-workers [118] predicted the trans-bent structure, and in 2000, the DFT calculations of Pak et. al.[104] yielded a near-planar trans-bent structure. Very recent (in 2002) infrared spectra taken by Andrews and Wang[122] suggested a trans-bent structure for the disilene. Predictions for the relative energy of the silylsilylene (H_3Si-SiH) isomer vary between 5 kcal/mol and 10 kcal/mol.[104,110,118,123–126] No bridged isomer of Si_2H_4 to our knowledge has previously been studied.

The present theoretical studies were motivated in part by recent laboratory measurements of the rotational spectra of two new silicon hydrides, detected by means of Fourier transform microwave (FTM) spectroscopy of a supersonic molecular beam: planar or nearly planar Si_2H_3 and an isomer of Si_2H_4 with experimental rotational constants that do not agree with those predicted for disilene or silylsilylene. Because of the somewhat contradictory theoretical predictions as to the true ground state equilibrium structures and the apparent lack of ab initio studies which fully explored the stability of bridge structures, we investigated Si_2H_3 and Si_2H_4 using highly correlated coupled-cluster theories [i.e. singles and doubles with a perturbative triples [CCSD(T)], and singles, doubles, and full triples (CCSDT)]. To our knowledge, this is the first time coupled-cluster theory has been used to study the ground electronic states of these two silicon hydrides. Scalar relativistic corrections were also included to determine accurate relative energies. A total of five isomers of Si_2H_3 and five isomers of Si_2H_4 were found to be stable. We conclude on the basis of the close agreement of the theoretical and experimental rotational constants that the new silicon hydride that has been detected in the laboratory is monobridged Si_2H_4, a low-lying isomer which is calculated to be quite polar ($\mu = 1.14$ D) and to lie only about 7 kcal/mol above disilene.

5.3 Theoretical Methods

The zeroth order descriptions of all isomers were obtained using single configuration SCF (restricted open-shell Hartree-Fock for Si_2H_3, and restricted closed-shell Hartree-Fock for Si_2H_4) wave functions. Correlation effects were included using coupled cluster with single and double excitations with perturbative triple excitations [CCSD(T)].[61] Correlation consistent polarized valence double-ζ (cc-pVDZ) and triple-ζ (cc-pVTZ) basis sets[73] were used for both hydrogen and silicon atoms.

The coupled cluster with single, double and full triple excitations (CCSDT), and the newly developed CCSD(2) theory[127] which has new class of correction that involves perturbatively expanding the similarity-transformed Hamiltonian from coupled-cluster gradient theory have also been employed for single point energy calculations. The CCSDT calculations are not feasible with the cc-pVTZ basis set due to the extremely high computational costs (a single point CCSDT/cc-pVTZ calculation for Si_2H_3 would take around 20 days on a 2.4 GHz pentium-4 machine). Therefore, the cc-pVDZ basis set was used for CCSDT calculations, whereas the larger cc-pVTZ basis set was used for CCSD(2) calculations. The effects of full triple coupled cluster excitations on relative energies were determined from the differences between the cc-pVDZ CCSDT and cc-pVDZ CCSD(T) results, and these effects were included on top of the cc-pVTZ CCSD(T) values to estimate the cc-pVTZ CCSDT results.

For the determination of the relativistic energy corrections, the one-electron Darwin term, which is always positive, and the mass-velocity term, which is always negative, were evaluated using first-order perturbation theory.[23,24] The Darwin term corrects the Coulomb attraction and the mass-velocity term corrects the kinetic energy of the system. This simple relativistic treatment gives satisfactory results for silicon compounds (and all atoms up to Z=40) compared to methods such as Dirac-

Hartree-Fock (DHF) and the use of relativistic effective core potentials (RECP). [26,76]

The geometries of the all isomers were optimized via analytic derivative methods [62,63] at the SCF and CCSD(T) levels. Harmonic vibrational frequencies were determined by means of finite differences of analytic gradients. Cartesian forces at optimized geometries were required to be less than 10^{-6} hartree/bohr in all geometry optimizations. Throughout our study, all computations were carried out using the ACES II package,[65] except for the CCSD(2) calculations which were performed using the Q-Chem package.[128] IBM RS/6000 workstations, an IBM SP2, and PC machines were used.

5.4 Results and Discussion

The optimized equilibrium geometries at the cc-pVTZ CCSD(T) level of theory are presented in Figure 5.1, 5.2, and 5.3 for isomers of Si_2H_3, and in Figure 5.5, 5.6, and 5.7 for isomers of Si_2H_4. The determined rotational constants for each isomer are also given in the figures. Figure 5.9 shows the structure of the transition state between two equivalent mono-bridged isomers of Si_2H_4. Experimentally obtained rotational spectrum of planar Si_2H_3 isomer is given in figure 5.4, and that of mono-bridged isomer of Si_2H_4 is shown in figure 5.8. The predicted dipole moments, harmonic vibrational frequencies, infrared intensities, and zero point vibrational energies (ZPVE) are presented in Table 5.1 for Si_2H_3, and in Table 5.5 for Si_2H_4. Tables 5.2, 5.3, and 5.4 report the relative energies of the different isomers of Si_2H_3, and Tables 5.6, 5.7, and 5.8 give the corresponding energies for the isomers of Si_2H_4. Tables 5.9 and 5.10 show the experimental and theoretical rotational constants of the planar H_2Si-SiH (structure **1a**) and the mono-bridged H_2Si-H-SiH (structure **2c**) isomers, respectively.

5.4.1 Structures

Si_2H_3

We have located five distinct minima on the doublet ground electronic state of Si_2H_3. The corresponding structure for each minimum is presented in Figure 5.1, 5.2, and 5.3.

The much studied planar form (structure **1a**, C_s, $^2A''$) and the H_3Si-Si isomer (structure **1b**, C_s, $^2A''$) were correctly located as well as three different mono-bridged structures; the H_2Si-H-Si like isomer (Structure **1c**, C_s, $^2A''$), trans-like H-Si-H-Si-H mono-bridged isomer (structure **1d**, C_2, ^2A), and cis-like H-Si-H-Si-H mono-bridged isomer (structure **1e**, C_1, ^2A). The shortest Si-Si bond distance was found to be in the H_2Si-H-Si like mono-bridged isomer (structure **1c**), which is 2.244 Å. The longest Si-Si bond length was found to be 2.379 Å, corresponding to the Si-Si distance of the H_3Si-Si like isomer (structure **1b**).

The geometrical parameters of the planar (structure **1a**) and the H_3Si-Si like isomer (structure **1b**) are very consistent with previous theoretical predictions, [104,111,118] except that all the previous studies found a near-planar (or quasi-planar) form for the H_2Si-SiH isomer. We did optimizations in both C_1 and C_s symmetry, and both of them gave the same perfectly planer structure with exactly the same energy. However, the geometrical parameters are very consistent with what were given for near-planar form. Two of the three mono-bridged isomers that we found, the H_2Si-H-Si like isomer (Structure **1c**) and trans-like H-Si-H-Si-H mono-bridged isomer (structure **1d**) were also predicted by Gong et. al.[107] However, although they mentioned the relative energies, Gong did not report geometrical parameters. Therefore, no literature data about these two mono-bridged isomers of Si_2H_3 have been found to compare with our structures. In addition, a third mono-bridged isomer (structure **1e**) has been successfully optimized at all levels of theory employed here.

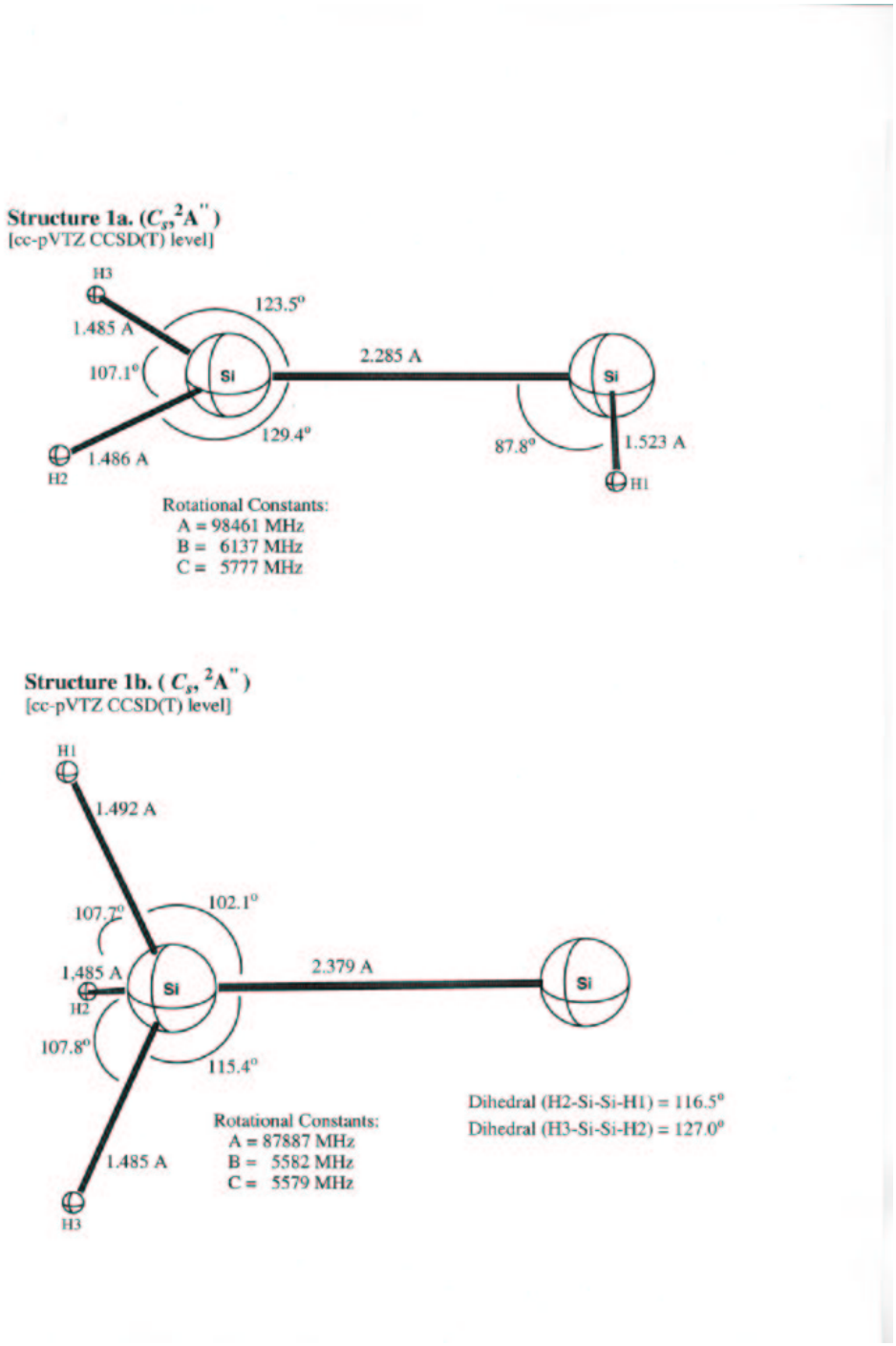

Figure 5.1: The structures **1a** and **1b**.

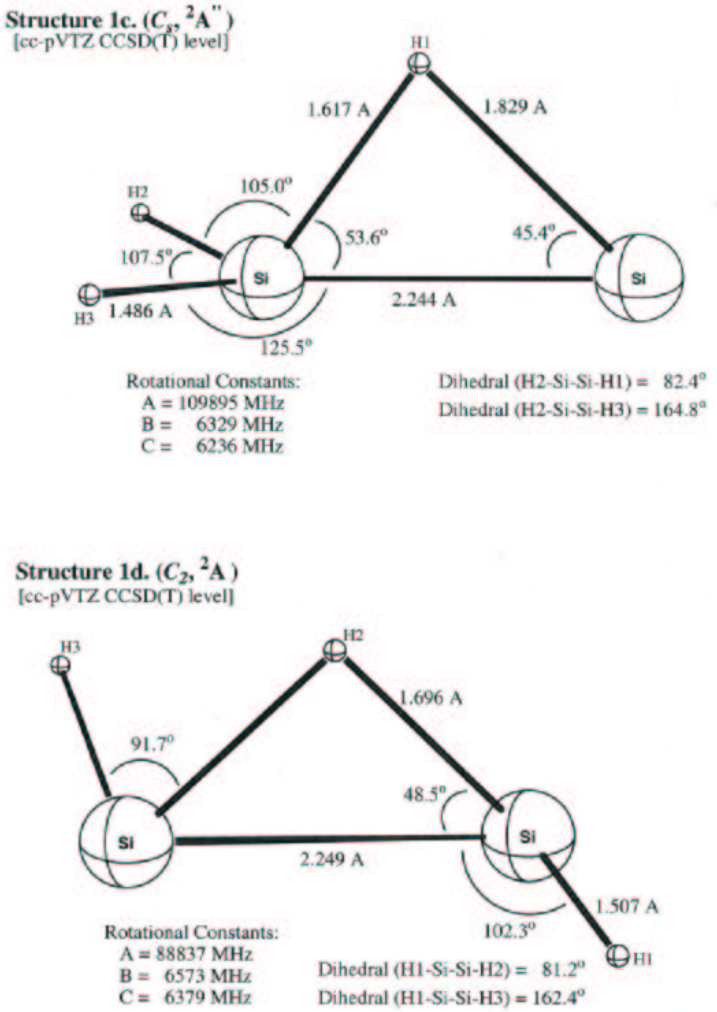

Figure 5.2: The structures **1c** and **1d**.

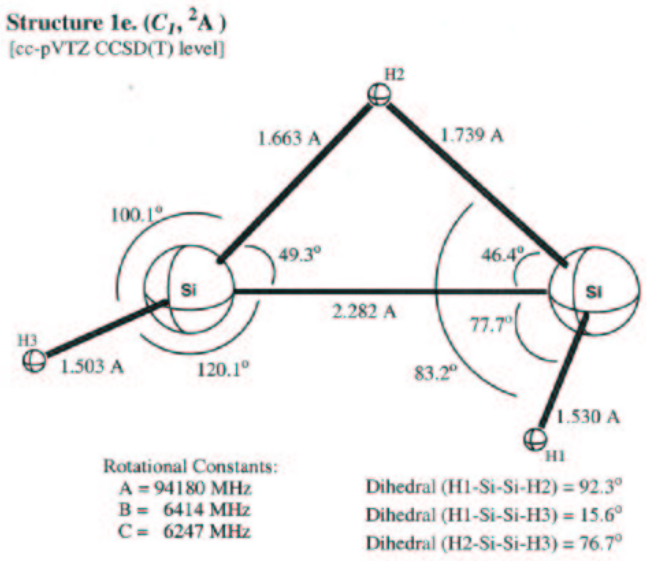

Figure 5.3: The structure **1e**.

This newly predicted mono-bridged isomer (structure **1e**) has no symmetry (C_1), and the distances of the bridged hydrogen to the two Si atoms are not equivalent. The two non-bridged hydrogen atoms are slightly out of the plane that contains the Si atoms (around 8 degrees and in the opposite directions). We have searched for a possible di-bridged or a tri-bridged isomer of Si_2H_3, without success. The rotational spectrum of planar Si_2H_3 (structure **1a**) has recently been measured in the laboratory, as have those of its rare ^{29}Si and ^{30}Si isotopic species and Si_2D_3. As shown in Fig. 5.4, owing to hyperfine structure from the three unequivalent hydrogen atoms and electron spin-rotation, all of which are comparable in magnitude, each rotational transition consists of many closely-spaced features. Conclusive evidence that the carrier of the observed lines is planar H_2SiSiH and no other molecule is provided by the close agreement of $B + C$ for the normal and isotopic species (Table 5.9). A more complete account of the laboratory observations, including tabulations of individual line frequencies and spectroscopic constants, will appear elsewhere. Laboratory searches are now underway for the monobridged H_2SiHSi whose fundamental $1 \rightarrow 0$ rotational transition is predicted to lie near 12.6 GHz.

Si_2H_4

The disilene (structure **2a**, C_{2h}, ^1A_g) and the silylsilylene (structure **2b**, C_s, $^1A'$) have been extensively studied.[104,110,111,118,120,129,130] In 1990, Trinquier[121] carried out DZP/CI calculations and found that two more di-bridged isomers, the trans di-bridged (structure **2d**, C_{2h}, ^1A_g) and cis di-bridged (structure **2e**, C_{2v}, $^1A_1$) should be minima. To our knowledge, there has been no report of a mono-bridged form of Si_2H_4. We have now located a mono-bridged isomer (structure **2c**, C_1, ^1A) which is very stable with respect to the other isomers [see the energetics section], and it is the only structure which has no symmetry. The high computational cost of optimizations

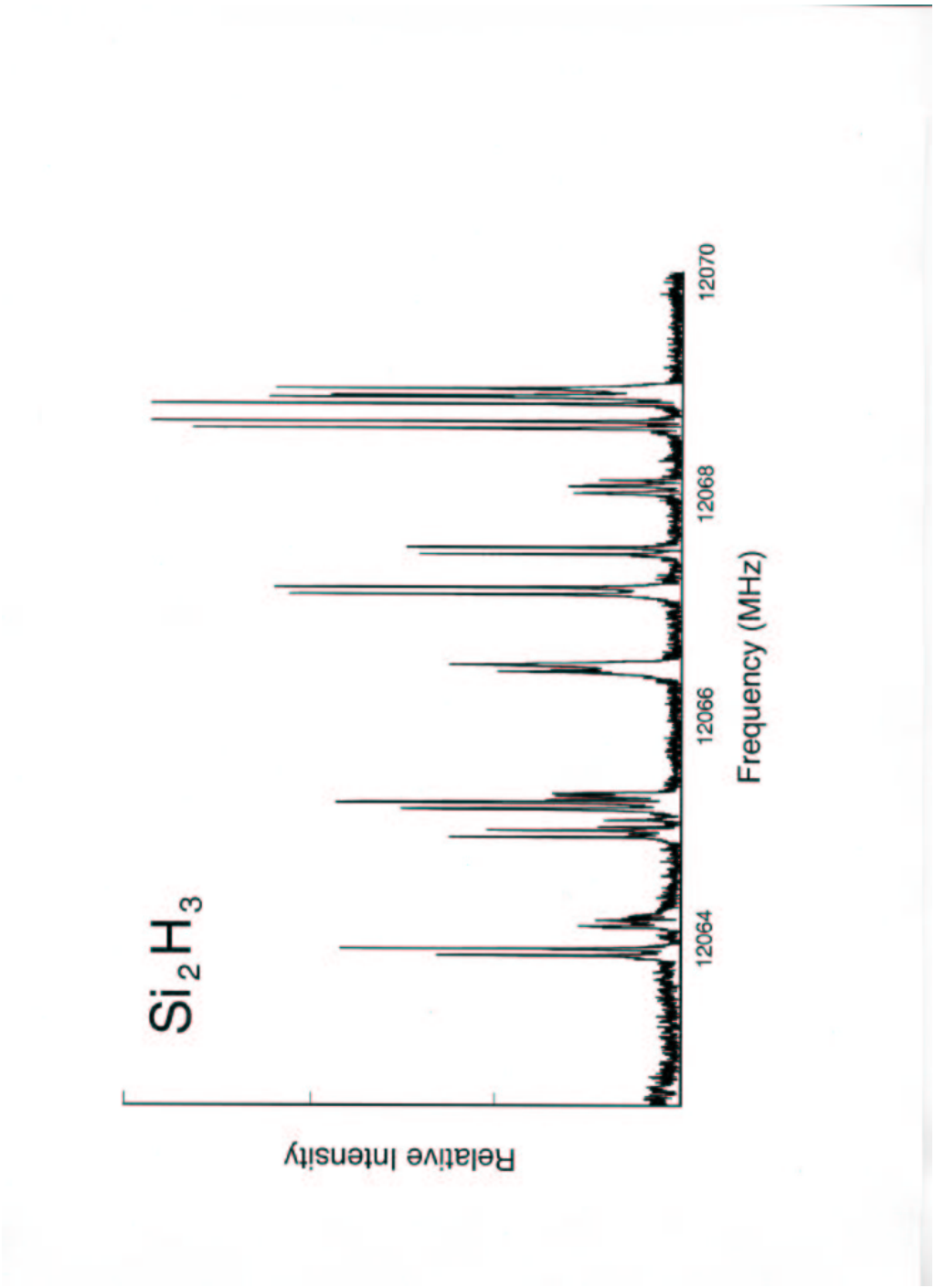

Figure 5.4: The $1_{0,1} \rightarrow 0_{0,0}$ transition of planar Si_2H_3 showing the complex spectral pattern which arises from spin-rotation of the unpaired electron and hyperfine structure from the three inequivalent hydrogen atoms. The integration time was approximately five hours.

in C_1 symmetry may be the reason it could not be located on the potential energy surface in previous theoretical studies.

The geometrical parameters for the much-studied silylsilylene (structure **2b**) are in very good agreement with the literature values.[104,110,111,118,120,129,130] For the disilene isomer (structure **2a**), both planar and trans-bent structures were reported. As explained in the introduction, Olbrich[120] reported that six of the eleven previous theoretical studies found disilene (H_2Si-SiH_2) to be planar, like ethylene, and five of them found it to be trans-bent structure. Recently, the DFT calculations of Pak et. al.[104] found a near-planar structure. Very recently (in 2002) infrared spectra taken by Andrews and Wang[122] suggested a trans-bent structure for the disilene. The reported deviations from the planarity predicted by previous theoretical studies do not in agree with each other. Many different values within the range 0-40 degrees were reported.[104,110,111,118,120,129,130] Our best level of theory, cc-pVTZ CCSD(T), gave a trans-bent disilene with a 18.9° deviation from the planarity. The predicted shapes of the trans and cis di-bridged isomers reported by Trinquier[121] are quite similar to what we determined (structures **2d** and **2e**). The largest discrepancy between our di-bridged structures and those given by Trinquier[121] is seen to be in the angles between the non-bridged hydrogens and the plane of two Si atoms. Angles of 89.1° and 94.2° were reported by Trinquier[121] for trans and cis like isomers, respectively; we determined the same angles to be 87.0° for structure **2d** and 91.2° for stucture **2e**. The reported Si-Si bond distances are in agreement with ours to within 0.01 Å for both trans- and cis-like structures.

The experimental rotational constants of the new silicon hydride, plausibly an isomer of Si_2H_4 on the basis of its rotational constants, are in extremely close agreement with those predicted here for monobridged Si_2H_4 (structure **2c**). As shown in Table 5.10, rotational constants for the normal isotopic species are within 2% of those predicted at the best level of theory, and this agreement alone makes it unlikely

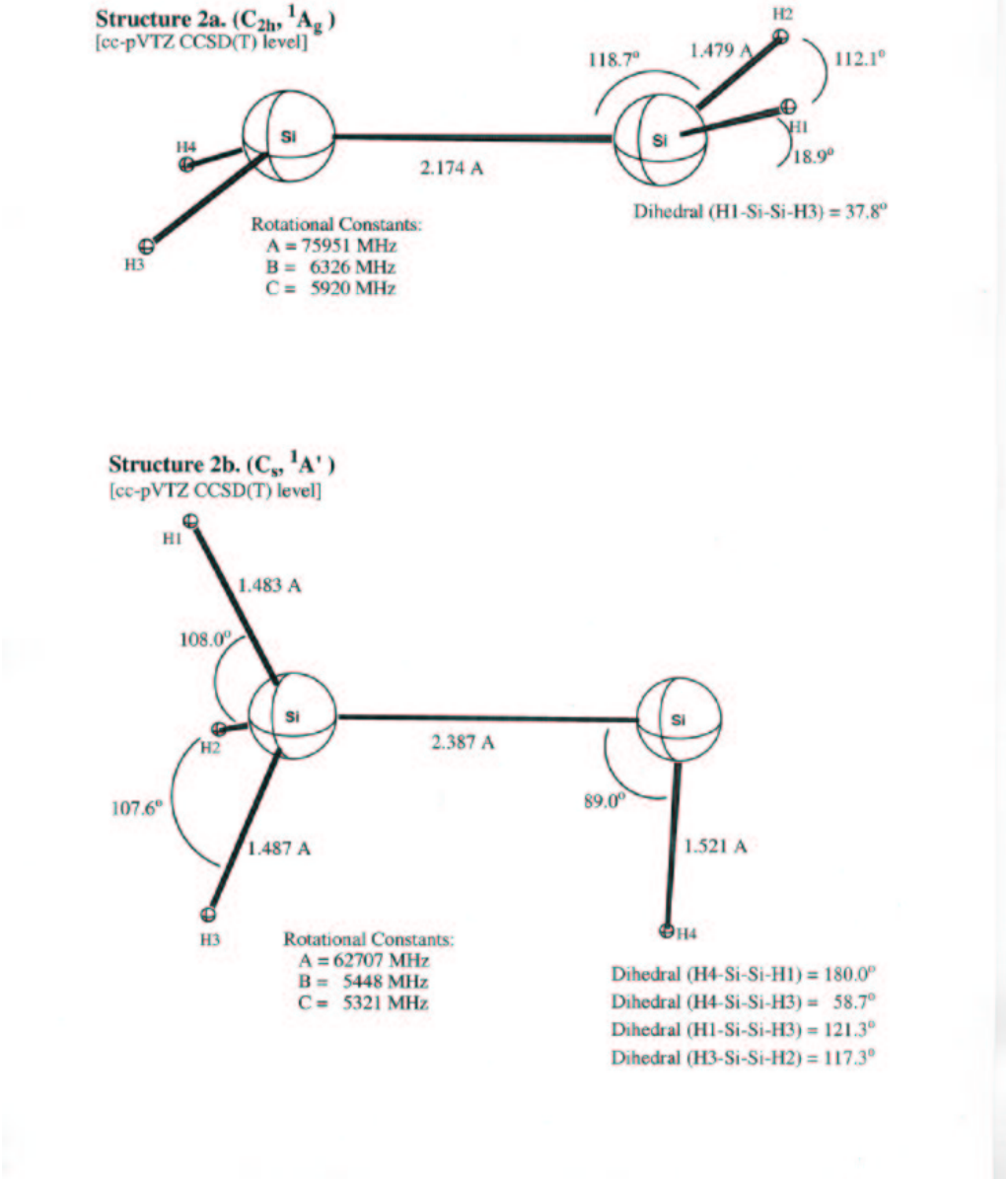

Figure 5.5: The structures **2a** and **2b**.

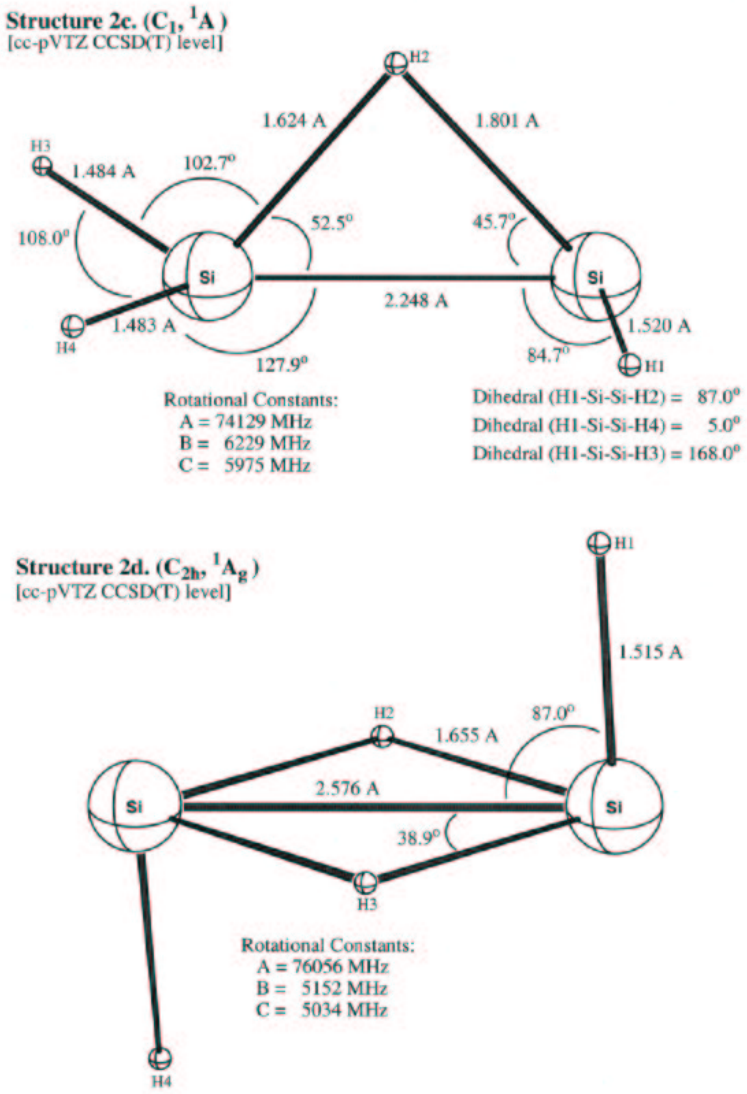

Figure 5.6: The structures **2c** and **2d**.

Structure 2e. (C_{2v}, $^1A_1$)
[cc-pVTZ CCSD(T) level]

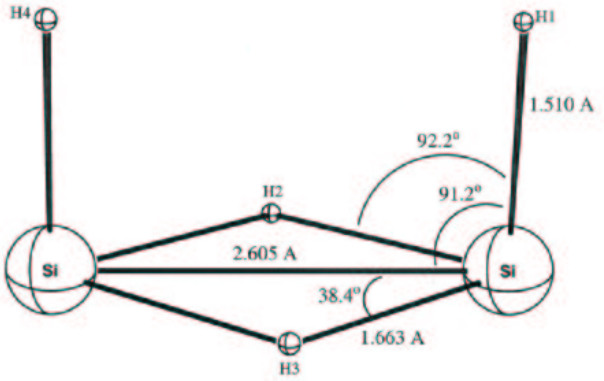

Rotational Constants:
A = 76558 MHz
B = 5019 MHz
C = 4907 MHz

Dihedral (H1-Si-Si-H2) = 92.0°
Dihedral (H2-Si-Si-H3) = 176.0°

Figure 5.7: The structure **2e**.

that we have discovered some other molecule. By comparison $B + C$=12.25 GHz for disilene (**2a**), 10.77 GHz for silylsilylene (**2b**), 12.21 GHz for the monobridged structure (**2c**), 10.19 GHz for the trans-like dibridged structure (**2d**), and 9.93 GHz for cis-like dibridged structure (**2e**). On this basis, all but disilene and the monobridged isomer can be eliminated from further consideration. Since disilene is nonpolar by symmetry it too can be eliminated as a candidate, leaving only H_2Si-H-SiH, which is calculated to possess a dipole moment of 1.14 debye at the cc-pVTZ CCSD(T) level of theory. Finally, conclusive evidence for the laboratory identification is provided by the detection of the ^{29}Si and ^{30}Si isotopic species and $D_2SiDSiD$ at precisely the expected isotopic shifts (see Table 5.10) for a molecule with this unusual monobridged geometry. A detailed account of the Si_2H_4 laboratory measurements and data analysis will appear separately.

There is evidence for inversion doubling in the rotational spectrum of monobridged (**2c**) Si_2H_4, since each rotational line consists of a closely-spaced doublet of equal intensity (Figure 5.8). The frequency separation between the two lines is so small — typically several tens of kHz — that it is only resolved in the present experiments because of the high spectral resolution of the FTM technique. This inversion implies that the molecule is interconverting between two equivalent structures, the magnitude of the splitting indicating that there is a fairly highbarrier to inversion motion. To consider whether this explanation is correct, we searched for a possible transition state (at the cc-pVDZ CCSD(T) level) that might lead to such motion. In fact, we have located a transition state which is presented in figure 5.9. As given in the figure, the structure has one imaginary harmonic vibrational frequency of $657i$ cm^{-1} which corresponds to the replacement of the terminal hydrogen of the monobridged isomer (structure **2c**) with the bridged hydrogen, producing the equivalent mono-bridged isomer. The barrier hight for this reaction is determined to be 10.9 kcal/mol at the cc-pVDZ CCSD(T) level. A single point computation at the cc-

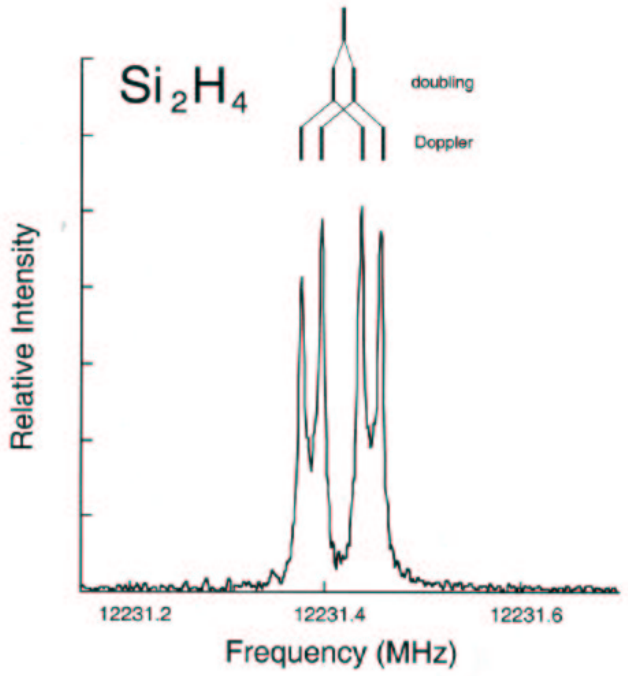

Figure 5.8: The $1_{0,1} \rightarrow 0_{0,0}$ transition of monobridged H_2Si-H-SiH showing the characteristic doubling of each rotational line which arises from inversion. Each feature possesses a double-peaked line shape owing to an instrumental artifact: the Doppler splitting which results from the interaction of the supersonic axial molecular beam with the standing wave of the confocal Fabry-Perot microwave cavity. The integration time was approximately 2 minutes.

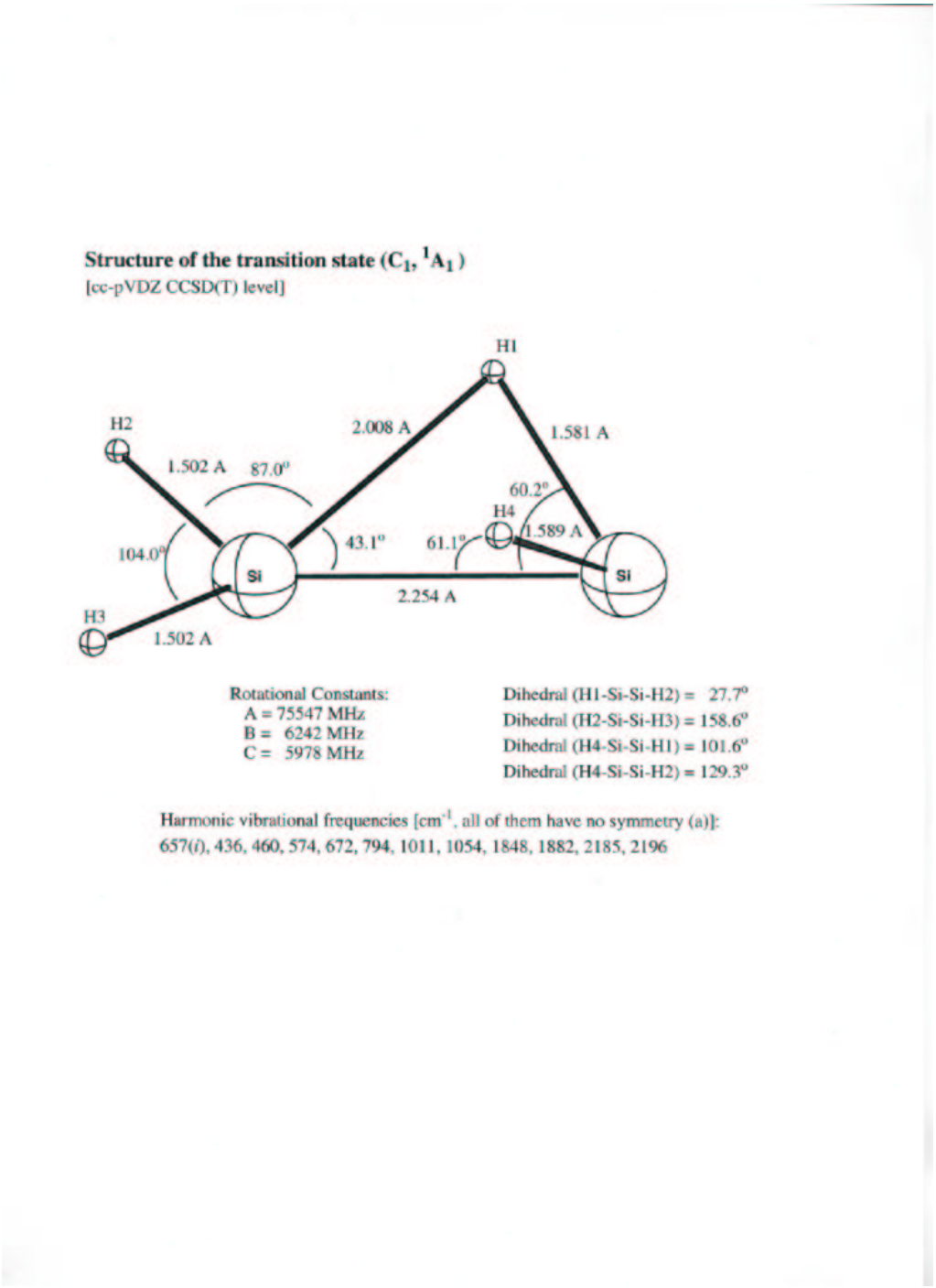

Figure 5.9: The structure of the transition state between two equivalent mono-bridged isomers of Si_2H_4.

Table 5.1: Dipole moments (debye), harmonic vibrational frequencies (cm^{-1}), and associated infrared intensities (km/mol, in parentheses) for the isomers of the Si_2H_3, determined at the cc-pVTZ CCSD(T) level.

Structure	μ_e	ZPVE	Harmonic vibrational frequencies (symmetries, infrared intensities)
1a (H_2Si-SiH, $^2A''$)	1.04	13.97	319(a″,2), 385(a″,12), 414(a′,4), 470(a′,10), 709(a′,36), 976(a′,85), 2047(a′,157), 2214(a′,100), 2237(a′,106)
1b (H_3Si-Si, $^2A''$)	0.30	15.60	396(a″,47), 416(a′,11), 486(a′,16), 898(a″,291), 964(a′,48), 989(a″,33), 2224(a′,105), 2266(a′,79), 2276(a″,95)
1c (H_2Si-H-Si, $^2A''$)	1.07	14.53	409(a″,7), 472(a′,2), 507(a′,26), 713(a″,13), 955(a′,33), 1016(a′,382), 1664(a′,94), 2210(a′,143), 2221(a″,101)
1d (H-Si-H-Si-H, ^2A)	0.11	14.74	471(a,0), 623(b,108), 658(a,7), 731(a,0), 844(b,591), 1210(b,1049), 1532(a,70), 2109(a,2), 2129(b,331)
1e (H-Si-H-Si-H, ^2A)	0.74	13.73	393(a,13), 423(a,5), 566(a,1), 643(a,47), 889(a,33), 1052(a,210), 1541(a,68), 2010(a,103), 2114(a,164)

pVTZ CCSD(T) level was carried out on the optimized transition state structure, and an energy barrier of 10.0 kcal/mol were found.

5.4.2 Dipole Moments

Dipole moments were determined as first derivatives of the total energies with respect to external electric fields. The cc-pVTZ CCSD(T) values for the dipole moments are given in Table 5.1 for Si_2H_3 and in Table 5.5 for Si_2H_4 molecule. The Si_2H_3 predicted dipole moments for the planar (structure **1a**) and newly predicted mono-bridged

(structure **1c**) isomers are very close to each other (1.04 and 1.07 debyes respectively). The trans-like mono-bridged isomer (structure **1d**) has a very small dipole, 0.30 debye, whereas the cis-like mono-bridged isomer (structure **1e**) has a relatively larger dipole moment of 0.70 debye. The most polar isomer of the Si_2H_4 molecule is the newly predicted mono-bridged isomer (structure **2c**). It has a permanent dipole moment of 1.14 debye which is close to that of mono-bridged isomer of Si_2H_3 (structure **1c**). The Si_2H_4 disilene (structure **2a**) and the trans dibridged (structure **2d**) isomers have no dipole moments by symmetry.

5.4.3 Harmonic Vibrational Frequencies

Although there are many theoretical studies of the structure and energetics of Si_2H_3 and Si_2H_4, there are only two literature studies that report the harmonic vibrational frequencies. Both of these are for the Si_2H_4 molecule. Therefore, to best of our knowledge, the present values for the harmonic vibrational frequencies as well as infrared intensities of the isomers of Si_2H_3 are the first predictions. We present our results in Table 5.1 for Si_2H_3. As seen in the table, all of the harmonic vibrational frequencies (varying from 319 cm^{-1} to 2276 cm^{-1}) are real, which confirms that the optimized structures are true minima on the potential energy surface. For the mono-bridged isomer of Si_2H_3 (structure **1c**), predicted to be the lowest energy isomer, an active mode with a infrared intensity of 382 km/mol is found. This mode corresponds to the bending of two terminal hydrogens, along with the motion of bridged hydrogen in the perpendicular plane. It has $a^{'}$ symmetry with a 1016 cm^{-1} harmonic vibrational frequency. This mode can be used to characterize our predicted mono-bridged isomer if infrared spectrum of Si_2H_3 is obtained.

Trinquier[121] predicted harmonic vibrational frequencies for three different isomers of Si_2H_4; the disilene (structure **2a**), the trans-like (structure **2d**) and cis-like di-bridged (structure **2e**) isomers. However, he found a planar disilene at his level of

computation (SCF/DZP). Therefore his results for disilene are quite different from our predictions. His predictions concerning the di-bridged structures are generally 60-90 cm^{-1} larger than our results. This is expected because correlated levels usually produce smaller harmonic vibrational frequencies. Another study of Si_2H_4 was reported by Andrews et. al.[122] in 2002. They experimentally obtained an infrared spectrum and also carried out B3LYP/6-31++G(d,p) calculations. They resolved a 858.5 cm^{-1} SiH_2 bending mode and a 2154.0 cm^{-1} Si-H stretching mode from their spectrum. Based on their B3LYP/6-31++G(d,p) predictions, they concluded that the observed peaks are associated with a trans-bent disilene. Their B3LYP/6-31++G(d,p) results showed three harmonic vibrational frequencies with large intensities. These are the two Si-H stretches, at 2264.0 cm^{-1} and 2231.1 cm^{-1}, and a SiH_2 bending mode. Our results showed that disilene has a b_u Si-H stretching at 2247 cm^{-1} with a 110 km/mol intensity, an a_u Si-H stretching at 2277 cm^{-1} with a 128 km/mol intensity, and a b_u SiH_2 bending at 922 cm^{-1} with 182 km/mol intensity. The experimentally observed values of 858.5 cm^{-1} and a 2154.0 cm^{-1} are close to our active modes of b_u Si-H stretching (2247 cm^{-1}) and b_u SiH_2 bending (922 cm^{-1}) symmetry.

5.4.4 Relative Energies

Si_2H_3

Sax and Kalcher[117] used the MRCI technique with double and triple-ζ quality basis sets, and investigated H_3Si-Si ($^2A''$) and the near-planar H_2Si-SiH isomers of the Si_2H_3 molecule. They predicted the H_3Si-Si ($^2A''$) isomer to be 1.1 kcal/mol more stable than the near-planar H_2Si-SiH isomer. In the same year, Curtiss et. al.[118] did G2 calculations and they reported that the lowest energy isomer is the H_3Si-Si ($^2A''$) structure, in agreement with the results obtained by Sax and Kalcher. They

Table 5.2: Relative Energies (kcal/mol) for the isomers of the Si_2H_3 at different level of theories (with the cc-pVTZ basis set).

Structure	SCF	CCSD(2)	CCSD(T)
1a (H_2Si-SiH, $^2A''$)	5.48	0.29	0.98
1b (H_3Si-Si, $^2A''$)	0.00	1.15	0.00
1c (H_2Si-H-Si, $^2A''$)	Not a Minimum	0.00	0.10
1d (H-Si-H-Si-H, ^2A)	20.20	4.57	4.27
1e (H-Si-H-Si-H, ^2A)	21.89	12.05	12.04

also stated that "mono-, di-, and tri- bridged structures were also investigated, but all bridged structures were found to be significantly higher in energy". However, in 1997, Gong et al[107] predicted a mono-bridged structure (HSi-H-SiH, C_2) to be the lowest energy isomer, after investigating six different structures: silylsilylidyne H_3Si-Si (C_s); the near-planar H_2Si-SiH (C_1); two mono-bridged isomers, HSi-H-SiH (C_2) and H_2Si-H-Si (C_s); a di-bridged; and a tri-bridged isomer. They also reported that the H_3Si-Si (C_s) like structure, which was predicted to be the lowest energy isomer by both Kalcher[117] and Pople[118], is 9.0 kcal/mol (0.39 eV) higher in energy. The tri-bridged isomer was found to be significantly higher in energy (0.64 eV). In 2001, Pak et. al.[104] reported B3LYP/DZP+ calculations and studied the H_3Si-Si (C_s), the near-planar H_2Si-SiH (C_1), and the mono-bridge (HSi-H-SiH, C_2) isomers. They reported that the H_3Si-Si (C_s) isomer and the near-planar H_2Si-SiH (C_1) isomer are almost equivalent in energy. Therefore, they pointed out that high level quantum chemical methods should be employed in order to tell which isomer is the lowest in energy.

As seen in Table 5.2, the H_3Si-Si (structure **1b**) is the lowest isomer at the SCF (Hartree-Fock) level, as predicted previously. At the same level of theory, the mono-bridged isomer (structure **1c**) could not be located. However, when the correlated levels [cc-pVDZ CCSD(T) and cc-pVTZ CCSD(T)] were employed, the mono-bridged isomer (structure **1c**) was found (with all real harmonic vibrational frequencies, see Table 5.1). The mono-bridged isomer (structure **1c**) is stabilized by both electron correlations and basis set expansion, as seen in Table 5.2 and 5.3. At the cc-pVDZ CCSD(T) level, the relative energy of the mono-bridged form (structure **1c**) with respect to the H_3Si-Si (structure **1b**) is +1.80 kcal/mol whereas at the cc-pVDZ CCSDT level, it is -0.31 kcal/mol. The CCSD(T) level of theory predicts the same energy difference as +0.10 kcal/mol with the cc-pVTZ basis set. When we add the effect of full triple corrections [cc-pVDZ CCSDT - cc-pVDZ CCSD(T)] to the estimated value at the cc-pVTZ CCSD(T) level (to predict cc-pVTZ CCSDT), as well as with the zero-point vibrational energy (ZPVE) and relativistic corrections, we found that the mono-bridged isomer (structure **1c**) is 3.15 kcal/mol *below* the H_3Si-Si isomer (structure **1b**), as given in Table 5.4. The planar Si_2H_3 isomer (structure **1a**), previously predicted[104,107,117,118] to be higher in energy than the H_3Si-Si (structure **1b**), is found to be stabilized by both correlation effects and basis set expansion. Although it is 5.48 kcal/mol higher in energy than the H_3Si-Si (structure **1b**) at the SCF level, it is only 0.98 kcal/mol higher in energy at the cc-pVTZ CCSD(T) level. Including all effects (ZPVE, full triples, and scalar relativity) to the cc-pVTZ CCSD(T) results, we predict that the planar form (structure **1a**) is *lower* in energy than the H_3Si-Si isomer by 2.92 kcal/mol. The mono-bridged isomer in C_2 symmetry (structure **1d**), which was predicted to be the lowest energy form by Gong et al[107], is found to be 4.20 kcal/mol *higher* than the mono-bridged structure in C_s symmetry (structure **1c**).

Table 5.3: The effects of full-triple coupled-cluster excitations on the relative energies of the isomers of the Si_2H_3, determined with the cc-pvDZ basis set [kcal/mol, values are with respect to the mono-bridged (**1c**) isomer]

Structure	CCSD(T)	CCSDT	Change
1a (H_2Si-SiH, $^2A''$)	0.15	0.03	-0.12
1b (H_3Si-Si, $^2A''$)	-1.80	0.31	+2.11
1c (H_2Si-H-Si, $^2A''$)	0.00	0.00	0.00
1d (H-Si-H-Si-H, ^2A)	4.46	4.36	-0.10
1e (H-Si-H-Si-H, ^2A)	12.03	11.99	-0.04

Table 5.4: Effects of full-triple coupled-cluster excitations, relativistic (MVD) corrections, and zero-point vibrational energy corrections on the relative energies of the isomers of Si_2H_3. The best estimates for the relative energies include all corrections on top of the cc-pVTZ CCSD(T) results [kcal/mol, all values are with respect to the mono-bridged (**1c**) isomer].

Structure	cc-pVTZ CCSD(T)	Full-Triples Corrections	Relativistic Corrections	ZPVE Corrections	Best Estimates
1a (H_2Si-SiH, $^2A''$)	0.88	-0.12	+0.03	-0.56	0.23
1b (H_3Si-Si, $^2A''$)	-0.10	+2.11	+0.07	+1.07	3.15
1c (H_2Si-H-Si, $^2A''$)	0.00	0.00	0.00	0.00	0.00
1d (H-Si-H-Si-H, ^2A)	4.17	-0.10	-0.08	+0.21	4.20
1e (H-Si-H-Si-H, ^2A)	11.94	-0.04	-0.10	-0.80	11.00

Table 5.5: Dipole moments (debye), harmonic vibrational frequencies (cm^{-1}), and associated infrared intensities (km/mol, in parentheses) for the isomers of the Si_2H_4, determined at the cc-pVTZ CCSD(T) level.

Structure	μ_e	ZPVE	Harmonic vibrational frequencies (symmetries, infrared intensities)
2a (H_2Si-SiH_2, ^1A_g)	0.00	19.58	317(a_g,0), 334(a_u,18), 441(b_u,21), 514(a_u,0), 566(a_g,0), 604(b_g,0), 922(b_u,182), 955(a_g,0), 2247(b_u,110), 2251(a_g,0), 2267(b_g,0), 2277(a_u,128)
2b (H_3Si-SiH, $^1A'$)	0.23	19.34	99(a'',10), 381(a',9), 386(a'',25), 434(a',17), 716(a',53), 879(a',230), 947(a',56), 970(a'',36), 2058(a',161), 2204(a',67), 2217(a'',96), 2239(a',117)
2c (H_2Si-H-SiH, ^1A)	1.14	19.76	389(a,7), 475(a,2), 518(a,13), 645(a,6), 694(a,35), 878(a,69), 972(a,68), 1074(a,328), 1645(a,96), 2060(a,140), 2228(a,131), 2247(a,109)
2d (H-Si-H_2-Si-H, ^1A_g)	0.00	20.31	264(b_u,2), 394(a_g,0), 733(a_u,14), 858(b_u,135), 859(a_g,0), 871(b_g,0), 1360(a_u,21), 1517(b_g,0), 1527(b_u,917), 1665(a_g,0), 2074(a_g,0), 2089(b_u,340)
2e (H-Si-H_2-Si-H, $^1A_1$)	0.50	20.03	363(a_1,0), 396(a_1,0), 645(a_2,0), 749(b_1,88), 866(b_2,14), 889(a_1,24), 1334(b_2,26), 1440(a_2,0), 1465(b_1,1214), 1656(a_1,0), 2092(b_1,20), 2115(a_1,300)

Table 5.6: Relative energies (kcal/mol) for the isomers of the Si_2H_4 at different levels of theory (with the cc-pVTZ basis set).

Structure	SCF	CCSD(2)	CCSD(T)
2a (H_2Si-SiH_2, ^1A_g)	0.00	0.00	0.00
2b (H_3Si-SiH, $^1A'$)	0.07	6.28	6.86
2c (H_2Si-H-SiH, ^1A)	Not a Minimum	7.01	6.64
2d (H-Si-H_2-Si-H, ^1A_g)	22.34	19.54	19.20
2e (H-Si-H_2-Si-H, $^1A_1$)	24.65	22.23	22.13

SI_2H_4

All previous Si_2H_4 theoretical studies found that the disilene (structure **2a**) lies lower in energy than silylsilylene (structure **2b**).[104,117,118,120,122] We similarly predict that disilene is 6.51 kcal/mol more stable than silylsilylene. However, the competition here is found to be between the newly predicted mono-bridged isomer (structure **2c**) and silylsilylene (structure **2b**). As we mentioned earlier, the newly predicted mono-bridged isomer is not found at the SCF level. At the cc-pVDZ CCSD(T) level, the silylsilylene (structure **2b**) is 1.49 kcal/mol more stable than the mono-bridged form. However, at the cc-pVTZ CCSD(T) level, the mono-bridged isomer was found to lie 0.22 kcal/mol lower than the silylsilylene (structure **2b**, see Table 5.6 and 5.7).

In other words, basis set expansion favors the mono-bridged form with respect to the silylsilylene. Both relativistic corrections and ZPVE corrections favor the silylsilylene. As seen in Table 5.8, the relativistic corrections (MVD) lower the relative energy of silylsilylene by 0.27 kcal/mol, and increase the relative energy of the

Table 5.7: The effects of full-triple coupled-cluster excitations on the relative energies of the isomers of the Si_2H_4 (kcal/mol, with the cc-pvDZ basis).

Structure	CCSD(T)	CCSDT	Change
2a (H_2Si-SiH_2, ^1A_g)	0.00	0.00	0.00
2b (H_3Si-SiH, $^1A'$)	6.44	6.60	+0.16
2c (H_2Si-H-SiH, ^1A)	7.93	8.15	+0.22
2d (H-Si-H_2-Si-H, ^1A_g)	19.42	20.12	+0.70
2e (H-Si-H_2-Si-H, $^1A_1$)	21.96	22.13	+0.17

Table 5.8: Effects of full-triple coupled-cluster excitations, relativistic (MVD) corrections, and zero-point vibrational energy corrections on the relative energies of the isomers of Si_2H_4. The best estimates for the relative energies include all corrections on top of the cc-pVTZ CCSD(T) results [kcal/mol, all values are with respect to the disilene (**2a**) isomer].

Structure	cc-pVTZ CCSD(T)	Full-Triple Corrections	Relativistic Corrections	ZPVE Corrections	Best Estimates
2a (H_2Si-SiH_2, ^1A_g)	0.00	0.00	0.00	0.00	0.00
2b (H_3Si-SiH, $^1A'$)	6.86	+0.16	-0.27	-0.24	6.51
2c (H_2Si-H-SiH, ^1A)	6.64	+0.22	+0.12	+0.18	7.16
2d (H-Si-H_2-Si-H, ^1A_g)	19.20	+0.70	-0.12	+0.73	20.51
2e (H-Si-H_2-Si-H, $^1A_1$)	22.13	+0.17	-0.11	+0.45	22.64

Table 5.9: Experimental and theoretical rotational constants of isotopic planar H_2SiSiH (in MHz).

Isotopic Species	$B+C$		Percent Difference
	Experiment	Theory	(%)
H_2SiSiH	12067	11914	−1.3
$H_2{}^{29}SiSiH$	11902	11748	−1.3
$H_2{}^{30}SiSiH$	11748	11588	−1.4
$H_2Si^{29}SiH$	11872	11717	−1.3
$H_2Si^{30}SiH$	11689	11527	−1.4
D_2SiSiD	10632	10484	−1.4

mono-bridged structure by 0.12 kcal/mol with respect to the disilene. The ZPVE for the mono-bridged form is estimated to be 0.42 kcal/mol larger than that for the silylsilylene (see Table 5.5). As a result, when we collected all of the corrections, the silylsilylene (structure **2b**) is found to be 0.65 kcal/mol *below* the mono-bridged form. As seen in Table 5.6, the cc-pVTZ CCSD(2) level of theory also predicts the silylsilylene to be more stable than the mono-bridged form by 0.73 kcal/mol. Both the trans (structure **2d**) and cis (structure **2e**) di-bridged forms of Si_2H_4 are estimated to be about 20 kcal/mol higher in energy than the disilene, the lowest energy form. As expected, the trans-like di-bridged form is found to be more stable than the cis-like di-bridged form. As a best value, 2.13 kcal/mol energy is estimated for the energy gap between the latter two isomers.

5.5 Concluding Remarks

A total of ten stable isomers of the Si_2H_3 and Si_2H_4 molecules have been located on the ground electronic state potential energy hypersurfaces. Scalar relativistic corrections and zero-point vibrational energy corrections were included in order to predict accurate energetic properties. For the first time, the mono-bridged H_2Si-H-Si isomer

Table 5.10: Experimental and theoretical rotational constants of isotopic mono-bridged $H_2SiHSiH$ (in MHz).

Isotopic Species	Rotational Constant	Experiment	Theory	Difference (%)
$H_2SiHSiH$	A	73012(187)	74129	1.5
	B	6243.731(1)	6229	−0.2
	C	5987.703(1)	5976	−0.2
$H_2{}^{29}SiHSiH$	A	73012[a]	74113	···
	B	6156(1)	6142	−0.2
	C	5911(1)	5895	−0.3
$H_2{}^{30}SiHSiH$	A	73012[a]	74097	···
	B	6077(1)	6058	−0.3
	C	5836(1)	5818	−0.3
$H_2SiH^{29}SiH$	A	73012[a]	74100	···
	B	6140(1)	6125	−0.2
	C	5894(1)	5879	−0.3
$H_2SiH^{30}SiH$	A	73012[a]	74072	···
	B	6045(1)	6024	−0.3
	C	5804(1)	5786	−0.3
$D_2SiDSiD$	A	37518[b]	37518	···
	B	5561.0(5)	5529	−0.6
	C	5171.9(5)	5144	−0.5

[a]Constrained to the value of the normal isotopic species.
[b]Constrained to the theoretical value of the fully deuterated isotopic species.

(C_s, $^2A''$) is predicted to be the lowest energy structure on the ground potential energy surface of Si_2H_3. One mono- and two di-bridged isomers are also found for the Si_2H_4. In addition to the much studied silylsilylene, H_3Si-SiH, we find that an unexpected monobridged isomer H_2Si-H-SiH (C_1, ^1A) is a minimum on the potential energy surface. By means of Fourier transform microwave spectroscopy of a supersonic molecular beam, the rotational spectrum of this novel mono-bridged Si_2H_4, as well as the for the planar (H_2Si-SiH) isomer of Si_2H_3, have been measured. Excellent agreement with theory has been observed. Harmonic vibrational frequencies as well

as infrared intensities for all isomers are predicted at the cc-pVTZ CCSD(T) level of theory.

Chapter 6

Conclusion

Challenging problems related with the electronic structures of the novel group IV small molecules have been attempted with the very sophisticated quantum mechanical ab initio methods such as coupled cluster with single and double excitations with perturbative triple excitations [CCSD(T)] and with full triple excitations CCSDT levels of theory. These problems include characterizations of the Renner-Teller splitting in the ground electronic states of HCSi and HCGe, the elusive ground state equilibrium structure of the GeC_2, and unanticipated mono- and di-bridged isomers of the Si_2H_3 and Si_2H_4 molecules. Scalar relativistic corrections and corrections due to the zero point vibrational energy (ZPVE) and core-valence interactions have been included, and large basis sets such TZ3P($2f$,$2d$)+$2diff$ and cc-pVQZ have been employed. Equation of motion coupled cluster theories were employed in order to determine some excited state properties that cannot be determined using standard quantum mechanical methods due to possible variational collapses.

Some of the very important results can be listed as follows;

- We have found that relativistic corrections do have some effects in the amount of Renner-Teller splitting. This is an indirect effect due to the relativistic changes in bending harmonic vibrational frequencies (see chapter 3).

- The equilibrium geometry for the GeC_2 molecule is predicted to be L-shaped. Both T-shaped and linear configurations have found to be transition states. This is a quite surprising finding because the isovalent SiC_2 molecule was

determined to be T-shaped in its ground state, after a 50 years wrong belief in the linear structure. Both the scalar relativistic corrections and core-valence corrections were found to favor the L-shape geometry with respect to T-shaped one (see chapter 4).

- Ten stable isomers of the Si_2H_3 and Si_2H_4 molecules have been located on the ground electronic state potential energy hypersurfaces. For the first time, the mono-bridged H_2Si-H-Si isomer (C_s, $^2A''$) is predicted to be the lowest energy structure. In addition, an unexpected monobridged isomer H_2Si-H-SiH (C_1, ^1A) is determined to be a minimum on the potential energy surface of the Si_2H_4 molecule. Collaborations with Harvard experimentalists confirmed that the predicted new monobridged Si_2H_4 isomer is stable (see chapter 5).

- The relativity and core-valence interactions produce very noticeable effects on the properties of the molecules that contain germanium atom. The effects are observed to be even larger for the energy gaps between two different electronic states. This is believed to be a consequence of the fact that total angular momentum of an electronic state is important for the amount of relativistic corrections.

In addition to the above results, physical and chemical properties such as bonding characters, equilibrium geometries, dipole moments, harmonic vibrational frequencies, rotational constants, excitation and relative energies, and infrared intensities have been studied, and reliable values have been determined with the coupled cluster theories. Comparison with the available experimental data suggested that coupled cluster theory is able to predict bond distances within ± 0.1 Å and energetic properties within ± 1 kcal/mol accuracy when it is employed with large basis sets.

Bibliography

[1] Čížek, J. *J. Chem. Phys.* **1966,** *45,* 4256.

[2] Čížek, J. *Adv. Chem. Phys.* **1969,** *14,* 35.

[3] Čížek, J. *Int. J. Quantum Chem.* **1971,** *5,* 359.

[4] Hurley, A. C. *Electron Correlation in Small Molecules;* Academic Press: London, 1976.

[5] Monkhorst, H. J. *Int. J. Quantum Chem. Symp.* **1977,** *11,* 421-432.

[6] Pople, J. A.; Krishnan, R.; Schlegel, H. B.; Binkley, J. S. *Int. J. Quantum Chem. Symp.* **1978,** *14,* 545.

[7] Bartlett, R. J.; Purvis, G. D. *Int. J. Quantum Chem.* **1978,** *14,* 561.

[8] Purvis, G. D.; Bartlett, R. J. *J. Chem. Phys.* **1982,** *76,* 1910.

[9] Purvis, G. D.; Bartlett, R. J. *J. Chem. Phys.* **1981,** *75,* 1284.

[10] Scuseria, G. E.; Lee, T. J.; Schaefer, H. F. *Chem. Phys. Lett.* **1986,** *130,* 236.

[11] Scuseria, G. E.; Scheiner, A. C.; Lee, T. J.; Rice, J. E.; Schaefer, H. F. *J. Chem. Phys.* **1987,** *86,* 2881.

[12] Lee, T. J.; Rice, J. E. *Chem. Phys. Lett.* **1988,** *150,* 406.

[13] Scuseria, G. E.; Janssen, C. L.; Schaefer, H. F. *J. Chem. Phys.* **1988,** *89,* 7382.

[14] Stanton, J. F.; Gauss, J.; Watts, J. D.; Bartlett, R. J. *J. Chem. Phys.* **1991,** *94,* 4334.

[15] Crawford, T. D.; Schaefer, H. F. *Rev. In Comp. Chem.* **2000,** *14,* 33.

[16] Schwarz, W. H. E.; van Wezenbeek, E. M.; Baerends, E. J.; Snijders, J. G. *J. Phys. B.* **1989,** *22,* 1515.

[17] Kellö, V.; Urban, M.; Sadlej, A. J. *Chem. Phys. Lett.* **1996,** *253,* 383.

[18] Pyykkö, P. *Relativistic Theory of Atoms and Molecules;* Springer-Verlag: Berlin, 1986.

[19] Balasubramanian, K. *Relativistic Effects in Chemistry Part A;* John Wiley Sons, Inc.: New York, 1997.

[20] Rose, E. M. *Relativistic Electron Theory;* Wiley: New York, 1961.

[21] Moss, R. E. *Advanced Molecular Quantum Mechanics;* Wiley: New York, 1973.

[22] Balasubramanian, K. *Relativistic Effects in Chemistry Part B;* John Wiley Sons, Inc.: New York, 1997.

[23] Cowan, R. D.; Griffin, D. C. *J. Opt. Soc. Am.* **1976,** *66,* 1010.

[24] Martin, R. L. *J. Phys. Chem.* **1983,** *87,* 730.

[25] Martin, R. L. *J. Chem. Phys.* **1983,** *78,* 5840.

[26] Dyall, K. G. *J. Chem. Phys.* **1992,** *96,* 1210.

[27] Thaddeus, P.; Cummins, S. E.; Linke, R. *Astrophys. J.* **1984,** *283,* L45.

[28] McCarthy, M. C.; Apponi, A. J.; Thaddeus, P. *J. Chem. Phys* **1999,** *110,* 10645.

[29] Ohishi, M.; Kaifu, N.; Kawaguchi, K.; Murakami, A.; Saito, S.; Yamato, S.; Ishikawa, S.; Fujita, Y.; Shiratori, Y.; Irvine, W. M. *Astrophys. J.* **1989,** *345,* L83.

[30] Cernicharo, J.; Gottlieb, C. A.; Guelin, M.; Thaddeus, P.; Vrtilek, J. M. *Astrophys. J.* **1989,** *341,* L25.

[31] Goldhaber, D. M.; Beltz, A. L. *Astrophys. J.* **1984,** *279,* L55.

[32] Herbst, E.; Miller, T. J.; Wlodek, S.; Bohme, D. K. *Astron. Astrophys. J.* **1989,** *222,* 205.

[33] Kaneko, T.; Sone, H.; Miyakawa, N.; Naka, M. *Jpn. J. Appl. Phys.* **1999,** *Part 1 38,* 2089.

[34] Lee, B.-T.; Kim, D.-K.; Moon, C.-K.; Kim, J. K.; Seo, Y. H.; Nahm, K. S.; Lee, H. J.; Lee, K. W.; Yu, K.-S.; Kim, Y.; Jang, S. J. *J. Mater. Res.* **1999,** *14,* 24.

[35] Pereya, I.; Carreno, M. N. P.; Tabacniks, M. H.; Prado, R. J.; Fantini, M. C. A. *J. Appl. Phys.* **1998,** *84,* 2371.

[36] Stapinski, T.; Ambrosone, G.; Coscia, U.; Giorgis, F.; Pirri, C. F. *Physica B.* **1998,** *254,* 99.

[37] Srinavas, R.; Sulzle, D.; Schwarz, H. *J. Am. Chem.* **1991,** *113,* 52.

[38] Han, D. S.; Rittby, C. M. L.; Graham, W. R. M. *J. Chem. Phys.* **1998,** *108,* 3504.

[39] Cireasa, R.; Cossart, D.; Vervleot, M. *Eur. Phys. J.* **1998,** *D 2,* 199.

[40] Smith, T. C.; Li, H.; Clouthier, D. J. *J. Am. Chem. Soc.* **1999,** *121,* 6068.

[41] Smith, T. C.; Li, H.; Clouthier, D. J.; Kingston, C. T.; Merer, A. J. *J. Chem. Phys.* **2000,** *112,* 3662.

[42] Cirease, R.; Cossart, D.; Vervloet, M.; Robbe, J. M. *J. Chem. Phys.* **2000,** *112,* 10806.

[43] Robbe, J. M.; Lavendy, H.; Flament, J. P.; Chambaud, G. *Chem. Phys. Letters* **1997,** *267,* 91-97.

[44] Herzberg, G.; Teller, E. *Z. Phys. Chem. Abt. B* **1933,** *21,* 410.

[45] Renner, R. *Z. Phys.* **1934,** *92,* 172.

[46] Hougen, J. T. *J. Chem. Phys.* **1962,** *36,* 1874.

[47] Jungen, C.; Merer, A. J. . In *Molecular Spectroscopy: Modern Research*, Vol. 2; Rao, K. N., Ed.; Academic Press: New York, 1976.

[48] Brown, J. M.; Jørgensen, F. *Adv. Chem. Phys.* **1983,** *52,* 117.

[49] Bunker, P. R.; Jensen, P. *Molecular Symmetry and Spectroscopy;* NRC Research Press: Ottawa, 2nd edition, 1998.

[50] Lee, T. J.; Schaefer, H. F.; Pitzer, R. M. *J. Chem. Phys* **1984,** *81,* 356.

[51] Yamaguchi, Y.; Alberts, I. L.; Goddard, J. D.; Schaefer, H. F. *Chem. Phys.* **1990,** *147,* 309.

[52] Burton, N. A.; Yamaguchi, Y.; Alberts, I. L.; Schaefer, H. F. *J. Chem. Phys.* **1991,** *95,* 7466.

[53] Crawford, T. D.; Stanton, J. F.; Allen, W. D.; Schaefer, H. F. *J. Chem. Phys.* **1997,** *107,* 10626.

[54] Herzberg, G. *Molecular Spectra and Molecular Structure III. Electronic Spectra and Electronic Structure of Polyatomic Molecules;* Van Nostrand: Princeton, NJ,, 1966.

[55] Mclean, A. D.; Chandler, G. S. *J. Chem. Phys* **1980,** *72,* 5639.

[56] Huzinaga, S. *Approximate Atomic Functions. II;* Department of Chemistry Report: University of Alberta, Edmonton, Alberta, Canada, 1971.

[57] Dunning, T. H. *J. Chem. Phys.* **1971,** *55,* 716.

[58] Huzinaga, S. *J. Chem. Phys.* **1965,** *42,* 1293.

[59] Woon, D. E.; Dunning, T. H. *J. Chem. Phys.* **1993,** *98,* 1358.

[60] Purvis, G. D.; Bartlett, R. J. *J. Chem. Phys.* **1982,** *76,* 1910.

[61] Raghavachari, K.; Trucks, G. W.; Pople, J. A.; Head-Gorden, M. *Chem. Phys. Lett.* **1989,** *157,* 479.

[62] Pulay, P. . In *Modern Theoretical Chemistry*, Vol. 4; Schaefer, H. F., Ed.; Plenum Press: New York, 1977.

[63] Yamaguchi, Y.; Osamura, Y.; Goddard, J. D.; Schaefer, H. F. *A New Dimension to Quantum Chemistry: Analytic Derivative Methods in Ab Initio Molecular Electronic Structure Theory;* Oxford University Press: New York, 1994.

[64] PSI 2.0.8; C. L. Janssen, E. T. Seidl, G. E. Scuseria, T. P. Hamilton, Y. Yamaguchi, R. B. Remington, Y. Xie, G. Vacek, C. D. Sherrill, T. D. Crawford, J. T. Fermann, W. D. Allen, B. R. Brooks, G. B. Fitzgerald, D. J. Fox, J. F. Gaw, N . C. Handy, W. D. Laidig, T. J. Lee, R. M. Pitzer, J. E. Rice, P. Saxe, A. C. Scheiner, and H. F. Schaefer, PSITECH, Inc., Watkinsville, GA, 30677, U.S.A., 1994.

[65] ACES II is a program product of the Quantum Theory Project, University of Florida. Authors: J. F. Stanton, J. Gauss, J. D. Watts, M. Nooijen, N. Oliphant, S. A. Perera, P. G. Szalay, W. J. Lauderdale, S. R. Gwaltney, S. Beck, A. Balkova, D. E. Bernholdt, K.-K. Baeck, P. Rozyczko, H. Sekino, C. Hober, and R. J. Bartlett. Integral packages included are VMOL (J. Almlöf and P. R. Taylor); VPROPS (P. Taylor); ABACUS (T. Helgaker, H. J. Aa. Jensen, P. Jørgensen, J. Olsen, and P. R. Taylor).

[66] Lavendy, H.; Robbe, J. M.; Duflot, D.; Flament, J. P. *AIP Conference Processing 312* **1994,** *343,*.

[67] Harper, W. W.; Ferrall, E. A.; Hilliard, R. K.; Stogner, S.; Grev, R. S.; Clouthier, D. J. *J. Am. Chem. Soc.* **1997,** *119,* 8361.

[68] Stogner, S. M.; Grev, R. S. *J. Chem. Phys.* **1998,** *108,* 5458.

[69] Hostutler, D. A.; Smith, T. C.; Li, H.; Clouthier, D. J. *J. Chem. Phys.* **1999,** *111,* 950.

[70] Smith, T. C.; Li, H.; Clouthier, D. J. *J. Am. Chem. Soc.* **1999,** *121,* 6068.

[71] Smith, T. C.; Li, H.; Clouthier, D. J.; Kingston, C. T.; Merer, A. J. *J. Chem. Phys.* **2000,** *112,* 8417.

[72] Schäfer, A.; Horn, H.; Ahlrichs, R. *J. Chem. Phys.* **1992,** *97,* 2571.

[73] Extensible Computational Chemistry Environment Basis Set Database, Version 1/29/01, as developed and distributed by the Molecular Science Computing Facility, Environmental and Molecular Sciences Laboratory which is part of the Pacific Northwest Laboratory, P.O. Box 999, Richland, Washington 99352, USA. http://www.emsl.pnl.gov:2080/forms/basisform.html.

[74] Jackson, P.; Diefenbach, M.; Schroder, D.; Schwarz, H. *Eur. J. Inorg. Chem.* **1999,** *8,* 1203-1210.

[75] Sari, L.; Gonzales, J. M.; Yamaguchi, Y.; Schaefer, H. F. *J. Chem. Phys.* **2001,** *114,* 4472.

[76] Ottschofski, E.; Kutzelnigg, W. *J. Chem. Phys.* **1995,** *102,* 1752.

[77] Venezuela, P.; Dalpian, G. M.; da Silva Antonio, J. R.; Fazzio, A. *Phys. Rev. B.* **2001,** *64,* 193202.

[78] Benzair, A.; Bouhafs, B.; Khelifa, B.; Mathieu, C.; Aourag, H. *Phys. Lett. A.* **2001,** *282,* 299.

[79] Jo, C.; Lee, K. *J. Chem. Phys.* **2000,** *113,* 7268.

[80] Li, S.-D.; Zhao, Z.-G.; Zhao, X.-F.; Wu, H.-S.; Jin, Z.-H. *Phys. Rev. B.* **2001,** *64,* 195312.

[81] Brazier, C. R.; O'Brien, L. C.; Bernath, P. F. *J. Chem. Phys.* **1989,** *91,* 7384.

[82] Jr., R. W. S.; Gingerich, K. A.; Kingcade, J. E. *J. Phys. Chem.* **1995,** *99,* 15294.

[83] Bruna, P. J.; Peyerimhoff, S. D.; Buenker, R. J. *J. Chem. Phys.* **1980,** *72,* 5437.

[84] Balasubramanian, K. *J. Mol. Spectrosc.* **1987,** *123,* 228.

[85] Izuha, M.; Yamanouchi, K. *J. Chem. Phys.* **1998,** *109,* 1810.

[86] Cangshan, X.; Taylor, T. R.; Burton, G. R.; Neumark, D. M. *J. Chem. Phys.* **1998,** *108,* 1395.

[87] Merrill, P. W. *Publ. Astron. Soc. Pac.* **1926,** *38,* 175.

[88] Bondybey, V. E. *J. Phys. Chem.* **1982,** *86,* 3386.

[89] Green, S. *Astrophys. J.* **1983,** *266,* 895.

[90] Grev, R. S.; Schaefer, H. F. *J. Chem. Phys.* **1984,** *80,* 3552.

[91] Michalopoulos, D. L.; Geusic, M. E.; Langridge-Smith, P. R. R.; Smalley, R. E. *J. Chem. Phys.* **1984,** *80,* 3552.

[92] Shepherd, R. A.; Graham, W. R. M. *J. Chem. Phys.* **1988,** *88,* 3399.

[93] Sari, L.; Yamaguchi, Y.; Schaefer, H. F. *J. Chem. Phys.* **2001,** *115,* 5932.

[94] Nielsen, I. M. B.; Allen, W. D.; Császár, A. G.; Schaefer, H. F. *J. Chem. Phys.* **1997,** *107,* 1195.

[95] Cernicharo, J.; Guelin, M.; Kahane, C.; Bogey, M.; Demuynck, C.; Destombes, J. L. *Astron. Astrophys.* **1991,** *246,* 213.

[96] Zhang, Y.; Zhao, C. Y.; Fang, W. H.; Lu, Z. H. *J. Mol. Struct.* **1998,** *454,* 31.

[97] Grev, R. S.; Janssen, C. L.; Schaefer, H. F. *J. Chem. Phys.* **1991,** *95,* 5128.

[98] Purnell, J. H.; Walsh, R. *Proc. R. Soc. London Ser. A* **1966,** *293,* 543.

[99] Ring, M. A.; O'Neal, H. E. *J. Phys. Chem.* **1992,** *96,* 10848.

[100] Newman, C. G.; Ring, M. A.; O'Neal, H. E. *J. Am. Chem. Soc.* **1978,** *100,* 5945.

[101] Agrawal, P. M.; Thomson, D. L.; Raff, L. M. *J. Chem. Phys.* **1988,** *88,* 5948.

[102] Colegrove, B. T.; Schaefer, H. F. *J. Phys. Chem* **1990,** *94,* 5593.

[103] Jasinski, J. M.; Meyerson, B. S.; Scott, B. A. *Annu. Rev. Phys. Chem.* **1987,** *38,* 109.

[104] Pak, C.; Rienstra-Kiracofe, J. C.; Schaefer, H. F. *J. Phys. Chem. A* **2000,** *104,* 11232.

[105] Tonokura, K.; Murasaki, T.; Koshi, M. *J. Phys. Chem.* **2002,** *106,* 555.

[106] Becerra, R.; Walsh, R. *J. Phys. Chem.* **1992,** *96,* 10856.

[107] Gong, X. G.; Guenzburger, D.; Saitovitch, E. B. *Chem. Phys. Lett.* **1997,** *275,* 392.

[108] Wirsam, B. *Theor. Chim. Acta* **1972,** *25,* 169.

[109] Blustin, H. P. *J. Organomet. Chem.* **1976,** *105,* 161.

[110] Sax, A. F. *J. Comput. Chem.* **1985,** *6,* 469.

[111] Ernst, M. C.; Sax, A. F.; Kalcher, J. *Chem. Phys. Lett.* **1993,** *216,* 189.

[112] Lischka, H.; Köhler, H. *J. Am. Chem. Soc.* **1983,** *105,* 6646.

[113] Bogey, M.; Bolvin, H.; Demuynck, C.; Destombes, J. L. *Phys. Rev. Lett.* **1991,** *66,* 413.

[114] Allen, W. D.; Schaefer, H. F. *Chem. Phys.* **1986,** *108,* 243.

[115] Hün, M. M.; Amos, R. D.; Kobayashi, R.; Handy, N. C. *J. Chem. Phys.* **1993,** *98,* 7107.

[116] Grev, R. S.; Schaefer, H. F.; Baines, K. M. *J. Am. Chem. Soc.* **1990,** *112,* 9458.

[117] Sax, A. F.; Kalcher, J. *J. Phys. Chem.* **1991,** *95,* 1768.

[118] Curtiss, L. A.; Raghavachari, K.; Deutsch, P. W.; Pople, J. A. *J. Chem. Phys.* **1991,** *95,* 2433.

[119] West, R.; Fink, M. J.; Michl, J. *Science* **1981,** *214,* 1343.

[120] Olbrich, G. *Chem. Phys. Lett.* **1986,** *130,* 115.

[121] Trinquier, G. *J. Am. Chem. Soc.* **1990,** *112,* 2130.

[122] Andrews, L.; Wang, X. *J. Phys. Chem.* **2002,** *106,* 7696.

[123] Poirier, R. A.; Goddard, J. D. *Chem. Phys. Lett.* **1981,** *80,* 37.

[124] Krogh-Jespersen, K. *J. Phys. Chem.* **1982,** *86,* 1492.

[125] Luke, B. T.; Pople, J. A.; Krogh-Jespersen, M. B.; Apeloig, Y.; Karni, M.; Chandrasekhar, J.; von R. Schleyer, P. *J. Am. Chem. Soc.* **1986,** *108,* 270.

[126] Ernst, M. C.; Sax, A. F.; Kalcher, J. *Chem. Phys. Lett.* **1993,** *216,* 189.

[127] Gwaltney, S. R.; Head-Gordon, M. *Chem. Phys. Lett.* **2000,** *323,* 21.

[128] Kong, J. *et al. J. Comput. Chem.* **2000,** *21,* 1532.

[129] Teramae, H. *J. Am. Chem. Soc.* **1987,** *109,* 4140.

[130] Somosundram, K.; Amos, R. D.; Handy, N. C. *Theoret. Chim. Acta* **1988,** *70,* 393.